



# *Solar Splash Technical Report*

## Boat #8



04 May 2015

### **Team Members**

Katelynne Burrell

Jacob Dubie

Jeremy Dumont

Peter Larson

Tieg Laskowske

Alex Rheaume

Josh Sykes

Jay White

Brian Wolf

### **Advisors**

Dr. Timothy Dewhurst

Dr. Gerry Brown

## **I. EXECUTIVE SUMMARY**

The overall goal of the Cedarville University 2015 Solar Boat team is to win the 2015 Solar Splash Competition and establish the viability of a hydrofoil system for the 2016 DONG Energy Solar Challenge (DSC). In order to accomplish these goals, we have set a target speed of 80.5 km/hr (50.0 mph) in the Sprint event and 14.5 km/hr (9.0 mph) in the Endurance event. With hydrofoil flight the Solar Splash boat goal speed is 19.3 km/hr (12.0 mph). To achieve these collective goals we focused on several individual projects including electronics and data acquisition, motors, propulsion, and hydrofoils.

For many years the Solar Boat team has been trying to develop a robust electronic control and instrumentation system. Based upon the work of previous teams, coupled with our own innovations, we have created a system with a very small form factor, robust noise immunity, and high modularity. This was done by optimizing the data acquisition and control systems from 2014 that served as a starting point for this year's system. Our new design uses faster and more powerful microprocessors along with the industry-standard Controller Area Network (CAN bus) protocol to communicate with a high number of devices; the newer microprocessors allow us to have better energy management and the CAN communication protocol greatly reduces noise in our data. The 2015 electrical system integrates the control panel, Energy Management System (EMS), motor current control, and the instrumentation and data acquisition system.

The EMS is an algorithm in the central microcontroller that takes into account Maximum Power Point Tracker (MPPT) current, battery State-of-Charge (SoC), and race time remaining to calculate the target battery current draw for any given point in the Endurance race. The new feedback control system uses a current sensor as its feedback, and controls the current going to the motor controller; this replaces the driver-set Pulse Width Modulation (PWM) control. The EMS allows us to have improved control of our battery current, thus allowing us to optimize our use of stored battery energy. The data acquisition system (DAQ) reads all measurements from the CAN bus and the central microcontroller and exports them to a Secure Digital (SD) memory card for analysis on a desktop computer.

The 2015 battery box design has been a two-year endeavor. In 2014 a battery box was designed with a Complex Programmable Logic Device (CPLD), using a "state machine," to automatically control the battery configuration for Sprint or Endurance. This was controlled by the driver interface on the boat's control panel. The system weighed 51 lb and was quite complex in both operation and construction; this was the source of some of our problems in the Endurance event in 2014. To make the system reliable and simple we have eliminated the CPLD control and limited the user control to switching between a power-conserving 12V battery mode and a high speed 24V battery mode. This decision allowed us to reduce the 2015 battery box from 51 lb to 37 lb, while increasing the system's robustness. The battery box communicates with the control panel via the CAN bus, instead of parallel signal communication. The 12V-24V system uses only a few switches and a purely analog circuit, therefore greatly increasing reliability and simplicity.

In 2014, we developed new motors for both the Sprint and Endurance races; these motors did not perform as expected and the primary goal in this area this year was to identify and fix the problems with these motors. We performed dynamometer tests with the 2014 Endurance motor and found it to be only 70% efficient at our rated torque and speed of 2.8 Nm and 3000 rpm. Through a series of tests, we discovered a short-to-ground in the motor's windings. We have designed a new motor that we are currently manufacturing, which is designed to be 93% efficient at our rated torque and speed. Similarly, the Sprint motor also had ground-shorts in two of the windings and we are rebuilding that motor as well.

To improve our propulsion system, we chose to design and manufacture a system with contra-rotating propellers (CRP). Such a design is promising since the aft propeller can recover much of the rotational energy imparted to the water by the fore propeller. We designed a new gear assembly that will utilize the current Endurance gearbox to drive a pair of CRPs. The new system will use a specially designed pod to allow the gearbox itself to rotate and power the outer shaft, while the inner shaft is driven by the sun gear.

Simultaneously, we have designed a new pair of CRP's using OpenProp software that we have modified for CRP design by implementing an iterative method that optimizes the propeller interactions. We used the CNC mill to create these new propellers.

For several years the Cedarville University Solar Boat team has attempted to increase boat speed through a hydrofoil system that reduces overall drag through elimination of hull drag. Toward this goal, previous teams have developed Computational Fluid Dynamics (CFD) modeling techniques, reduced the overall weight of the boat, and developed foil manufacturing techniques. The last concerted hydrofoil attempt (2013) achieved flight but with a hindered performance due to excessive boat weight and drag of the struts. This year, the hydrofoil sub-team attempted to make an improved, complete hydrofoil system. To accomplish this we learned how to use two fluid analysis programs: the Athena Vortex Lattice (AVL) and Ansys Fluent. AVL is a quick and simple program that we intended to use to test a wide range of foils quickly. Fluent is a powerful program that can model very complex geometries and 2-phase flow that we intended to use for refining the design achieved with AVL. A large portion of the work this year was devoted to validating AVL as a design tool and confirming the results from both AVL and Fluent with published experimental data. First we focused on resolving discrepancies between the results from AVL and Fluent. We found that AVL uses a "lifting panel" technique that only calculates lift-induced drag. Thus, we developed a new code that combines AVL output with additional calculations for other types of drag; we now have agreement between our various analysis codes. We then began to identify a hydrofoil system that would produce the desired performance characteristics. Manufacturing techniques were changed to improve speed of manufacturing and foil strength; this enabled a wider range of possible designs. These changes included adding a wood core and optimizing the amount of carbon fiber present in the foil. With these improvements we are closer to our goal of creating a full, robust, and stable hydrofoil system for use in future Solar Splash Endurance races.

These concurrent projects have been a full-team effort to improve on the work of previous years and perform competitively in both 2015 and the future. With improvements to pre-existing electronic control algorithms we have optimized the power flow from the batteries to the motors of both races. We have created an electronic system which is capable of running the boat successfully for several hours in race conditions. Through extensive testing we have identified winding short-circuits for the 2014 Sprint and Endurance motors. We have created a CRP design tool for public use and have used it to design a pair of contra-rotating propellers for the Endurance race this year. Using AVL and Fluent software we have shown that several analysis techniques are practical validators for hydrofoil designs applicable to the Endurance race. With improvements in core type and sealant technique we have identified a hydrofoil manufacturing process that can implement the new design

## II. TABLE OF CONTENTS

I. EXECUTIVE SUMMARY .....	i
II. TABLE OF CONTENTS.....	iii
III. PROJECT GOALS AND OBJECTIVES .....	1
IV. CURRENT DESIGN AND PROBLEM DEFINITION .....	1
A. Solar System .....	2
B. Electrical System .....	2
C. Power Electronics .....	6
D. Hull Design .....	9
E. Drivetrain and Steering.....	12
F. Data Acquisition and Communication.....	16
V. PROJECT MANAGEMENT .....	18
G. Team Organization.....	18
H. Project Planning and Schedule.....	18
I. Financial and Fund-raising .....	18
J. Continuity and Sustainability.....	18
VI. CONCLUSIONS AND RECOMMENDATIONS .....	19
K. Conclusions.....	19
L. Summary of Goal Completion.....	19
M. Where do we go from here?.....	19
N. Recommendations.....	20
BIBLIOGRAPHY .....	21

### III. PROJECT GOALS AND OBJECTIVES

The primary goal of the 2015 Cedarville University Solar Splash team is to win the Solar Splash competition in June of 2015. In order to accomplish our primary goal of winning, we have set specific goals for each event based upon the past several years' performances.

For the Endurance event our goal is to travel at an average speed of 9 mph (14.5 km/hr) for both of the two-hour races. Our goal for the Sprint portion of the competition is to complete our run in under 20 seconds. We calculate that we can obtain a top speed of 50 mph (61 km/hr). Our goal for the Slalom event is to complete the course in 31 seconds or less. To attain these speeds we created a power budget to determine performance specifications for each subsystem. Fig. 1 shows a visual representation the power budget for the Endurance event without hydrofoils.

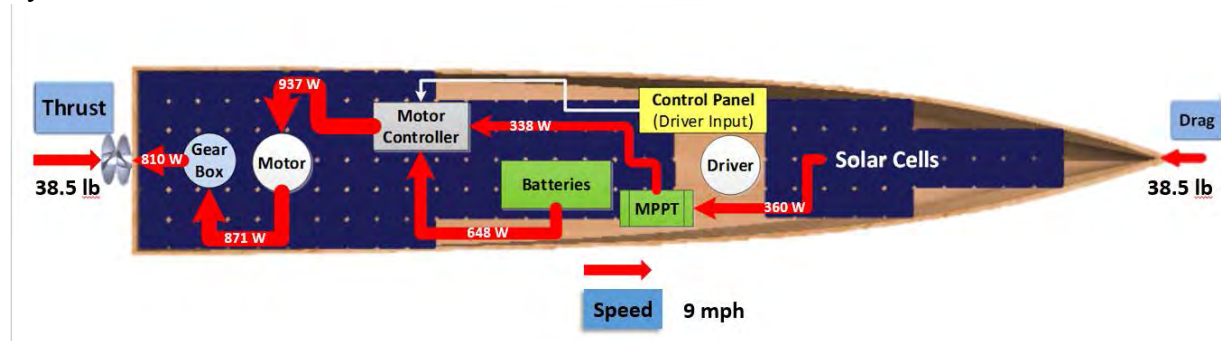


*Fig. 1. Power flow diagram for the Solar Splash Endurance event.*

Fig. 2 shows the power flow for the Sprint event. The power values shown are determined by using the efficiencies specified in the power budget. During the Sprint event the solar cells are not in use which explains why there are 0 W coming into the motor controller from the cells.

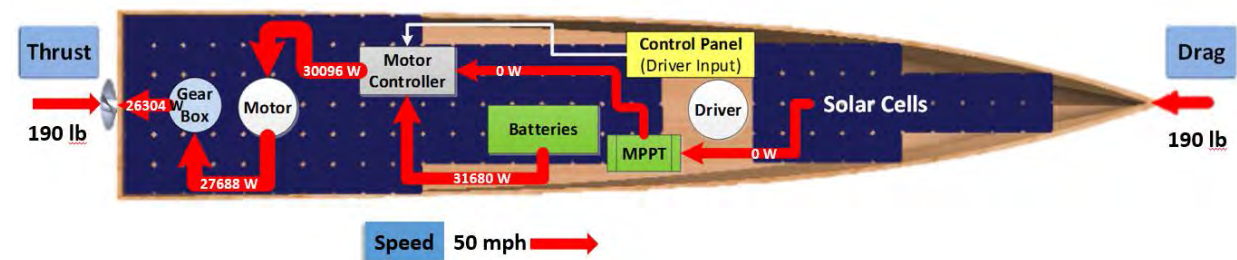


*Fig. 2. Power flow diagram for Solar Splash Sprint event*

These figures show the amount of power coming into and going out of each component, which are based on target efficiencies for each component and thus dictate performance specifications for the solar panels, MPPT, batteries, motor controller, motor, gear box, and propellers. The full power and weight budgets are shown in Appendix E-Power and Weight Budgets.

### IV. CURRENT DESIGN AND PROBLEM DEFINITION

The Cedarville University Solar Splash team has made several improvements to the 2014 boat design. These changes are reflected in the following sections: Solar System, Electrical System, Power Electronics, Hull Design, Drivetrain and Steering, and Data Acquisition and

## IV. CURRENT DESIGN AND PROBLEM DEFINITION

Communication. Documentation of the boat batteries, flotation calculations, proof of insurance, and team roster are located in Appendices A, B, C, and D respectively.

### A. Solar System

1) **Current Design:** The solar panels designed and used in 2014 allow for more low-angle light to enter the solar panels by changing the top layer of the panels to one with triangular prisms rather than a flat top. The layout of the solar cells was then finalized, as shown in Fig. 3.

2) **Analysis of Design Concepts:** We used an optics analysis to develop the surface texture to capture low-angle light. Calculations showing that we meet the competition requirements can be found in Appendix V- Solar Array Electrical Calculations.

3) **Design Testing and Evaluation:** These panels were tested using our custom solar-panel test bench (funded in part by a NASA Space Grant); results showed that the panels produce up to 40% more power under low-angle light conditions. This design proved useful in the 2014 competition and will be used again by the 2015 team.

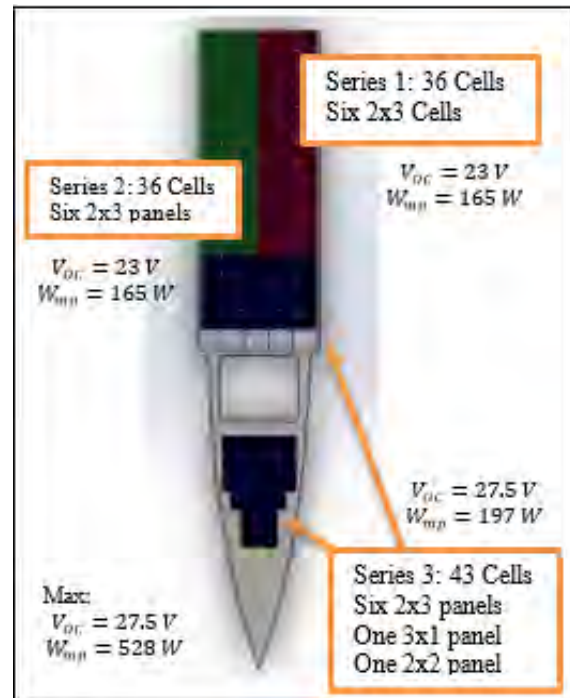


Fig. 3. Solar array layout for three series

### B. Electrical System

#### 1) Current Design:

Last year we fabricated two circuit cards for the electrical system. One performed the following tasks: collect and store/transmit data at appropriate speeds; interpret strain gauge data for torque and thrust gauges; send and receive logic between the CPLD on the battery controller circuit and send appropriate signals to the motor controllers. We also designed a circuit card that implemented a current feedback system using Uno32 and Max32 microcontrollers with an Allegro current sensor to limit motor current.

We ran the board on 12/24 V coming from the battery controller circuit, depending on system voltage. All of the signals going into the microcontrollers were between 0 and 3.3 V, due to input constraints of the microcontroller. We ran most signals directly to each corresponding box as an analog system. This led to high noise on our signals and to inaccurate results. The system was only suitable for Solar Splash where the race length is a set time; we prefer a system that is versatile and can be used for races of a set distance as well.

We had issues last year with ground loops and voltage spikes that destroyed multiple devices. Also, the Uno32 precluded a feedback system since its current draw cannot be dictated by the Max32; it cannot operate as a slave device.

2) **Analysis of Design Concepts:** The overall electrical system block diagram is shown in Fig. 4. The Instrumentation and control system consists of the control panel, motor control box, and sensor boxes. The subsystems communicate with each other using the CAN bus protocol. This diagram also shows the power flow from the solar panel and batteries to the motor as well as the way in which the driver interacts with the power system through the control panel. The



#### IV. CURRENT DESIGN AND PROBLEM DEFINITION

Data acquisition system is discussed in the Data Acquisition/Communication section of this report.

##### a) Control panel and

**Software:** The control panel circuit card consists of a PIC18F46K22 as our central microcontroller. This device is capable of using interrupts so we have the ability to utilize our processing power more efficiently. We use a GPS module to determine our speed, and a keypad to allow the driver to control the LCD display. We also have a Bluetooth module to add a wireless display in the near future. An image of the control panel PCB is shown in Fig. 5.

The control panel is also the center of data collection and logging. The software design has many layers. We interface with a large number of devices and this is accomplished by using interrupts for nearly all of our protocols. One of the main techniques we use is memory mapping. Memory mapping consists of writing to a buffer that is used to send commands to various devices. For example, below we have a buffer called LCDBuffer that can be seen in Fig. 6 which contains four buffers, one for each row. The buffers are continually written to, but also we are continually sending commands to update the LCD.

We use the OpenLog SD card writer to log the data. This board uses USART communication to the GPS and Bluetooth modules. Since there are only 2 hardware USART modules on the PIC18F46K22, we designed a third serial port using a “bit-bang” approach. This method uses a Capture/Compare port to trigger at 9600 Hz and we created a variable called SDbuffer into which we continually write variables. We also give each variable a start and stop bit, and each time the “compare interrupt” variable is triggered we send out another bit. A visual example of this is given in Fig. 7.

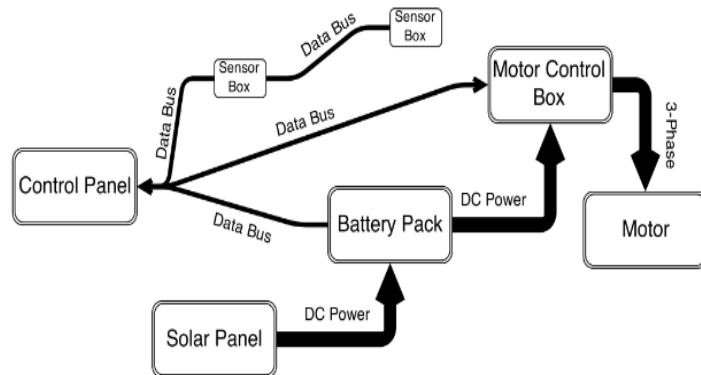


Fig. 4. Overall electrical system block diagram

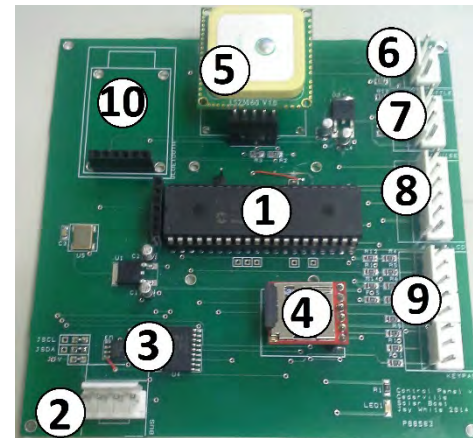


Fig. 5. The control panel circuit card; 1) PIC18F46K22 micro-controller; 2) CAN bus; 3) CAN controller; 4) SD card; 5) GPS; 6) Throttle encoder; 7) Energy management activate; 8) LCD; 9) keypad

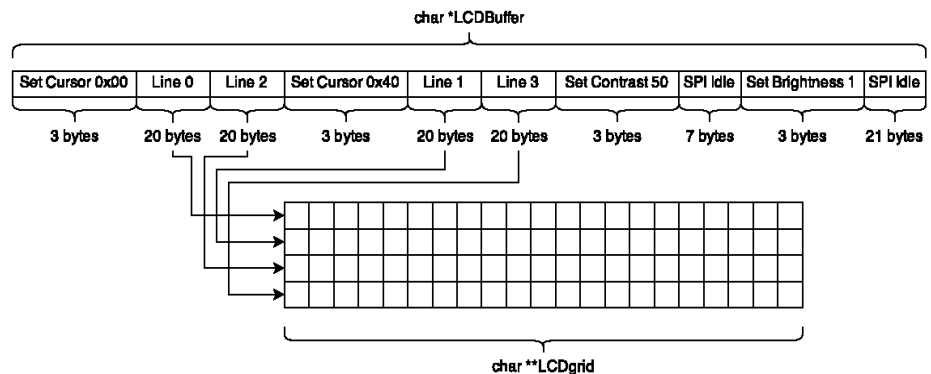


Fig. 6. Our main method of working with external devices is called memory mapping. This consists of updating a buffer containing everything being sent to the device. The example above is for the LCD

#### IV. CURRENT DESIGN AND PROBLEM DEFINITION

The data collected comes via the CAN bus, or directly into the Control Panel Circuit Card. The data on the CAN bus can come from CAN I/O Expanders, such as those in the Battery Box, or from other microcontrollers, such as the one on the Motor Control Cards. This data is stored in a memory map that can be accessed by other parts of the Control Panel software, such as the LCD display, the Energy Management System, or the SD Logger.

To use the CAN bus, a microcontroller needs to interface with a MCP2515 CAN controller chip. The microcontroller uses an SPI interface to communicate with the MCP2515. The MCP2515 contains registers that must be configured so that the MCP2515 can talk on the CAN bus. The MCP2515 is then connected to a MCP2561 CAN transceiver which converts the RX and TX signals from the MCP2515 to the differential pair signals on the bus.

**b) Energy management:** The Control Panel also contains the Energy Management System. The goal of this system is to allow the boat to automatically determine the speed, in order to optimize the usage of the energy in the batteries. While the algorithm is in the Control Panel software, it uses data collected from several parts of the boat. The energy management algorithm output is motor amps,  $I_{motor}$ , but our energy remaining is mainly determined by battery amps,  $I_{batt}$ . The battery current can be found by subtracting the MPPT current,  $I_{PPT}$ , from the motor current. The algorithm considers the voltage of the batteries,  $V_{batt}$ , and  $I_{batt}$  with a lookup table to determine the energy remaining,  $U_{batt}$ , because our goal is to drive at constant battery power. The target power is found in Equation 1. All currents are measured at the battery voltage, for example  $I_{PPT}$  is the MPPT output current and  $I_{motor}$  is the motor controller input current.

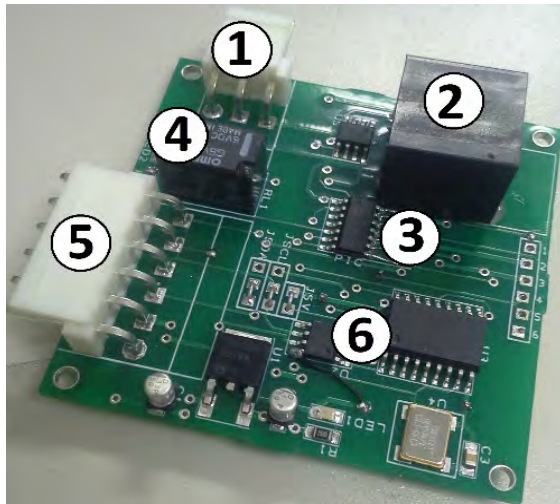


**Fig. 8.** The Motor Control Card; 1) PWM signal to the motor controller; 2) current sensor input; 3) PIC16F1825 microcontroller; 4) PWM select relay; 5) CAN bus; 6) CAN controller

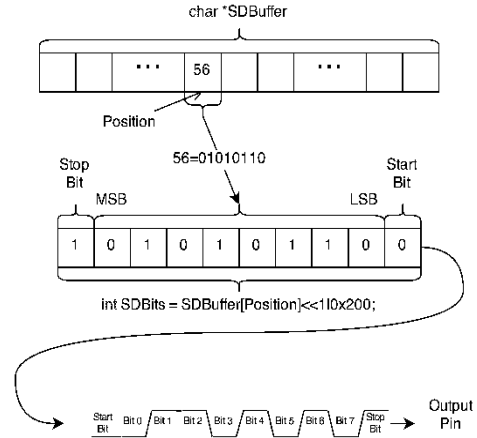


**Fig. 7.** A visual representation of the "bit bang" approach; we use a Capture/ Compare module from the  $\mu C$  to trigger at 9600 Hz and we send out bits using SDBuffer

$$P_{target_{batt}} = \frac{U_{batt}}{\Delta t} = V_{system} I_{target_{batt}} \quad (1)$$

Therefore the target battery current can be found using Equation 2

$$I_{target_{batt}} = \frac{U_{batt} \Delta t}{V_{system}} \quad (2)$$

Equation 3 shows the formula for the target current for the motor.

$$I_{target_{motor}} = \frac{U_{batt} \Delta t}{V_{system}} + I_{PPT} \quad (3)$$

**c) Motor control box:** The motor control box contains the circuitry to send power to the motor. It contains three main components: the motor controller(s), the current sensor(s), and Motor Control Card(s) (MCC). The component that we spent the most time designing was the motor control card, shown in Fig. 8. The full schematic



#### IV. CURRENT DESIGN AND PROBLEM DEFINITION

and PCB layout of an MCC is shown in Appendix F- Circuit Diagrams, Figures F.5 and F.6, respectively.

Instead of controlling our motors based on a PWM signal we have designed a system that will send a modulated signal to achieve a target current. This prevents excessive current draw that would endanger the motor controller circuitry (a problem in 2014).

To set the current to the motor controller, the value from the current sensor is sent to the analog input of the microcontroller on the MCC. A 50 Hz PWM signal is generated by this microcontroller. On every cycle the current measurement is compared with the target. If it is too high, the PWM pulse width is decremented by  $1\ \mu\text{s}$  and if it is too low, the PWM pulse width is incremented by  $1\ \mu\text{s}$ . Additionally, if the current rises above a pre-programmed threshold the CAN bus is notified and the PWM is set to stop the motor controller.

For the Endurance event we use a Mamba XL2 and for the Sprint event we use four Jeti SPIN Pro 300 motor controllers. However, they are all controlled by a PWM control signal from the Motor Control Card. The current sensor is connected to the DC input to the motor controller. Due to their simplicity and light weight, we used GMW BBM-01 current sensors throughout the boat to measure current. This field-effect sensor is placed on a bus bar through which the DC current flows. The Endurance motor control box is seen in Fig. 9.



**Fig. 9.** Endurance motor control box. It consists of a Mamba XL2 motor controller, Motor Control Card, and GMW current sensor



**Fig. 10.** A separate motor control card is used to control each motor for our Sprint system. Each Motor Control Card communicates with the CAN bus

MCP25050, which connects it to the CAN bus. This allows the Control Panel to read the analog values of the various sensors around the boat. The MCP25050 CAN I/O expanders work similarly to the MCP2515 CAN controller but have much of the hardware built in. As a result, only the MCP2561 CAN transceiver is needed for these to work. The expanders are “once-programmable” and assigned different ID's so that each expander can be accessed separately. They are configured so that they periodically send the analog data along the CAN bus. For more

There are two configurations: Sprint and Endurance. For the Endurance race, we run a single motor with a single Mamba XL2 motor controller and one MCC. For the Sprint race, we run four motors on a single shaft with four Jeti SPIN Pro 300 motor controllers and four MCCs. Because there are four MCCs their CAN bus connections are daisy-chained together as seen in Fig. 10.

**d) Sensor boxes:** The goal of the Sensor Cards is to allow for data from various parts of the boat to be collected. The core of the box is a MCP25050 CAN I/O expander. The cards also contain instrumentation circuitry for each sensor with analog outputs that can be read by the

## IV. CURRENT DESIGN AND PROBLEM DEFINITION

complex sensors, such as the propeller tachometer, a microcontroller can be used in tandem with the MCP2515 CAN controller.

### 3) *Design Testing and Evaluation:*

The control panel processes all of the measurements and control logic of the boat. The measurements and calculations are recorded to an SD card. The Control Panel has a deadman, motor switch, and other driver interface devices. The Control Panel also contains the Energy Management System, which optimally uses the allowable energy in the boat to be at approximately 5 % SoC at the end of any Endurance race.

The motor control box successfully limits the DC current going into the motor controllers with a current feedback system. The sensor boxes can be implemented anywhere on our main bus. They use the MCP25050 CAN expander chip to measure and transport analog and digital inputs. The Communication Bus uses the CAN protocol to send information to all subsystems in the electrical system. Fig. 11 shows our current target point (yellow), our actual current (blue), and our speed (orange).

After some initial tests with the EMS we found that a convenient way for the driver to control the boat is to have the driver press the Cruise Control push-button to enable the EMS. The LED in the button lights up to show that the EMS is enabled. To override the system, the driver simply turns the throttle, which disables the Energy Management System, takes the target current directly from the throttle. When overridden, the target current is adjusted from its last value, instead of the absolute position of the dial.

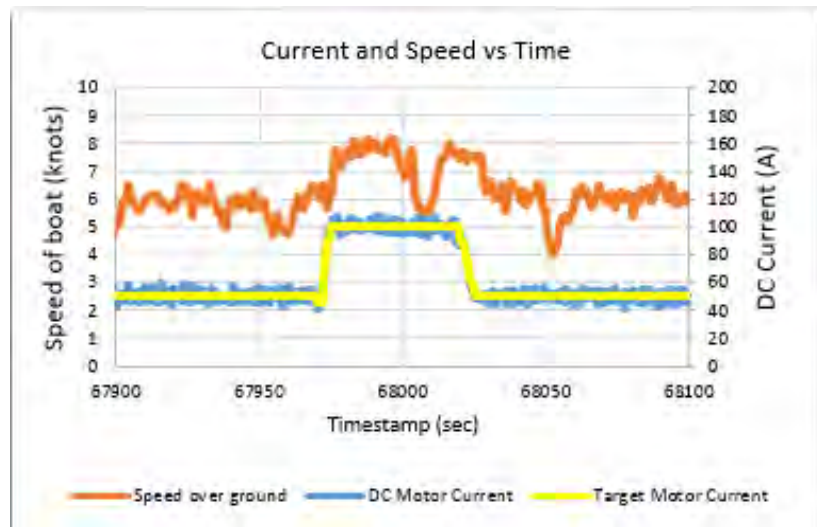


**Fig. 11.** Current control capabilities. The current set-point is in yellow, the actual current is in blue, and the speed in knots from the GPS is in orange. Note how the actual current tracks the target current very closely

After initial tests with both Sprint and Endurance controllers, we found that the power loss in the controllers is too high and the resulting temperature rise is too much for the devices to handle. For Endurance we added a heat sink with a fan and have found that it significantly reduces the temperature rise. For the Sprint system we have added larger heat sinks and fans for greater heat dissipation. For both controllers we have also optimized the timing advance setting and switching frequency to better match the extremely low impedance of our custom motors which also reduces the controller temperature.

### C. Power Electronics

1) **Current Design:** We designed and constructed a Battery Controller Box (BCB) for the Endurance race of the 2014 Solar Splash competition. The BCB consisted of nine 1-1414939-4 relays and three PN-9012 solenoids that were controlled by a CPLD with inputs from the driver interface. The BCB allowed the user to connect the lead-acid batteries in parallel or series according to the finite state machine algorithm within the CPLD. The algorithm also allowed the user to switch the battery voltage from 12 V DC (nominal mode) to 24 V DC (high power mode

#### IV. CURRENT DESIGN AND PROBLEM DEFINITION

for passing and creating enough lift for hydrofoils) under load. The BCB can also perform battery-to-battery charging through an auxiliary charging unit, but this function still needs to be optimized. The BCB was completed in time for competition, but time did not allow for sufficient testing and functionality was lost during competition. The box turned out to weigh 51 lb (plus 100 lb of batteries).

The 12V-24V high power mode system was designed to change the configuration of the three 12V batteries to a 24V system with one battery in series with two paralleled batteries. In 2014 we designed a current controller card to limit and stabilize the current in the Solar Splash races. We were not able to implement this function because of general time constraints and the Sprint motor's delayed completion.

##### 2) *Analysis of Design Concepts:*

###### a) *Battery monitoring card:*

The Endurance motor runs on 12 V nominal voltage and the Sprint motor is designed to run on 26V (load voltage), which is an open circuit voltage of 36V. We are using either three Genesis 42 EP Lead-Acid batteries or nine Genesis 13 EP Lead-Acid batteries. (Appendix A provides the required battery documentation.) When the nine 13 EP batteries are used, we permanently put three in parallel with each other to give "three 12V batteries." The three 42 EP batteries weigh 98.34 lb and the nine 13 EP batteries weigh 97.2 lb. Therefore we satisfy the 100 lb max battery limit. We have designed a battery management card to monitor the analog inputs of the battery pack. The schematic and printed circuit file for the battery management circuit card is found in Appendix F – Circuit Diagrams, Figures F.1 and F.2, respectively. We condition the analog inputs with Op-Amp circuits and convert the analog signals to digital signals, which are sent over the CAN bus via the MCP25050 I/O CAN expander chip to be recorded in the control panel. The I/O expander chip communicates with the MCP2561 CAN transceiver. Also, the battery management circuit card has a Vicor 50 W, 7.5V power supply that will go on the main communication bus to power all of the boards in the system. The 7.5V is regulated down to 5V on each board to eliminate noise picked up on the bus. A picture of our board is shown in Fig. 12.

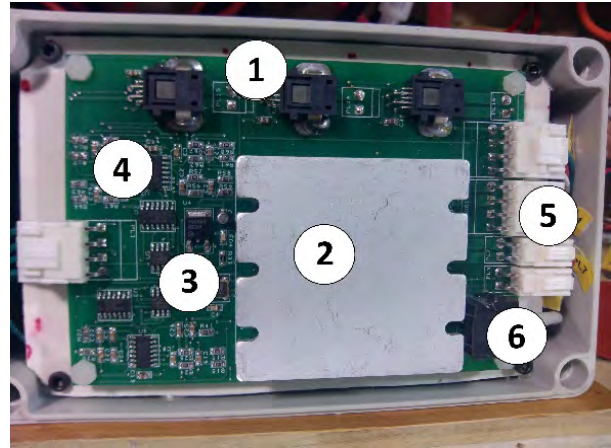


**Fig. 12.** The battery monitoring card. 1) PPT sensors; 2) Vicor power supply; 3) CAN devices and voltage regulators; 4) signal conditioning circuits; 5) four wire bus; and 6) current sensor input

###### b) *12 V-24 V switching circuit:*

The 12V-24V system high power mode is designed to change the parallel configuration of the three 12V batteries into a 24V system with one battery in series with two paralleled batteries. This allows us to pass quickly and to rise up on hydrofoils. The system is shown in Fig. 13. When only Switches 1 and 2 are closed, the load receives 12V and the batteries share the load equally. To switch to 24V mode, we open Switches 1 and 2, resulting in Switches 1-3 being open. The load receives

**Table 1.** States of Switches 1-3 for each mode in the Solar Splash Endurance race

	SW1	SW2	SW3
12V mode	CLOSED	CLOSED	OPEN
Switching mode	OPEN	OPEN	OPEN
24V mode	OPEN	OPEN	CLOSED



#### IV. CURRENT DESIGN AND PROBLEM DEFINITION

a voltage slightly less than 12V because of the voltage drop across the diodes, but drive current continues to flow to the motor, which is one of our objectives. When only Switch 3 is closed, the load receives 24V. The different modes are shown in Table 1.

The next crucial step of the 12V-24V high power mode was deciding how to drive the relays, because without a short delay in the switching sequence, or if the switching occurs in the wrong order, we will have a short circuit on the battery. The relays are model 1-1414939-4, a bi-stable relay driven with a 2.5 A pulse (min. 200 ms). Last year, we used a CPLD to perform a series of tasks to configure the batteries but there were several design issues with ground loops and voltage spikes that destroyed multiple devices.

This year we decided to use an analog solution, because the simplicity of an analog circuit would decrease the amount of testing needed to develop a reliable solution. We went through many revisions and settled on a solution that uses only seven components: two capacitors, two relays, two resistors, and one push button. A schematic of our design is shown in Fig. 13.

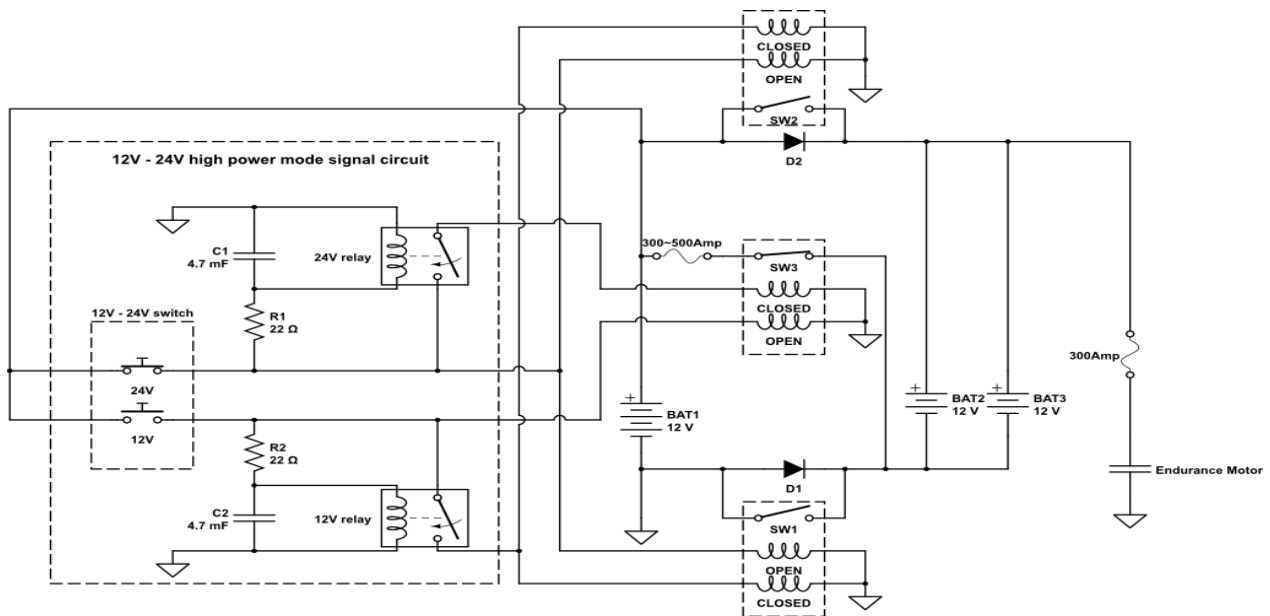


**Fig. 13.** 12V-24V high power mode circuit. On the left is the signal circuit that has only 7 components; one switch, two resistors, two capacitors, two relays. On the right is the power circuit consisting of three bi-stable relays

We implemented the 12V to 24V signal circuit on a prototype board. Since we have so few components, we kept that as the permanent solution, shown in Fig. 14. Once we established the internal circuitry of the battery box we began the manufacturing process. For the starting point we decided to use a battery box from previous years that was light weight for its size. To develop the 12V - 24V mode capability of the system we decided to lay out a to-scale cardboard mock-up version of the battery box allowing us to configure the layout in various ways to find the optimal set-up (Fig. 15). Once we were satisfied with a battery box configuration we began the manufacturing process.



**Fig. 14.** 12V-24V circuit; the cylindrical bodies are the capacitors and the orange cubes are the relays

### 3) *Design Testing and Evaluation:*

The 12V-24V switching circuit has been tested under various environments including a two hour drawdown test on the water. It successfully switches in and out of high power mode while under load. The battery box also communicates all relevant data to the boat via the CAN bus.

When the battery box was completed we performed efficiency tests to ensure the battery box is not consuming a large amount of power during normal Endurance operation. We found that at 56 A DC and a system voltage of 12 V DC the power loss in the cables and contactors is 1%. During switching mode the losses increase dramatically to about 7.5%, due to the voltage drop across the diode. This is an acceptable amount of loss, because this mode has been designed to operate when some kind of failure occurs in the system, such as a

relay malfunction or circuit board failure. A mode that can operate after a component failure, with a power loss of 7.5 %, is acceptable for a backup system that adds robustness to the system.

A thermal analysis was carried out for the diode assembly and the system is designed to safely handle diode losses of 180 W. (Equation 4):

$$V_{diode} I_{pack} = (0.9 V \times 200 A) = 180 W \quad (4)$$

The final weight of the battery box without the batteries is 37 lb; a 14 lb reduction from last year with increased robustness and simplicity, but with less automation.

### D. Hull Design

#### 1) *Current Design:*

**a) Hull:** The existing design for the Solar Splash hull shape is very good and will not be modified. The current hull is designed to be a planing hull for the Sprint event, and a displacement hull for the Endurance Event. In 2014 the team manufactured a hull using a Kevlar shell and a honeycomb core. Analysis indicated that a 1 inch core was sufficient to meet the strength and stiffness requirements. Also, by using core we are able to meet the Solar Splash buoyancy requirements without using bulkheads or other means of buoyancy. Buoyancy calculations, showing that our hull meets Solar Splash regulations, are provided in Appendix C. Additionally, we used wooden gunnels for increased stiffness, aesthetics, and to provide a means of attaching the steering system and deck. The current hull weighs just under 70 lb (311 N). Two-phase flow Fluent analysis was completed for the 2014 hull.

**b) Hydrofoil system:** A hydrofoil system for the Cedarville team was designed and implemented in 2013 for the Solar Splash boat. This design included two front foils and one rear lifting foil. The front foils were articulated by surface followers which helped the boat maintain flight. The boat was flown in October 2014 and the team observed that the surface followers and struts caused excessive drag. Only single-phase flow Fluent analysis has been used previously to evaluate the 2013 hydrofoil system.

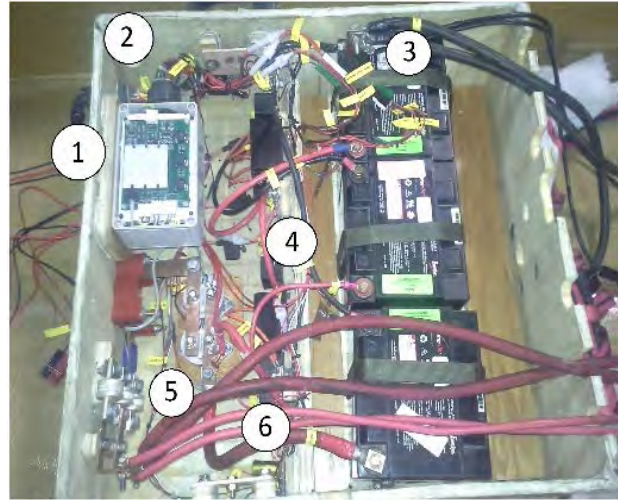


**Fig. 15.** Final layout of the Solar Splash battery box; 1) battery monitoring card, 2) Deutsch connectors going out to the control panel, 3) battery signal connectors (there is one for each race), 4) 12V-24V high power connectors equipped with heat sink, 5) protection devices, 6) 12V-24V signal circuit



## 2) *Analysis of Design Concepts:*

**a) Hull:** The existing design for the Solar Splash hull shape will not be modified this year. In 2014 the team utilized a composite construction schedule which helped in reducing the weight of the hull. The design used was a composite design with a honeycomb Nomex core and Kevlar. Fluent analysis was completed in 2014 to determine the drag on the hull using two-phase flow. From analysis it was estimated that the drag on the hull at 9 mph (14.4 km/hr) would be 24 lb (107 N) at a boat weight of 500 lb (2222 N).

Last year we carried out two-phase flow, hull drag analysis using a grant from Ohio State University's Supercomputing Center. We have performed extensive hull drag modeling using our predicted boat weight of 615 lb (2736 N), operating at 9 mph. To validate our numerical results, we developed a technique for applying 6 strain gages on the inside of the Endurance downleg to measure propeller torque and thrust, and from that we were able to determine hull drag.

**b) Hydrofoil system:** Fluent analysis has been used in the past to evaluate drag and lift on hydrofoils, however Fluent is a very complex and time consuming program to use. The Athena Vortex Lattice program provides a simpler and quicker solution to solving for lift and induced drag. A description of this program is outlined in Appendix G- Description of AVL. Analyses run in both Fluent and AVL showed discrepancies between the results. This was due to the lack of viscous effects in our AVL model. We then developed a MATLAB based program, Additional Hydrofoil Analysis (AHA), to predict the total drag on the hydrofoil system using AVL results coupled with formulae from S.F. Hoerner's *Fluid-Dynamic Drag* to account for skin friction, form and interference drag on the hydrofoil system. The AHA program can be found in Appendix H- Additional Hydrofoil Analysis (AHA) Program.

The process developed to design a hydrofoil system is outlined in Fig. 16. The parameter studies conducted in the development of the hydrofoil system included profile shape, aspect ratio, taper, and angle of attack (see Appendix I – Hydrofoil Design Analysis, for a detailed description of the design process for the hydrofoil system). From the results of these tests, the hydrofoil system was constructed to

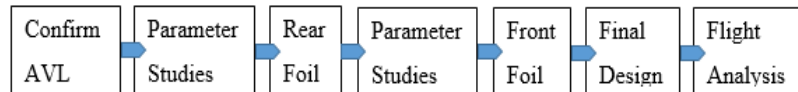


**Fig. 16** Progression of the Design Process for a hydrofoil system

obtain 615 lb (2736 N) of lift as specified by the weight budget with a maximum drag of 29 lb (129 N) at 12 mph (19.3 km/h) based on our power budget. The budgets can be found in Appendix E-Power and Weight budgets.

CFD analysis was conducted using Ansys Fluent software. Our models incorporated two-phase flow in a series of parameter studies. First, struts were analyzed in Fluent and the drag values compared. We then conducted a study on the surface effects arising from a foil flying close to the water surface. This showed the allowable limit for foil rise before lift was lost. The final results obtained agree with published experimental data that shows significant loss of lift as the foil rises to within 1½ chord lengths of the surface.

In order to conduct these studies we needed more computing power and an appropriate meshing technique for the smaller hydrofoil-and-strut bodies present in the physical system. To increase computational power, we obtained a research project under the Ohio State Supercomputer system (see Appendix J – Ohio Supercomputer Input Files) and improved our meshing through the implementation of a boundary layer mesh (see Appendix K – Boundary Layer Mesh Procedure).

#### IV. CURRENT DESIGN AND PROBLEM DEFINITION

The foil manufacturing process must yield a smooth surface finish and an accurate foil profile to  $\pm 0.05''$  ( $\pm 1.3$  mm) in the thickness direction. The material used to manufacture the foil must be of adequate strength to withstand a 400 lb (1780 N) load (65% of the total boat weight) applied as a point load in the center of the rear foil. For the designed foil profile, this correlates to a 7.5 ksi (51.7 MPa) required material bending strength.

In order to manufacture the hydrofoil design, we made an attempt to replicate a method used by the 2013 Cedarville team. This method used a foam core wrapped in carbon fiber sheets which was placed inside a mold. Resin was infused into this mold using a vacuum and allowed to cure. The resulting foil has a smooth surface finish with no voids in the resin. Due to problems with achieving the vacuum, an alternative method was used in which the resin was brushed onto the carbon-wrapped foam core, and the mold was simply clamped tightly over the foil to squeeze out excess resin. Three point bend testing showed that the carbon shell with a foam core would not be strong enough for our hydrofoil design because the carbon fiber shell failed in buckling. Several alternative material combinations were considered to achieve the strength necessary for the new hydrofoil design. Of the options considered, a wooden core covered with two layers of carbon fiber provided sufficient strength and was actually lighter than a fully carbon/resin foil. Manufacturing this foil consists of machining a wooden core to the correct shape (using models created as described in Appendix L), covering the foil with carbon fiber, brushing resin into the carbon fiber, placing the entire foil into a vacuum bag, and sanding the surface smooth. The wooden core reduces the tendency of the carbon layers to buckle.

##### 3) **Design Testing and Evaluation:**

**a) Hull:** The current design has proven useful in past competitions, and data has been collected to determine that the predictions made using Fluent are realistic. We tested the boat on the lake to collect data that can be compared to the Fluent results. From this, we found the results to match within 10%. The drag recorded using the strain gages mounted in the Endurance downleg resulted in a measurement of 39 lb (173 N) of drag on the 2014 hull.

**b) Hydrofoil design:** Using AVL and the corresponding AHA program, a hydrofoil system was designed which consists of two foils, front and rear, each with a NACA 4412 foil profile and a root chord of 0.63 ft (0.19 m). The front foil which will be articulated using a surface follower has a taper ratio of 75% and a span of 3.3 ft (1 m). The rear foil which will be at a constant angle of attack has a taper ratio of 50% and a span of 6.3 ft (1.9 m). Each foil is supported by a single NACA 0012 strut at the center. The final design is shown in Fig. 17.

This system would produce the necessary lift of 615 lb (2736 N), however it could only fly at 10 mph (16.1 km/h) with a drag of 34 lb (151 N) as specified by our power and weight budgets. To achieve our target speed we will have to decrease the weight of the boat. This will allow for smaller foils (less lift would be needed), which would consequently reduce the drag. More information on the design process and results can be found in Appendix I- Hydrofoil Design Analysis.

To confirm that the AHA program was accurate, a test was conducted using experimental data for comparison with Fluent (Beaver). The NACA 66014 strut was analyzed in Fluent and in

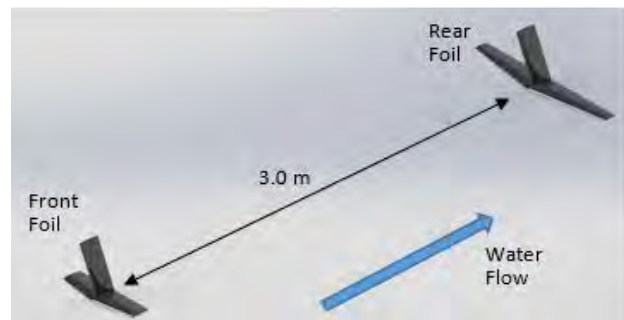


**Fig. 17.** Preliminary Design of Hydrofoil System; weight distribution is 35%-65%, front to back; generates 620 lb of lift and 34 lb of drag at 10 mph

#### IV. CURRENT DESIGN AND PROBLEM DEFINITION

the AHA program. These results (Fig. 18) were compared with the experimental drag value of 2.72 lb (12.1 N) (Beaver). More data on this test can be found in Appendix M- Moth Foil Results.

Fig. 19 indicates that the ideal operating point of a hydrofoil system is with each foil submerged at 1.5 chord lengths; lift is not compromised but each strut contributes minimal drag due to less submerged surface area. Further information may be found in Appendix N-Raw Free-Surface Study Data.

Another test conducted was for the verification of realistic flow patterns modeled in Fluent. Fig. 20 shows the general agreement between the “rising action” of the water observed in the physical and experimental strut bodies.

Finally, the manufacturing of the foils was analyzed, and the three point bend test for the foam core showed a much lower strength value than the wood core. We chose to move on with the wood core encased in two layers of carbon fiber as this foil proved to be stronger and lighter than the foil using a foam core.

#### E. Drivetrain and Steering

##### 1) Current Design:

**a) Endurance drivetrain:** The 2014 Cedarville team created a 12 V brushless motor which was used during the 2014 competition. This motor was measured to have 88% efficiency by the 2014 team, but tests this year showed it to be only 70% efficient.

**b) Sprint drivetrain:** Due to manufacturing issues, the Sprint Motor designed and built in 2014 was not used at competition, and has previously only worked for two seconds. The design consists of four motors sharing a common shaft. The motor was not in working condition when we began.

**c) Propellers:** The current propeller design is a single propeller in a forward facing pod attached by a downleg to the hull of the boat. The steering system is connected to this downleg. The pod houses the motor and the 5:1 planetary gear box in line with the Endurance motor.

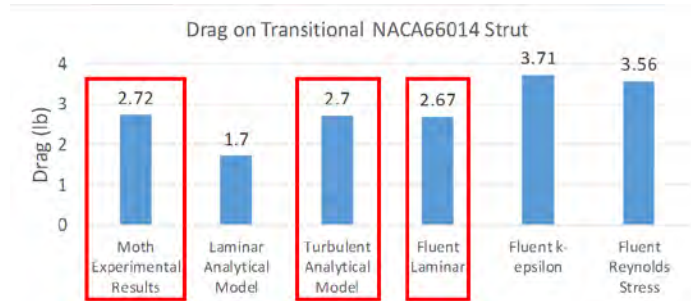


**Fig. 18.** Agreement of Experimental, Analytical and Fluent laminar models for determining drag on a surface-piercing NACA 66014 strut at a Reynolds number of 623000

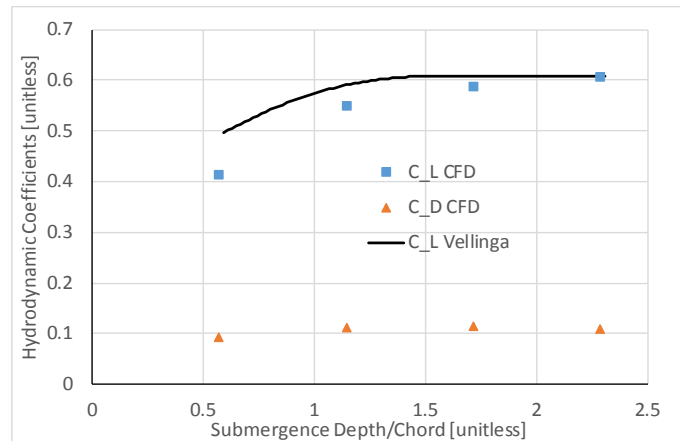


**Fig. 19.** Free-surface interaction behavior of a hydrofoil as predicted both by experimental and 2-phase VOF CFD solutions; the CFD simulation clearly shows the loss of lift reported experimentally

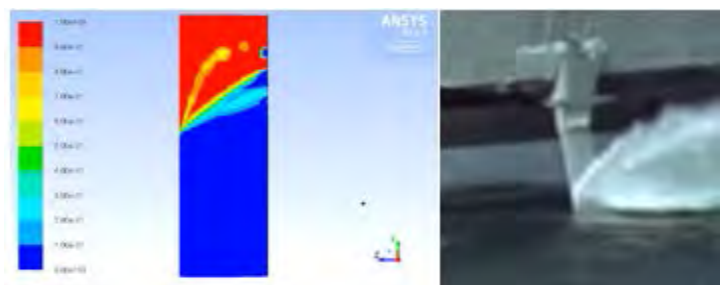


**Fig. 20.** Spray on surface piercing struts. Left: Fluent Analysis. Right: Observation; both display “rising action” and spray from the surface-piercing member

#### IV. CURRENT DESIGN AND PROBLEM DEFINITION

##### 2) *Analysis of Design Concepts:*

**a) *Endurance drivetrain:*** According to the 2015 team goal of winning Solar Splash, the Endurance motor should run at 3000 rpm with a torque of 2.07 ft-lb (2.8 Nm) while being 93% efficient as described in the Power Budget.

Preliminary analysis of the 12 V motor led to an efficiency of 70%. After determining the low efficiency in the 12 V motor a series of tests were conducted in order to determine if the efficiency problem lay with the test setup, motor controller, or the motor. Partial throttle tests were conducted with the 12 V motor at torques between 1.5-3 ft-lb (2-4 N-m) over a speed range of 2000 to 4000 rpm to determine how efficient the motor was at different operating points. The majority of our dynamometer tests were performed at partial throttle because that is how the motor is run at competition. We performed WOT (wide open throttle) tests with the 12 V motor to test the hypothesis that the motor controller is more efficient when it is run wide open. We wanted to see how much the motor controller affected the motor's efficiency. A series of voltage and current tests were performed to attempt to narrow down the reason for the 12 V motor's inefficiency. We used an oscilloscope during several of the dynamometer tests to view the current and voltage waveforms going into each of the motor's three wires. The last series of tests performed to determine the motor's efficiency problem consisted of measuring resistances to find possible short circuits or ground faults in the windings.

After this series of tests we found that we needed to build a new motor. We planned for the new motor to run at the same efficiency and speed as described in our power budget, and it needed to be constrained to the same outer diameter and approximate length as the current motor so that it could fit into the motor pod. These constraints limited the number of modifications we could make on the motor. To meet our design specifications, Jeff Keesaman made several changes to the laminations. The number of poles was increased from 9 to 36 and the inner diameter was increased from 42.3 mm to 56.4 mm. Keesaman also designed and built the magnet sleeve to go around the rotor. The new lamination pattern is shown in Fig. 21. A positive side effect of the new lamination design is that it requires a shorter stack than the 2014 motor. The shorter stack will take up less space and allow more room to fit the windings within the housing (a source of the ground-faults in the 2014 motor). This left us to design and build the housing, rotor shaft, rotor slugs and end bells. The design process is further explained in Appendix O – 2015 Endurance Motor Design and the new design can be seen in Fig. 22.

**b) *Sprint drivetrain:*** We began by testing the motor designed in 2014 for the Sprint event. The motor is a combination of four identical brushless DC motors mounted on a common shaft. It was

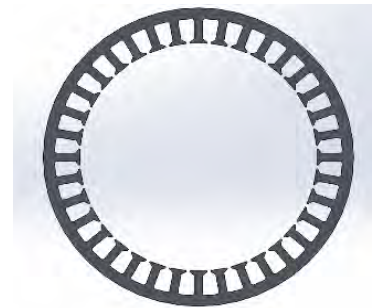


**Fig. 21.** Lamination pattern of new 12 V motor

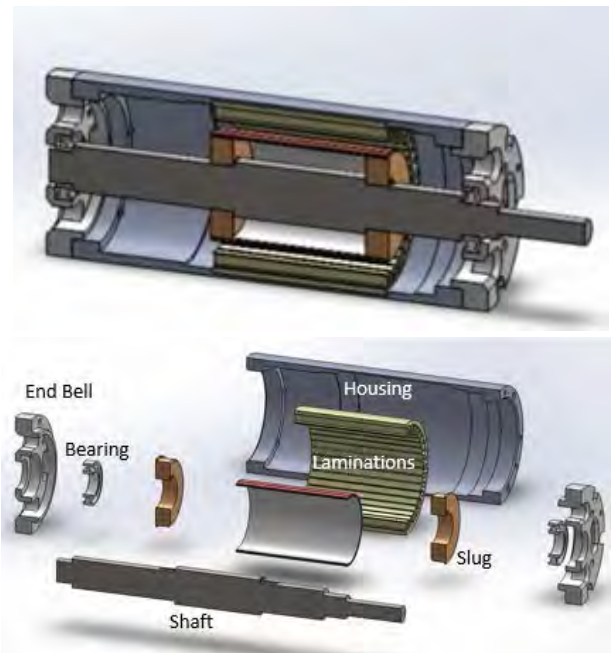


**Fig. 22.** Cross-sectional (above) and exploded cross-sectional views of the 2015 Endurance event motor



#### IV. CURRENT DESIGN AND PROBLEM DEFINITION

predicted to have a 92% efficiency when run at 5000 rpm (524 rad/s) and 39 ft-lb (52.9 N-m). These efficiencies would allow us to achieve our goal of 50 mph (80.5 km/h) for the Sprint race.

c) To evaluate the motor performance a search began for a dynamometer which would be useful for obtaining test results. However, we were not able to purchase a dynamometer this year and had to fall back on alternative options for testing. The primary option we decided to pursue was to run one or two sections of the motor while operating one or two other sections as generators. This process only required a load to dissipate the generated power, a place for the motor to be located when the tests were being performed, and the motor to be in working condition.

We knew there was a problem with the motor's wiring. We tested the motor with an ohmmeter to locate the ground faults and found one on the third stage of the motor. Before running the motor on the lake, we decided to have the stators remanufactured to correct the problems with ground faults in the windings.

d) **Propellers:** The goal this year is to achieve a gearbox efficiency of 93% or higher for a coaxial CRP system without negatively impacting the form factor. The gear assembly must accept input speeds of 4000 RPM at 10 ft-lb (13.6 N-m). The CRP's must have the requirements outlined in Table 2. These figures are dictated by the power budget specifications for motor, propellers, and hull.

*Table 2. Specifications for CRP's*

Specification	SI	English	Other
Torque/prop	11.6 Nm	8.6 lb-ft	-
Angular Velocity/prop	34.9 rad/s	-	333 RPM
Input Power/prop	405 W	-	-
Total Input Power	810 W	-	-
Total Thrust	171 N	38.5 lb	-
Total Output Power	689 W	-	-
Boat Velocity	4.0 m/s	9.0 mph	14.5 km/hr
Total Efficiency	85%	-	-
Total Weight	2.3 kg	5.0 lb	-

For the CRP gear assembly, we chose to utilize the same planetary gearbox that we use in the single propeller Endurance drivetrain. We observed that in a simple system of planetary gears, the rotation of the sun gear (power input) causes the planet ring (power output) to rotate by pushing against the ring gear (stationary and attached to the body of the gearbox). This concept is shown in Fig. 23. We designed a new shaft and gearbox configuration that allows a second propeller to be affixed to the gearbox housing. This configuration allows the force exerted on the ring gear to be transmitted to the rear propeller, rotating it in the opposite direction. The new shaft configuration is shown in Fig. 24. More information on the design of the contra-rotating gear box can be found in Appendix P – Contra-Rotating Gear Box Design.

In design of the propellers, we first compared computational tools available for propeller design. OpenProp is an open source MATLAB-based program that the team has used in the past. We learned more about CRP design using OpenProp by first replicating a simplified method of CRP design, which our team had implemented in 2009, using the 2013 version of OpenProp. Then, we moved on to implement

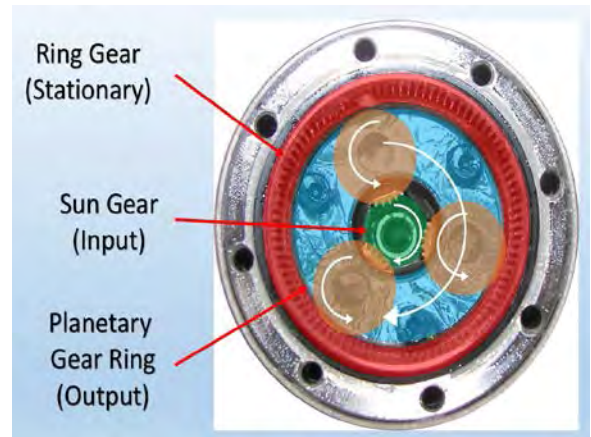


*Fig. 23. Planetary gearbox primary components*



#### IV. CURRENT DESIGN AND PROBLEM DEFINITION

Laskos's 'uncoupled' method (Laskos). The basic idea of his 'uncoupled' method is to optimize the front propeller without regard to the rear propeller, then calculate the induced velocities at the plane of the rear propeller, then optimize the rear propeller, calculate the velocities the rear propeller induces at the plane of the front propeller and repeat this procedure until convergence is achieved.

We identified the functions which would be used for optimization and the induced velocity calculations. We also identified each component that would need to be modified or added to the code. The first modification that we made was to add a second structure variable for the additional propeller to the output file. Second, we modified the output figures to show the results of both propellers. Third, we modified the input GUI to allow specification of the direction of rotation, the axial distance between the propeller planes, and a different diameter, number of blades, and torque for each propeller. Fourth, we modified the code to optimize the propellers based on a torque specification rather than a thrust specification. Fifth, we incorporated the iterative process from Laskos's code to implement the optimization routine. Finally, we modified the off-design analysis to make it applicable for analysis of CRPs. To validate the modifications we made to OpenProp, we compared the results with published data. Instructions to use the modified version of OpenProp, a sample of the primary input and output figures, and a basic description of how the program works can be found in Appendix Q – Instructions, Sample Inputs, and Outputs from Iterative CRP Version of OpenProp. Appendix R – CRP Design Process provides further details of our CRP design process.

##### 3) **Design Testing and Evaluation:**

**a) Endurance drivetrain:** The 2015 Endurance motor has not yet been completed so no testing has been done with that motor. However, many hours of testing were completed with the 2014 12 V and 24 V motors to confirm that the team needed a replacement. The set up for these tests is shown in Fig. 25. A full detailed description of the 12 V Endurance motor testing may be found in Appendix S- 12V Endurance Motor Testing and Evaluation.

**Sprint drivetrain:** We knew there was a problem with the motor's wiring since the beginning of the year, but didn't work on it until the beginning of spring semester. We tested the motor with an ohmmeter to locate the ground faults and found one on the first and fourth motor, so our preliminary testing was done on the second and third motor. Because of this problem with short circuits in our windings, we found that the reliability of the motor windings we low. This led us to approach Neu Motors about rewinding the Sprint motors to eliminate the ground fault issues and increase the reliability of the drivetrain.

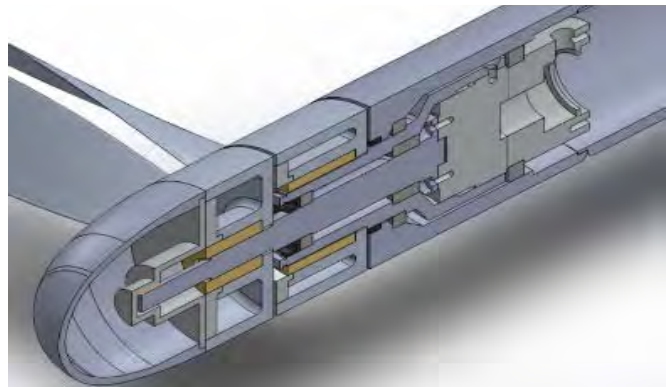


**Fig. 24.** Cross-sectional CAD model of revised CRP gearbox design including shafts

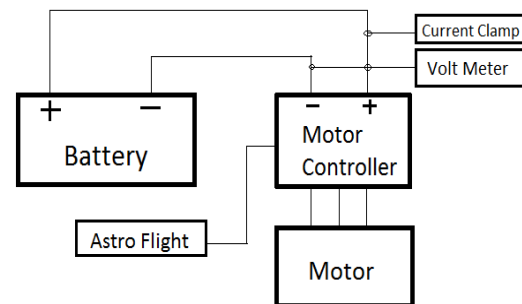


**Fig. 25.** Motor efficiency test set-up

## IV. CURRENT DESIGN AND PROBLEM DEFINITION

The motor has been reassembled and fixed so that two motors work and has been tested on the water. From this test we found that the motor controller was very inefficient at low loads and this was fixed by changing the timing angle of the motor controller. Additionally we found that the propeller for the system experiences ventilation due to surface proximity, which was fixed by adding a splash guard.

**b) Propellers:** Since the contra rotating gear assembly has not been manufactured yet, there has been no testing. When the gear assembly is completed, it will be tested with the pair of contra-rotating Endurance propellers and the efficiency of the combined system can be determined.

The CRP set designed with the modified version of OpenProp predicts an overall efficiency of 91%, which is 6% greater than the 85% specified in the power budget. We also reduced the blade thickness to give the propellers a lower pressure drag and confirmed, using the stress analysis tool, that the blade was still strong enough for both steady-state and accelerating conditions. We also examined the off-design performance curve and concluded that the off-design performance was acceptable since the efficiency is predicted to be fairly good on either side of the design point (see Fig. 26). Other than the thickness, the sample outputs shown in Appendix R are the outputs from this design. The interface between the propeller hubs and the gearbox shafts has been finalized and the overall propeller assembly is predicted to be well under the weight specification.

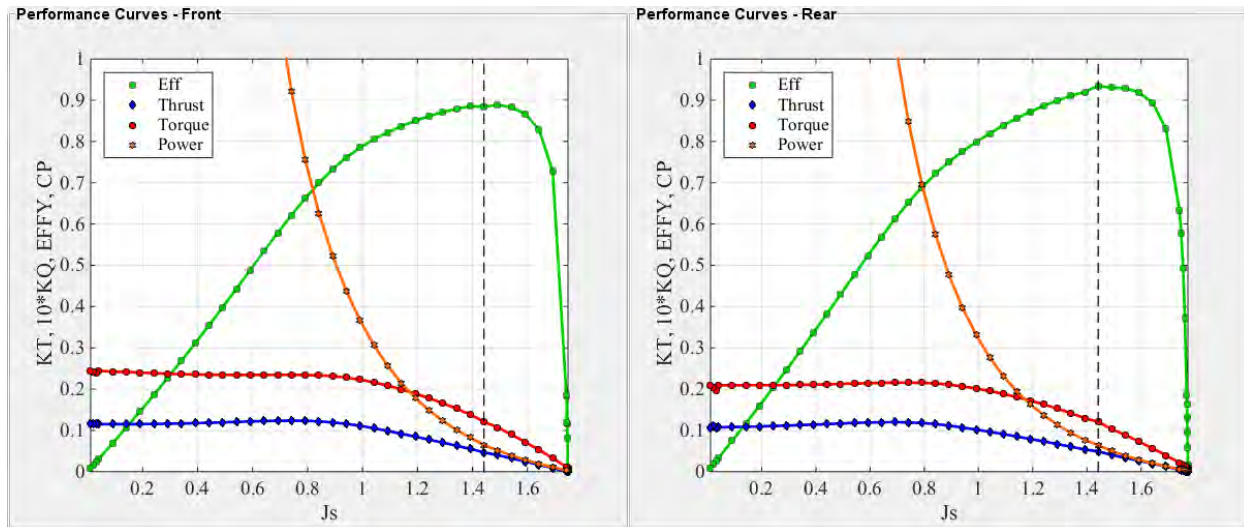


Fig. 26. The CRP performance curves show predicted off-design performance; the design point is the dashed line

We plan to test the combined thrust of the CRPs using strain gauges installed inside the motor downleg. Of the strain gauges installed on the forward-facing downleg in 2014, only the four aft strain gauges are still working. Construction of a circuit for sending the strain gauge signal to the data logger has begun.

### F. Data Acquisition and Communication

#### 1) Current Design:

In previous years, the team has had mixed results in data acquisition. One previous method used NI Labview software, which needed a laptop with careful handling requirements to store data. In 2012, the team developed an inboard data acquisition system to monitor and record measurements during the Frisian Solar Challenge competition. These developments were not fully successful, but set the foundation for designing a data acquisition system for the Solar

#### IV. CURRENT DESIGN AND PROBLEM DEFINITION

Splash competition. In 2014, we were successful in monitoring data, but failed to fully achieve recording.

2) **Design Analysis:** The Instrumentation and Data Acquisition system must be able to measure and record the following:

- Voltage, current, and temperature information from the battery pack
- Voltage output of the MPPT with accuracy of  $\pm .05\text{V}$  and range of 0-52 V
- Current output from the MPPT with an accuracy of  $\pm .05\text{ A}$  and range of 0-15 A
- Current to each motor controller with an accuracy of  $\pm .05\text{ A}$  and range of 0-300 A
- Propeller speed with an accuracy of  $\pm 10\text{ rpm}$  and range of 0-10,000 rpm
- Temperature of the motor controllers with an accuracy of  $3^\circ\text{C}$  and a range of  $-20^\circ$ - $175^\circ\text{ C}$
- Temperature of the batteries with a range of  $-20^\circ - 175^\circ\text{ C}$  and accuracy of  $3^\circ\text{C}$
- Thrust of the motor with an accuracy of 25 N and maximum thrust of 1100 N
- Torque from the motor with an accuracy of 5 N-m and maximum torque of 75 N-m
- Speed of the boat with an accuracy of .25 knots

The system must be able to measure these values at a rate of at least 50 samples per second to allow for testing and analysis of the boat's electrical and mechanical performance and efficiency. The system logs to an SD card which allows for easy data analysis in tools like Excel.

We are using a Controller Area Network (CAN) bus to send data between the subsystems of the boat. This is because CAN is an industry standard, so there are many parts that will interface well. Also, because it is differential pair, CAN is highly noise immune. Our bus has only 4 wires, the CAN high and low signals, a +7.5V power wire, and a ground wire.

The CAN bus protocol contains an ID field and several data bytes. This allows the messages from each device to be distinguishable from each other.

#### 3) **Design Testing and Evaluation:**

Measurements have successfully been recorded using the new data acquisition system. We have performed many tests recording all of these measurements, and many of them have greater accuracy than what we claimed in our specifications. An example of our CAN communication protocol can be seen in Fig. 27.

We've found that the CAN protocol should be in one continuous transmission, due to transmission line effects. This required us to find the characteristic impedance of our cable, which we found to be approximately  $180\ \Omega$  for the cable we are using. Terminating the transmission line with a  $180\ \Omega$  resistor allows us to add a device anywhere on the line, without transmission line effects.

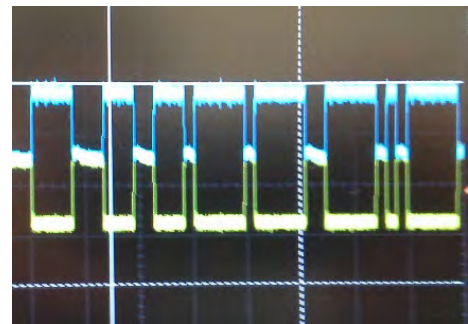


**Fig. 27.** The CAN communication protocol signal consists of a differential high (blue) and low (yellow) pulse; the wires are in twisted pair configuration and allow the signal be very noise resistant

## V. PROJECT MANAGEMENT

### ***G. Team Organization***

Cedarville University's Solar Splash teams have primarily been composed of senior mechanical engineering students as part of their capstone courses, Mechanical Engineering Senior Design I and II. This year two senior Electrical Engineers were a part of the team as part of their capstone course as well. The team was split up into four sub teams.

- Electrical
  - Battery systems
  - Data Acquisition and Energy Management
- Motors
  - Sprint Motor
  - Endurance Motor
- Propulsion
  - Contra-rotating Gear Box
  - Contra-rotating Propellers
- Hydrofoils
  - Design using AVL
  - Computation Fluid Dynamic (Fluent) Analysis
  - Manufacturing and Flight Control

The whole team met for one hour each week with the faculty advisors to discuss progress. Each sub team also met for one hour each week with the advisors to discuss design strategy.

Our team is advised by two faculty members: one mechanical engineer and one electrical engineer. In a paper written by our faculty advisors, Dewhurst and Brown (2013), they explain their approach to advising in light of three different educational models: the teacher-student model, the manager-engineer model, and the master-apprentice model. They attribute much of the solar boat team's past success to the mentoring—which balances different aspects of each of these three types of relationships—that they have provided as faculty to students on the solar boat team.

### ***H. Project Planning and Schedule***

We organized this year's team in August 2014 and each team member decided on measureable individual milestones to track their progress (see Appendix T- Team Member Task Gantt Charts). We have struggled to meet the timetable proposed in the Gantt chart.

### ***I. Financial and Fund-raising***

The Cedarville University engineering department provides our team with a budget to complete some design work and fabricate and/or purchase components and parts (Appendix U- Monetary Budget Summary). We focused on getting materials donated.

### ***J. Continuity and Sustainability***

Team continuity remains a challenge for Cedarville's Solar Splash teams. Since the project is part of a capstone course, there are few underclassmen who remain involved in the project throughout the year. The most important means of project continuity has been the shared network drive that enables each team to access work completed by previous teams. It helps maintain research, contacts, part specifications, reports, and test data, passing all of the information from team to team. The end-of-the-year reports are especially useful as a summary of work completed as well as the extensive appendices detailing specific work. This year the team focused on creating tutorials, maintaining the network drives to decrease clutter, and organize our work in a concise and straight forward manner.

### VI. CONCLUSIONS AND RECOMMENDATIONS

#### ***K. Conclusions***

The following discussion addresses our overall project strengths and weaknesses from this year:

Strengths:

- We have tested the Endurance motor and made necessary changes to improve the efficiency so as to achieve our objective of an average speed of 9 mph (14.5 km/hr) in the Endurance event
- We have produced a CRP design which will allow for greater efficiency of the boat during the Endurance event
- 12 V-24 V switching allows us to pass other teams in the Endurance event, but conserve power throughout

Weaknesses:

- We have not yet manufactured hydrofoils or the contra-rotating drivetrain. The new Endurance and Sprint motors are also not complete.

#### ***L. Summary of Goal Completion***

Our goal is to win the 2015 Solar Splash Challenge and prepare next year's team for the 2016 DSC. These objectives were used to set individual system goals.

- We have complete an electrical system which includes data logging, motor control, and a driver interface, that can be compatible with both the 2016 DSC boat and the 2015 Solar Splash Boat.
- We have redesigned, and are currently producing, a 12 V motor for the Endurance race that would allow us to achieve 9 mph (14.5 km/hr) and a Sprint motor which would allow us to achieve 50 mph (80.5 km/hr) in the Sprint event
- We have developed an analysis tool to design contra-rotating propellers. We have used this code to design CRPs and have made them on our CNC machine. We have designed a contra-rotating drivetrain but have not yet manufactured it.
- We have further developed analysis tools (AVL, AHA, Fluent) for hydrofoil design and have developed a system of hydrofoils appropriate for Solar Splash. We are still developing a means to control foil height during the race. We will not be using hydrofoils in Solar Splash 2015. We have designed, built and tested a battery box capable of protecting our batteries during a fault and send battery measurements to the Control Panel for processing. The battery box performs a 12V-24V high power mode-switching operation reliably.

While many of the above objectives were completed for our senior capstone projects, there is significantly more progress to be made in terms of completion of manufacturing and testing the Sprint and Endurance drivetrains. While the hydrofoil design is finalized, hydrofoils must also still be manufactured. The electronics are completed and have been tested for the upcoming competition. Ultimately the boat has been successfully tested on the lake for the Endurance event and run for two hours straight.

#### ***M. Where do we go from here?***

Our team has made significant progress refining the 2014 boat. The manufacturing of hydrofoils needs to be completed along with continuing work on the Sprint motor. The contra-rotating gear box must be manufactured along with the CRP's and the Endurance motor. In future years, teams should pursue hydrofoil design and manufacturing, improving upon the methods we established this year. The analytical methods using AVL and CFD presented in this technical report will also be published in the 13th International Conference on Fast Sea



## VI. CONCLUSIONS AND RECOMMENDATIONS

Transportation, held in 2015 (Burrell, Sykes). The weight of the Sprint and Endurance motors should be decreased.

### ***N. Recommendations***

- Future teams must continue to document and annotate their work: part design files, analysis work, test procedures, test data, and user guides for each process. Good documentation greatly helps future students understand the work already completed.
- At the beginning of the year, set goals that advisors think are realistic: teams may have to underestimate what they think they can complete. Once those deadlines are in place, resolve to follow them as closely as possible.
- Future teams should develop the process of designing and manufacturing a hydrofoil system.
- Use crystals for the clock of the microcontroller instead of an external crystal oscillator. The clock out pin of one chip could drive the clock for the rest of the board.
- For microcontrollers that need to use the CAN bus, a chip that has a CAN hardware module built in should be used instead of the CAN controller chip. This could significantly reduce code.

## BIBLIOGRAPHY

- Beaver, Bill and Zselezky, John. "Full Scale Measurements on a Hydrofoil International Moth". *Proceedings of the 19<sup>th</sup> Chesapeake Sailing Yacht Symposium, Annapolis, Maryland, March 2009*. Internet. 7 Apr. 2015.
- Buckle, A. K., and C. Beason. *Hydrofoil Vessels*. London: Lloyd's Register of Shipping, 1965. Print.
- Burrell, Katelynne et al. "Use of Athena Vortex Lattice Program in the Design of a Hydrofoil System for a Solar Boat." *Proceedings of the 13th International Conference on Fast Sea Transportation, Washington, D.C., September 2015*. In progress.
- Drela, Mark, and Harold Youngren. "AVL 3.30 User Primer." 18 Aug. 2010. Internet. 7 Apr. 2015.
- Hoerner, Sigward F. *Fluid-dynamic Drag: Practical Information on Aerodynamic Drag and Hydrodynamic Resistance*. Albuquerque, N.M.: Dr. Hoerner Fluid Dynamics, 1965. Print.
- Laskos, Dimitrios. "Design and Cavitation Performance of Contra-Rotating Propellers." *DSpace@MIT* 1 (2010): n. pag. *DSpace@Mit*. Internet. 3 Sept. 2013.
- Munson, Young & Okiishi, "Fundamentals of Fluid Mechanics," Wiley, 1998. Print.
- Sykes, Joshua et al. "Use of Computational Fluid Dynamics to Model Free-Surface Effects on Hydrofoil Systems." *Proceedings of the 13th International Conference on Fast Sea Transportation, Washington, D.C., September 2015*. In progress.
- Vellinga, Ray. *Hydrofoils: Design, Build, Fly*. Gig Harbor, Wash.: Peacock Hill Pub., 2009. Print.

## VII. APPENDICES

Appendix A - Solar Splash Batteries .....	22
Appendix B - Solar Splash Insurance .....	26
Appendix C- Solar Splash Buoyancy .....	27
Appendix D- Solar Splash Team Roster .....	29
Appendix E – Power and Weight Budgets .....	30
Appendix F – Circuit Diagrams .....	33
Appendix G - Description of AVL .....	40
Appendix H –Full Hydrofoil Drag Program .....	44
Appendix I - Hydrofoil Design Analysis .....	50
Appendix J - Ohio Supercomputer Input Files .....	53
Appendix K – Boundary Layer Mesh Procedure .....	55
Appendix L – SolidWorks Model of Foil and Mold .....	60
Appendix M - Moth Foil Results .....	63
Appendix N – Raw Free-Surface Study Data .....	66
Appendix O - 2015 Endurance Motor Design .....	68
Appendix P – Contra-Rotating Gear Box Design .....	75
Appendix Q - Instructions, Sample Inputs, and Outputs from Iterative CRP Version of OpenProp .....	77
Appendix R – CRP Design Process .....	95
Appendix S - 12 V Endurance Motor Testing and Evaluation .....	98
Appendix T – Team Member Task Gantt Charts .....	104

### Appendix A - Solar Splash Batteries

This year we will be utilizing one of each battery pack that has been used in the past. A set of three Genesis 42EP batteries weighting 32.9 lb (14.9 kg) each giving us a total weight of 98.34 lb (44.7 kg) for the first set. The second set we will use the Genesis 13EP batteries, each weighing 10.8 lb (4.9 kg); we will use 9 of these for the second set of batteries for a total weight of 97.2 lb (44.1 kg). This is in compliance with the new Solar Splash rule 7.4.1 having both of the battery sets under the 100 lb (45.5kg) limit.

The specification and MSDS sheets for these two types of batteries, which were selected from the available batteries provided by Genesis as shown in Figure A.1, are on the following pages in Figure A.2.

#### GENESIS PRODUCT FAMILY (All capacities at 10 hr. rate 25°C to 1.67 vpc)

##### GENESIS EP:

Product (capacity)	Part Number	Internal res. of fully charged battery mΩ @ 25°C	Nominal short circuit current for charged battery	DIMENSIONS				
				Length in. (mm)	Width in. (mm)	Height in. (mm)	Weight lb. (kg)	Brass Terminal (metric)
G13EP (13Ah)	0770-2007	8.5	1,400A	6.910 (175.51)	3.282 (83.36)	5.113 (129.87)	10.8 (4.9)	M6 w/SS hardware
G13EPX (13Ah)	0770-2003	8.5	1,400A	6.998 (177.75)	3.368 (85.55)	5.165 (131.19)	12.0 (5.4)	M6 w/SS hardware
G16EP (16Ah)	0769-2007	7.5	1,600A	7.150 (181.61)	3.005 (76.33)	6.605 (167.77)	13.5 (6.1)	M6 w/SS hardware
G16EPX (16Ah)	0769-2003	7.5	1,600A	7.267 (184.58)	3.107 (78.92)	6.666 (169.32)	14.7 (6.7)	M6 w/SS hardware
G26EP (26Ah)	0765-2001	5.0	2,400A	6.565 (166.75)	6.920 (175.77)	4.957 (125.91)	22.3 (10.1)	M6 w/SS hardware
G26EPX (26Ah)	0765-2003	5.0	2,400A	6.636 (168.55)	7.049 (179.04)	5.040 (128.02)	23.8 (10.8)	M6 w/SS hardware
G42EP (42Ah)	0766-2001	4.5	2,600A	7.775 (197.49)	6.525 (165.74)	6.715 (170.56)	32.9 (14.9)	M6 w/SS hardware
G42EPX (42Ah)	0766-2003	4.5	2,600A	7.866 (199.80)	6.659 (169.14)	6.803 (172.80)	35.1 (15.9)	M6 w/SS hardware
G70EP (70Ah)	0771-2001	3.5	3,500A	13.020 (330.71)	6.620 (168.15)	6.930 (176.02)	53.5 (24.3)	M6 w/SS hardware
G70EPX (70Ah)	0771-2003	3.5	3,500A	13.020 (330.71)	6.620 (168.15)	6.930 (176.02)	56.0 (25.4)	M6 w/SS hardware

Figure A.1. Genesis 13EP and Genesis 42EP battery specifications

**Section I - Product and Manufacturer Identity**

Product Identity:

Sealed Lead Battery

Cyclon®, Genesis®, SBS, SBS J, Hawker XE™ Odyssey® or Trolling Thunder™

Manufacturer's Name and Address:

EnerSys Energy Products Inc. (formerly Hawker Energy Products Inc.)

617 North Ridgeview Drive

Warrensburg, MO 64093-9301

Emergency Telephone Number: (660) 429-2165

Customer Service Telephone Number: 800-964-2837

**Section II – Ingredients**

Hazardous Components	CAS #	OSHA PEL-TWA	% (By weight)
Lead	7439-92-1	50µg/m <sup>3</sup>	45 - 60 %
Lead Dioxide	1309-60-0	50µg/m <sup>3</sup>	15 - 25 %
Sulfuric Acid Electrolyte	7664-93-9	1.0 mg/m <sup>3</sup>	15 - 20 %
Non-Hazardous Materials	N/A	N/A	5 - 10 %

**Section III - Physical/Chemical Characteristics**

Boiling Point - N/A

Specific Gravity (H<sub>2</sub>O=1) - NA

Vapor Pressure (mm Hg.) - N/A

Melting Point - N/A

Solubility in Water - N/A

Appearance &amp; Color - N/A

**Section IV - Fire & Explosion Hazard Data****Flash Point (Method Used):** N/A**Flammable Limits:** N/A**LEL:** N/A**UEL:** N/A**Extinguishing Media:**Multipurpose Dry chemical, CO<sub>2</sub> or water spray.**Special Fire Fighting Procedures:**

Cool Battery exterior to prevent rupture. Acid mists and vapors in a fire are toxic and corrosive. Unusual Fire and Explosion Hazards: Hydrogen gas may be produced and may explode if ignited. Remove all sources of ignition.

**Section V - Reactivity Data and Shipping/Handling Electrical Safety**

Conditions to Avoid: Avoid shorting, high levels of short circuit current can be developed across the battery terminals. Do not rest tools or cables on the battery. Avoid over-charging. Use only approved charging methods. Do not charge in gas tight containers.

Requirements for Safe Shipping and Handling of Cyclon® Cells: Warning – Electrical Fire Hazard – Protect Against Shorting

- Terminals can short and cause a fire if not insulated during shipping.

Figure A.2. Enersys and Odyssey MSDS Sheets (1 of 3)



- Cyclon® product must be labeled "NONSPILLABLE" during shipping. Follow all federal shipping regulations. See section IX of this sheet and CFR 49 Parts 171 through 180, available anytime online at [www.gpoaccess.gov](http://www.gpoaccess.gov).

#### Requirements for Shipping Cyclon® Product as Single Cells

- Protective caps or other durable inert material must be used to insulate each terminal of each cell unless cells are shipping in the original packaging from EnerSys, in full box quantities.
- Protective caps are available for all cell sizes by contacting EnerSys Customer Service at 1-800-964-2837.

#### Requirements for Shipping Cyclon® Product Assembled Into Multicell Batteries

- Assembled batteries must have short circuit protection during shipping.
- Exposed terminals, connectors, or lead wires must be insulated with a durable inert material to prevent exposure during shipping.

### Section VI - Health Hazard Data

**Routes of Entry:** N/A

**Health Hazards (Acute & Chronic):** N/A

#### Emergency & First Aid Procedures:

Battery contains acid electrolyte which is absorbed in the separator material. If battery case is punctured, completely flush any released material from skin or eyes with water.

#### Proposition 65:

Warning: Battery posts, terminals and related accessories contain lead and lead compounds, chemicals known to the State of California to cause cancer and reproductive harm. Batteries also contain other chemicals known to the State of California to cause cancer. Wash hands after handling.

### Section VII - Product and Manufacturer Identity

#### Steps to be taken in case material is released or spilled:

Avoid contact with acid materials. Use soda ash or lime to neutralize. Flush with water.

#### Waste Disposal Method:

Dispose of in accordance with Federal, State, & Local Regulations. Do not incinerate. Batteries should be shipped to a reclamation facility for recovery of the metal and plastic components as the proper method of waste management. Contact distributor for appropriate product return procedures.

### Section VIII - Control Measures - Not Applicable

### Section IX - Transportation, Shipping and Handling

EnerSys Energy Products Inc. batteries are starved electrolyte batteries which means the electrolyte is absorbed in the separator material. The batteries are also sealed. As of September 30, 1995, EnerSys Energy Products Inc. batteries were classified as "nonspillable batteries", and as such are not subject to the full requirements of 49 CFR § 173.159. The previous exempt classification, "Dry Batteries, Not Restricted" was discontinued effective September 30, 1995. "Nonspillable" batteries are excepted from the regulation's

Figure A.2 (cont.). EnerSys and Odyssey MSDS Sheets (2 of 3)

comprehensive packaging requirements if the following conditions are satisfied: (1) The battery is protected against short circuits and is securely packaged. (2) For batteries manufactured after September 30, 1995, the battery and outer packaging must be plainly and durably marked "NONSPILLABLE" or "NONSPILLABLE BATTERY". (3) The battery is capable of withstanding vibration and pressure differential tests specified in 49 CFR § 173.159(d). (4) At a temperature of 55 °C (131°F), the battery must not contain any unabsorbed free-flowing liquids, and is designed so that electrolyte will not flow from a ruptured or cracked case.

EnerSys Energy Products Inc. batteries have been tested by WYLE Scientific Services & Systems Laboratories Group and determined to be in compliance with the vibration and pressure differential tests contained in 49 CFR § 173.159(d), and therefore as of September 30, 1995, excepted from the DOT requirements set forth in 49 CFR § 173.159, other than paragraph (d).

Battery shipments from EnerSys Energy Products Inc. Warrensburg location, will be properly labeled in accordance with applicable DOT regulations.

**Packaging changes performed at other locations may require additional labeling, since in addition to the battery itself containing the required marking, the outer packaging of the battery must also contain the required marking: "NONSPILLABLE" OR "NONSPILLABLE BATTERY".** Because the batteries are classified as "Nonspillable" and meet the three conditions above, [from § 173.159(d)] they do not have an assigned UN number nor do they require additional DOT hazard labeling.

The regulation change effective September, 1995, was to clarify and distinguish to shippers and transporters, all batteries that have been tested and determined to be in compliance with the DOT Hazardous Material Regulations, the International Civil Aeronautics Organization (ICAO), and the International Air Transport Association (IATA) Packing Instruction 806 and Special Provision A67, and therefore excepted from all other requirements of the regulations and classified as a "nonspillable battery".

Per 42 USC Section 14322 (US Code Title 42 – The Public Health and Welfare), packaging must be marked with the following: "Contains Sealed Lead Battery" and "Battery Must Be Recycled".

### **Section X - Additional Information**

The EnerSys Energy Products Inc. sealed lead acid battery is determined to be an "article" according to the OSHA Hazard Communication Standard and is thereby excluded from any requirements of the standard. The Material Safety Data Sheet is therefore supplied for informational purposes only.

The information and recommendations contained herein have been compiled from sources believed to be reliable and represent current opinion on the subject. No warranty, guarantee, or representation is made by EnerSys Energy Products Inc., as to the absolute correctness or sufficiency of any representation contained herein and EnerSys Energy Products Inc. assumes no responsibility in connection therewith, nor can it be assumed that all acceptable safety measures are contained herein, or that additional measures may not be required under particular or exceptional conditions or circumstances.

N/A or Not Applicable - Not applicable for finished product used in normal conditions.  
Informational MSDS Part Number 2602-0043 Rev. 2 (09/07/06)

**Figure A.2 (cont.).** EnerSys and Odyssey MSDS Sheets (3 of 3)



**Appendix B - Solar Splash Insurance**

		CEDAR-3      OP ID: CW DATE (MM/DD/YYYY) 04/17/2015	
CERTIFICATE OF LIABILITY INSURANCE			
THIS CERTIFICATE IS ISSUED AS A MATTER OF INFORMATION ONLY AND CONFERS NO RIGHTS UPON THE CERTIFICATE HOLDER. THIS CERTIFICATE DOES NOT AFFIRMATIVELY OR NEGATIVELY AMEND, EXTEND OR ALTER THE COVERAGE AFFORDED BY THE POLICIES BELOW. THIS CERTIFICATE OF INSURANCE DOES NOT CONSTITUTE A CONTRACT BETWEEN THE ISSUING INSURER(S), AUTHORIZED REPRESENTATIVE OR PRODUCER, AND THE CERTIFICATE HOLDER.			
IMPORTANT: If the certificate holder is an ADDITIONAL INSURED, the policy(ies) must be endorsed. If SUBROGATION IS WAIVED, subject to the terms and conditions of the policy, certain policies may require an endorsement. A statement on this certificate does not confer rights to the certificate holder in lieu of such endorsement(s).			
PRODUCER Wallace & Turner, Inc. P. O. Box 209 30 Warder Street #200 Springfield, OH 45501-0209 Patrick E. Field		CONTACT NAME: PHONE (A/C, No, Ext):      FAX (A/C, No): E-MAIL: ADDRESS:  INSURER(S) AFFORDING COVERAGE      NAIC # INSURER A: Cincinnati Insurance Company      10677 INSURER B: INSURER C: INSURER D: INSURER E: INSURER F:	
INSURED Cedarville University 251 North Main Street Cedarville, OH 45314			
COVERAGES      CERTIFICATE NUMBER:      REVISION NUMBER:			
THIS IS TO CERTIFY THAT THE POLICIES OF INSURANCE LISTED BELOW HAVE BEEN ISSUED TO THE INSURED NAMED ABOVE FOR THE POLICY PERIOD INDICATED. NOTWITHSTANDING ANY REQUIREMENT, TERM OR CONDITION OF ANY CONTRACT OR OTHER DOCUMENT WITH RESPECT TO WHICH THIS CERTIFICATE MAY BE ISSUED OR MAY PERTAIN, THE INSURANCE AFFORDED BY THE POLICIES DESCRIBED HEREIN IS SUBJECT TO ALL THE TERMS, EXCLUSIONS AND CONDITIONS OF SUCH POLICIES. LIMITS SHOWN MAY HAVE BEEN REDUCED BY PAID CLAIMS.			
INSUR LTR	TYPE OF INSURANCE	ADDL SUBR INSR WVD	POLICY NUMBER
POLICY EFF (MM/DD/YYYY)	POLICY EXP (MM/DD/YYYY)	LIMITS	
A <input checked="" type="checkbox"/> GENERAL LIABILITY <input checked="" type="checkbox"/> COMMERCIAL GENERAL LIABILITY <input type="checkbox"/> CLAIMS-MADE <input checked="" type="checkbox"/> OCCUR <input checked="" type="checkbox"/> Empl Liab Defense GEN'L AGGREGATE LIMIT APPLIES PER: <input type="checkbox"/> POLICY <input type="checkbox"/> PRO-JECT <input type="checkbox"/> LOC	SIP0003158 07/01/2013    07/01/2016	EACH OCCURRENCE \$ 1,000,000 DAMAGE TO RENTED PREMISES (Ea occurrence) \$ 500,000 MED EXP (Any one person) \$ 10,000 PERSONAL & ADV INJURY \$ 1,000,000 GENERAL AGGREGATE \$ 3,000,000 PRODUCTS - COMP/OP AGG \$ 3,000,000	
A <input checked="" type="checkbox"/> ANY AUTO <input type="checkbox"/> ALL OWNED AUTOS <input checked="" type="checkbox"/> HIRED AUTOS <input type="checkbox"/> SCHEDULED AUTOS <input checked="" type="checkbox"/> NON-OWNED AUTOS	SIP0003158 07/01/2013    07/01/2016	COMBINED SINGLE LIMIT (Ea accident) \$ 1,000,000 BODILY INJURY (Per person) \$ BODILY INJURY (Per accident) \$ PROPERTY DAMAGE (PER ACCIDENT) \$	
A <input checked="" type="checkbox"/> UMBRELLA LIAB <input type="checkbox"/> EXCESS LIAB <input checked="" type="checkbox"/> OCCUR <input type="checkbox"/> CLAIMS-MADE DED. <input checked="" type="checkbox"/> RETENTION \$ 0	SIP0003158 07/01/2013    07/01/2016	EACH OCCURRENCE \$ 15,000,000 AGGREGATE \$ 15,000,000	
A WORKERS COMPENSATION AND EMPLOYERS' LIABILITY ANY PROPRIETOR/PARTNER/EXECUTIVE OFFICER/MEMBER EXCLUDED? (Mandatory in NH) If yes, describe under DESCRIPTION OF OPERATIONS below	Y/N N/A SIP0003158 07/01/2013    07/01/2016	WC STATUTORY LIMITS    OTHER E.L. EACH ACCIDENT \$ 500,000 E.L. DISEASE - EA EMPLOYEE \$ 500,000 E.L. DISEASE - POLICY LIMIT \$ 500,000	
DESCRIPTION OF OPERATIONS / LOCATIONS / VEHICLES (Attach ACORD 101, Additional Remarks Schedule, if more space is required)			
Event: Solar Splash 2015 held June 10-14th, 2015 at Venue Eastwood Metro Park, Dayton, Ohio			
CERTIFICATE HOLDER		CANCELLATION	
ASMECOM  SOLAR SPLASH c/o Jeffrey H. Morehouse PhD PE Mechanical Engineering Dept University of South Carolina Columbia, SC 29208		SHOULD ANY OF THE ABOVE DESCRIBED POLICIES BE CANCELLED BEFORE THE EXPIRATION DATE THEREOF, NOTICE WILL BE DELIVERED IN ACCORDANCE WITH THE POLICY PROVISIONS.  AUTHORIZED REPRESENTATIVE Patrick E. Field	

© 1988-2010 ACORD CORPORATION. All rights reserved.

ACORD 25 (2010/05)

The ACORD name and logo are registered marks of ACORD

**Figure B.1.** Cedarville University Solar Splash 2015 Certificate of Insurance

### **Appendix C- Solar Splash Buoyancy**

The surface area of the new hull which utilizes 1 layer of 1.25 inch of Nomex honeycomb is 65.0 ft<sup>2</sup> and the surface area which utilizes 2 layers of 0.472 inches of Nomex honeycomb is 7.1 ft<sup>2</sup>. Thus, the buoyant force provided by the hull alone, neglecting the Kevlar skins is given by the following Equation C.1.

$$\begin{aligned}
 B_H &= (\sum_{i=1}^n A_i t_i) \rho_{water} & (C.1) \\
 &= \left( 65.0 \text{ ft}^2 * 1.25 \text{ in} * \frac{\text{ft}}{12 \text{ in}} + 7.1 \text{ ft}^2 * 2 * 0.472 \text{ in} * \frac{\text{ft}}{12 \text{ in}} \right) \frac{62.4 \text{ lb}}{\text{ft}^3} \\
 &= 468 \text{ lb}
 \end{aligned}$$

Where  $B_H$  is the buoyant force on the hull when submerged,  $A_i$  is the surface area covered by a given core thickness,  $t_i$  is thickness of the core in a given region, and  $\rho_{water}$  is the density of water. Because the batteries are secured to the hull, their buoyant force also contributes the overall buoyant force on the boat (Equation C.2). The volume of 3, 42 EP batteries is less than that of 12, 13 EP batteries, and will therefore be used for our calculations.

$$\begin{aligned}
 B_B &= 3V_{42EP} \rho_{water} & (C.2) \\
 &= 3 * 0.175 \text{ ft}^3 * 62.4 \frac{\text{lb}}{\text{ft}^3} \\
 &= 33 \text{ lb}
 \end{aligned}$$

Where  $B_B$  is the buoyant force of the batteries and  $V_{42EP}$  is the volume of the Genesis 42EP batteries. Therefore, the maximum possible buoyant force exerted on the hull is given by the following Equation C.3.

$$\begin{aligned}
 B_{tot} &= B_H + B_B & (C.3) \\
 &= 468 \text{ lb} + 33 \text{ lb} \\
 &= 501 \text{ lb}
 \end{aligned}$$

Also, the weight of the hull, as given by the power budget is shown in Table C.1. Based on our calculations, our hull can easily support its own weight plus a small safety factor as the buoyant force of 501 lb is greater than the required buoyant force of 491 lb.



**Table C.1.** *Weight Budget for 2015 Solar Splash Boat*

Components	Weight [lb]	
	2014 Sprint	2014 Endurance
Solar Array	N/A	42
Batteries	137	137
Sprint Drivetrain & Controllers	107	107
Endurance Drivetrain	34	34
Hull	70	70
MPPT	N/A	4
Control Panel	5	5
Miscellaneous	10	10
<b>Total</b>	<b>363</b>	<b>409</b>
<b>120% Total (Rule 7.14.2)</b>	<b>436</b>	<b>491</b>

**Appendix D- Solar Splash Team Roster**

<b>Name</b>	<b>Degree Program</b>	<b>Year</b>	<b>Role</b>
Katelynne Burrell	BSME	Senior	Hydrofoil Design with AVL
Jacob Dubie	BSEE	Senior	Battery and Energy Management
Jeremy Dumont	BSME	Senior	Sprint Motor Drivetrain
Peter Larson	BSME	Senior	Endurance Motor Drivetrain
Tieg Laskowske	BSME	Senior	Contra-Rotating Propellers
Alex Rheume	BSME	Senior	Contra-Rotating Gear Box
Josh Sykes	BSME	Senior	Computational Fluid Dynamics
Jay White	BSEE	Senior	Data Acquisition Systems
Brian Wolf	BSME	Senior	Hydrofoil Manufacturing and Flight Control

## Appendix E – Power and Weight Budgets

Table E.1. 2015 Power budget for the Solar Splash Endurance event

Variable Name	Variable	Value	Unit (metric)	Value	Unit (US)	Comments	Governing Equation
<b>SOLAR PANELS</b>							
PV Power Gain	PV_Pgain	360	W			Assuming avg of 75% of one sun condition max (Insolation data for Dayton OH in June)	$PV\_Pgain = 480W * (\% \text{ of one sun conditions})$
PV Voltage	PV_V	16	V				
PV Current	PV_I	22.5	A				$PV\_I = PV\_Pgain / PV\_V$
PV Output Power	PV_Pout	360	W				$PV\_Pout = PV\_Pgain$
<b>PEAK POWER TRACKER</b>							
MPPT Efficiency	MPPT_e	0.94				Assuming 94% efficiency	
MPPT Current	MPPT_I	28.2	A			Assuming current stays same from panels to PPT	$MPPT\_I = MPPT\_Pout / MPPT\_V$
MPPT Voltage	MPPT_V	12	V				$MPPT\_V = Batt\_V$
MPPT Power Gain	MPPT_Pgain	-21.6	W				$MPPT\_Pgain = MPPT\_Pout - PV\_Pout$
MPPT Output Power	MPPT_Pout	338.4	W				$MPPT\_Pout = MPPT\_e * PV\_Pout$
<b>BATTERIES</b>							
Battery Voltage	Batt_V	12	V			Three 12 V Endurance batteries in series	
Battery Current	Batt_I	54	A			Based on available amp-hours in 2 hour race	
Battery Power Gain	Batt_Pgain	648	W				$Batt\_Pgain = Batt\_Pout$
Battery Output Power	Batt_Pout	648	W				$Batt\_Pout = Batt\_V * Batt\_I$
<b>MOTOR CONTROLLER</b>							
Controls Efficiency	C_e	0.95				Assuming 95% efficiency	
Controls Voltage	C_V	12.0	V				$C\_V = Batt\_V$
Controls Current	C_I	82.2	A				$C\_I = MPPT\_I + Batt\_I$
Controls Power Gain	C_Pgain	-49.32	W				$C\_Pgain = (Batt\_Pout + MPPT\_Pout) + C\_Pout$
Controls Output Power	C_Pout	937.08	W				$C\_Pout = (Batt\_Pout + MPPT\_Pout) * C\_e$
<b>MOTOR</b>							
Motor Efficiency	M_e	0.93				Assuming 93% efficiency	
Motor Torque	M_T	2.8	N*m	2.0460129	lbs*ft		$M\_T = M\_Pout / M\_omega$
Motor Angular Velocity	M_omega	314.2	rad/s	3000	RPM	Motor designed most efficient at 4000 RPM	$M\_n = GR * GB\_n$
Motor Power Gain	M_Pgain	-66	W				$M\_Pgain = M\_Pout - C\_Pout$
Motor Output Power	M_Pout	871	W				$M\_Pout = Cont\_Pout * Mot\_e$
<b>GEAR BOX</b>							
Gear Box Efficiency	GB_e	0.93				Assuming 93% efficiency	
Gear Ratio	GR	9				Gear box designed with 5:1 gear ratio	
Gear Box Torque	GB_T	23.2	N*m	17.125128	lbs*ft		$GB\_T = GB\_Pout / GB\_omega$
Gear Box Torque per CRP	GB_T_i	11.6	N*m	8.562564	lbs*ft		$GB\_T\_i = GB\_T / 2$
Gear Box Angular Velocity	GB_omega	34.9	rad/s	333.33333	RPM	Due to gear ratio	
Gear Box Power Gain	GB_Pgain	-61	W				$GB\_Pgain = GB\_Pout - Mot\_Pout$
Gear Box Power Output	GB_Pout	810	W				$GB\_Pout = M\_Pout * GB\_e$
<b>PROP</b>							
Prop Efficiency	Prop_e	0.85				Assuming 85% efficiency	
Prop Thrust	P_Thrust	171	N	38.5	lb		$P\_Thrust = Prop\_Pout / (P\_v * (1000/3600))$
Prop Thrust front CRP	P_Thrust_i	86	N	18.3	lb	Approximate. Rear prop will have higher thrust.	
Prop Velocity	P_v	14.5	km/hr	9	MPH	Desired goal speed	
Prop Power Gain	Prop_Pgain	-122	W				$Prop\_Pgain = Prop\_Pout - GB\_Pout$
Prop Output Power	Prop_Pout	689	W				$Prop\_Pout = GB\_Pout * Prop\_e$
<b>HULL</b>							
Hull Drag	H_Drag	171	N	38.493488	lb		
Hull Velocity	H_v	14	km/hr	9	MPH		$P\_Thrust = Prop\_Pout / (P\_v * (1000/3600))$
Hull Power Gain	Hull_Pgain	-689	W				
Hull Power Output	Hull_Pout	0	W				$Prop\_Pgain = Prop\_Pout - GB\_Pout$
<b>PROP</b>							
Prop Efficiency	Prop_e	0.85				Assuming 85% efficiency	
Prop Thrust	P_Thrust	128	N	28.870116	lb		$P\_Thrust = Prop\_Pout / (P\_v * (1000/3600))$
Prop Velocity	P_v	19.3	km/hr	12	MPH	Desired goal speed	
Prop Power Gain	Prop_Pgain	-122	W				$Prop\_Pgain = Prop\_Pout - GB\_Pout$
Prop Output Power	Prop_Pout	689	W				$Prop\_Pout = GB\_Pout * Prop\_e$
<b>HYDROFOIL</b>							
Hull Drag	H_Drag	128	N	28.870116	lb		
Hull Velocity	H_v	19.3	km/hr	12	MPH		$P\_Thrust = Prop\_Pout / (P\_v * (1000/3600))$
Hull Power Gain	Hull_Pgain	-689	W				
Hull Power Output	Hull_Pout	0	W				$Prop\_Pgain = Prop\_Pout - GB\_Pout$
Denotes Input Value	Efficiencies	Inputs	Output Power	Represents power in the system directly after the given component			
Total Distance		77.24832	km	48	mi	4 hours of runtime	

**Table E.2.** 2015 Power budget for the Solar Splash Sprint event

Variable Name	Variable	Value	Unit (metric)	Value	Unit (US)	Comments	Governing Equation
<b>BATTERIES</b>							
Battery Impedance	Batt_Z	0.008	$\Omega$				
Nominal Battery Voltage	Batt_N	36	V				
Battery Voltage under load	Batt_VFL	26	V			Sprint batteries	
Battery Current	Batt_I	1200	A			Design to draw power at this current	
Battery Power Gain	Batt_Pgain	31680	W				$Batt\_Pgain = Batt\_V * Batt\_I$
Battery Power Output	Batt_Pout	31680	W				$Batt\_Pout = Batt\_Pgain$
<b>CONTROLS</b>							
Controls Efficiency	C_e	0.95				Assuming 95% efficiency	
Controls Voltage	C_V	25.1	V				$C\_V = C\_Pout / C\_I$
Controls Current	C_I	1200	A			Assume current is the same as from batteries	$C\_I = Batt\_I$
Controls Power Gain	C_Pgain	-1584	W				$C\_Pgain = C\_Pout - Batt\_Pout$
Controls Power Output	C_Pout	30096	W				$C\_Pout = Batt\_Pout * C\_e$
<b>MOTOR</b>							
Motor Efficiency	M_e	0.92				per conversations w/ Neu Motors (12/03/13)	
Motor Torque	M_T	52.9	N*m	39	lbs*ft		$M\_T = M\_Pout / M\_w$
Motor Angular Velocity	M_w	524	rad/s	5000	RPM	design motor speed for 5000 at 26.4 V	
Motor Power Gain	M_Pgain	-2408	W				$M\_Pgain = M\_Pout - C\_Pout$
Motor Power Output	M_Pout	27688	W				$M\_Pout = C\_Pout * M\_e$
<b>LOWER GEAR UNIT</b>							
Drive Train Efficiency	DT_e	0.95				Assuming 95% efficiency	
Drive Train Torque	DT_T	50.2	N*m	37	lbs*ft		$DT\_T = Mot\_T$
Drive Train Angular Velocity	DT_omega	524	rad/s	5000	RPM		$DT\_w = DT\_Pout / DT\_T$
Drive Train Power Gain	DT_Pgain	-1384	W				$GP\_Pgain = DT\_Pout - Mot\_Pout$
Drive Train Power Output	DT_Pout	26304	W				$GB\_Pout = Mot\_Pout * DT\_e$
<b>PROP</b>							
Prop Efficiency	Prop_e	0.72				Assuming 72% efficiency	
Prop Thrust	P_Thrust	847	N	190	lb		$P\_Thrust = Prop\_Pout / (P\_v * (1000/3600))$
Max Prop Velocity	P_v	80.5	km/hr	50.0	MPH	Desired goal speed	
Total Run Time	T	20.0	s			Desired run time	
Average Prop Velocity	P_v_avg	54.0	km/hr	33.6	MPH	300 m run	$P\_v\_avg = (300\text{ m}) / (T * 3600 / 1000)$
Prop Power Gain	Prop_Pgain	-7365	W				$Prop\_Pgain = Prop\_Pout - DT\_Pout$
Prop Power Output	Prop_Pout	18939	W				$Prop\_Pout = DT\_Pout * Prop\_e$
<b>HULL</b>							
Hull Drag	H_Drag	847	N	190	lb		$H\_Thrust = P\_Thrust$
Hull Velocity	H_v	80.5	km/hr	50.0	MPH		$H\_v = P\_v$
Hull Power Gain	Hull_Pgain	-18939	W				$Hull\_Pgain = Hull\_Pout - Prop\_Pout$
Hull Power Output	Hull_Pout	0	W			All the power should be used	
Denotes input value	Efficiencies		Output Power	Represents power in the system directly after the given component			

**Table E.3.** Weight Budget for the 2015 Solar Splash Sprint event

<b>SOLAR SPLASH - Sprint</b>		
	<b>Weight [lb]</b>	<b>Mass [kg]</b>
Solar Array	N/A	N/A
Batteries	100.0	45.4
Battery Box	37.0	16.8
Sprint Drivetrain & Controllers	107.1	48.6
Endurance Drivetrain	34.1	15.5
Pod and Downleg	14.1	6.4
Motor	9.3	4.2
Cables	3.3	1.5
Gearbox	2.4	1.1
Propeller	5.0	2.3
Hull (with Bilge Pump, Steering and Motor Mount)	69.7	31.6
Driver	155.0	70.3
PPT	N/A	N/A
Control Panel	5.0	2.3
Hydrofoils	45.0	20.4
Miscellaneous	10.0	4.5
<b>Total</b>	<b>562.9</b>	<b>255.3</b>

**Table E.4.** Weight Budget for the 2015 Solar Splash Endurance event

<b>SOLAR SPLASH - Endurance</b>		
	<b>Weight [lb]</b>	<b>Mass [kg]</b>
Solar Array	40.6	18.4
Batteries	95.7	43.4
Battery Box	37.0	16.8
Sprint Drivetrain & Controllers	107.1	48.6
Endurance Drivetrain	34.1	15.5
Pod and Downleg	14.1	6.4
Motor	9.3	4.2
Cables	3.3	1.5
Gearbox	2.4	1.1
Propeller	5.0	2.3
Hull (with Bilge Pump, Steering and Motor Mount)	69.7	31.6
Driver	155.0	70.3
PPT	10.4	4.7
Control Panel	9.7	4.4
Hydrofoils	45.0	20.4
Miscellaneous	10.0	4.5
<b>Total</b>	<b>614.3</b>	<b>278.6</b>



## Appendix F – Circuit Diagrams

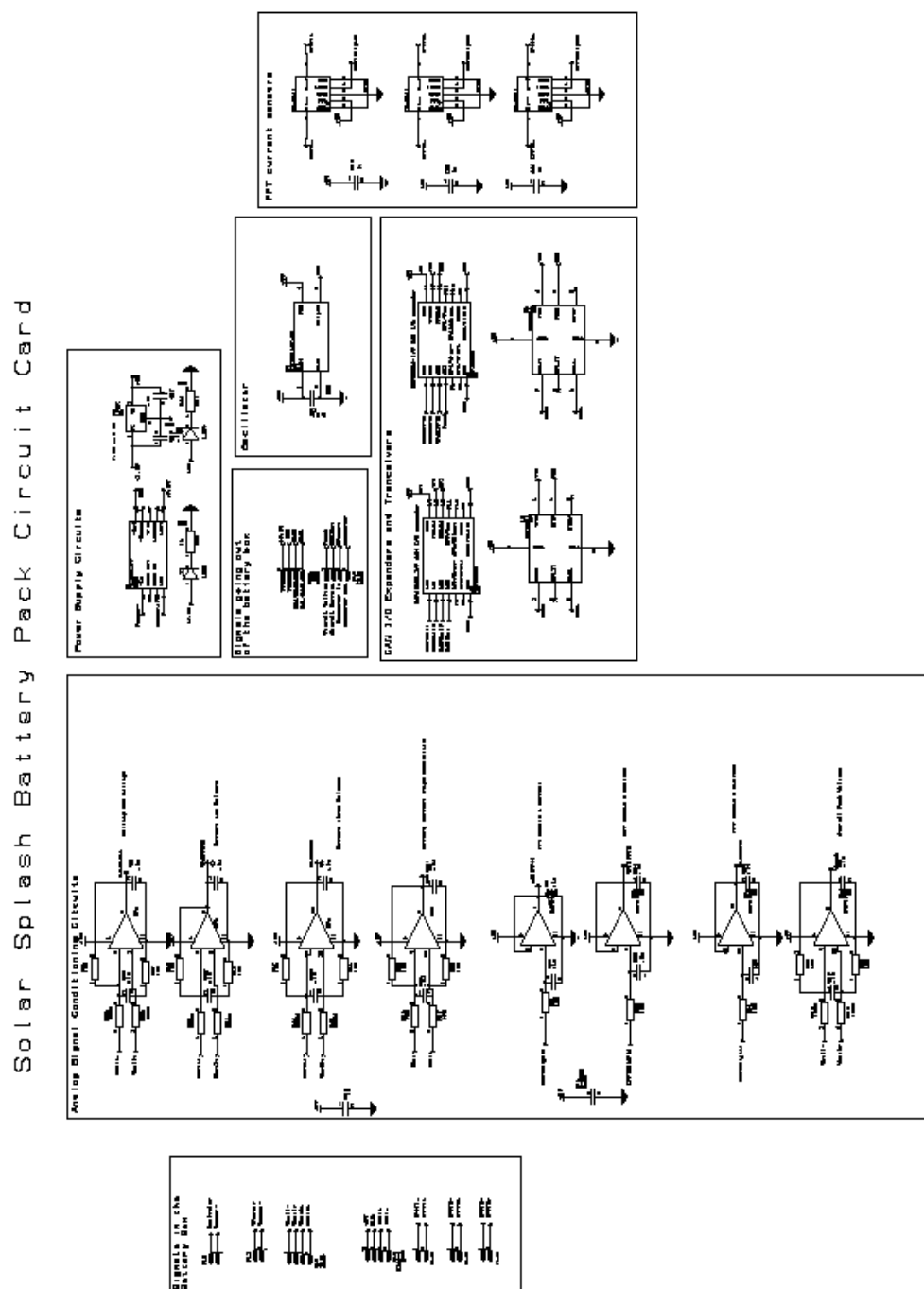


**Figure F.1.** Solar Splash Battery Monitoring Circuit Card Schematics from 2015. In the bottom block are Op-Amp gain circuits, in the top block are current controllers, and the middle right box has the CAN I/O expanders and the CAN transceivers

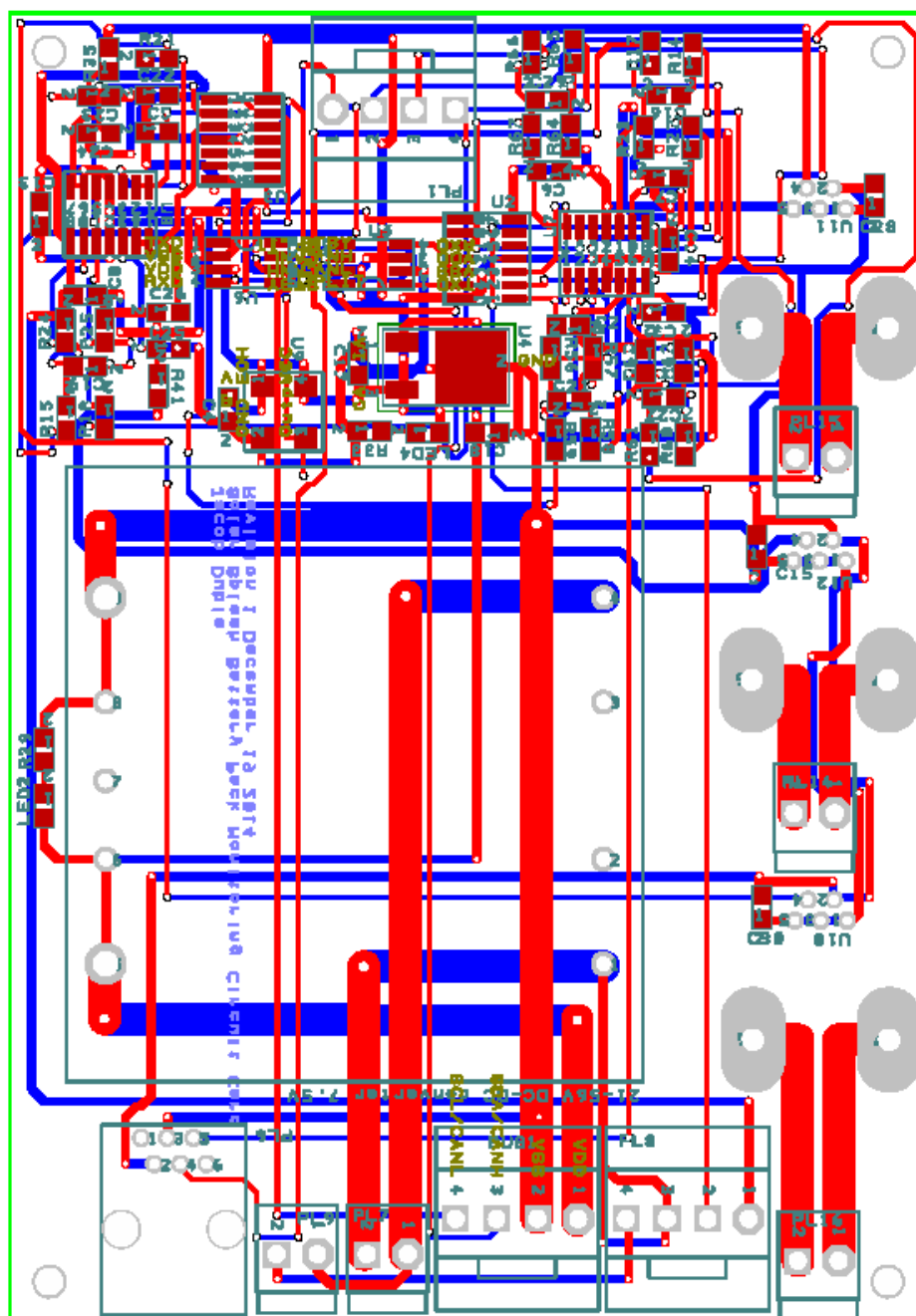


**Figure F.2.** Battery Monitoring Card Printed Circuit Board schematic; the top circuitry are the signal conditioning circuits; the large component in the center is the Vicor power supply and the right hand devices are the current sensors

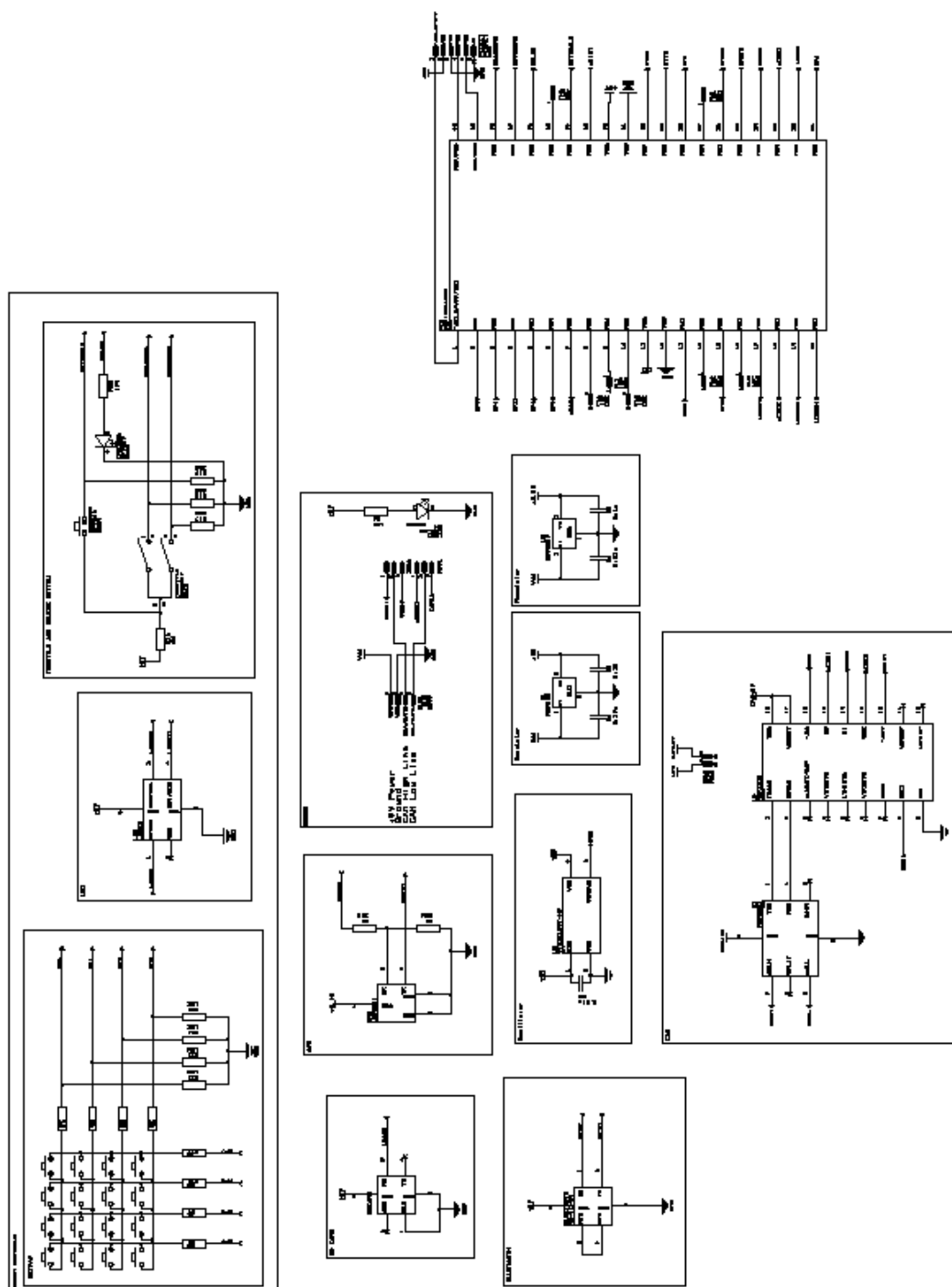


**Figure F.3.** Control panel schematic; starting clockwise and spiraling in: the encoder for throttle control, the PIC18F46k22 micro controller, the CAN controller, Bluetooth, SD card reader, keypad, and GPS

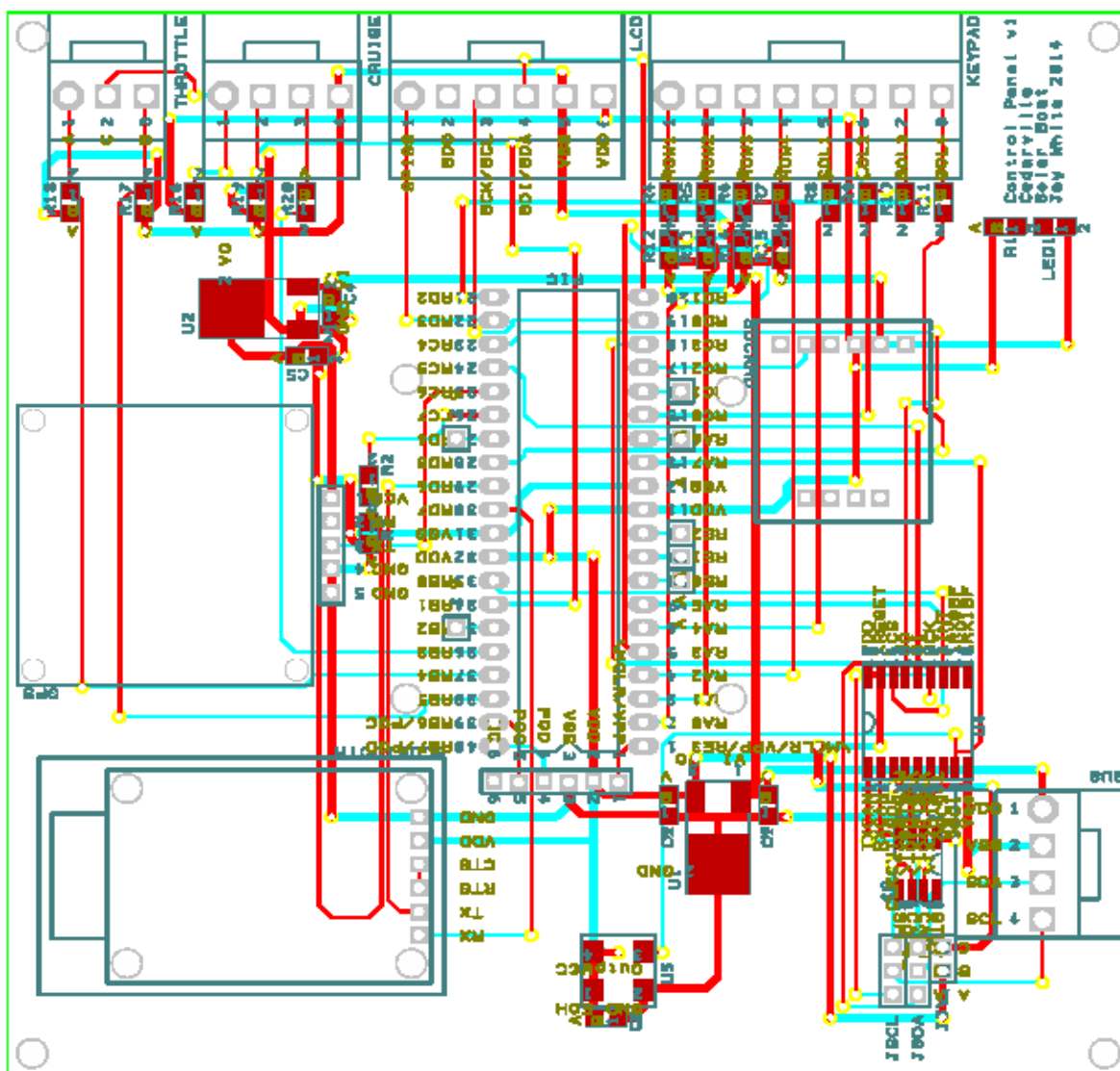


**Figure F.4.** Printed circuit board schematic for the control panel; refer to Figure T.3 for details of the design

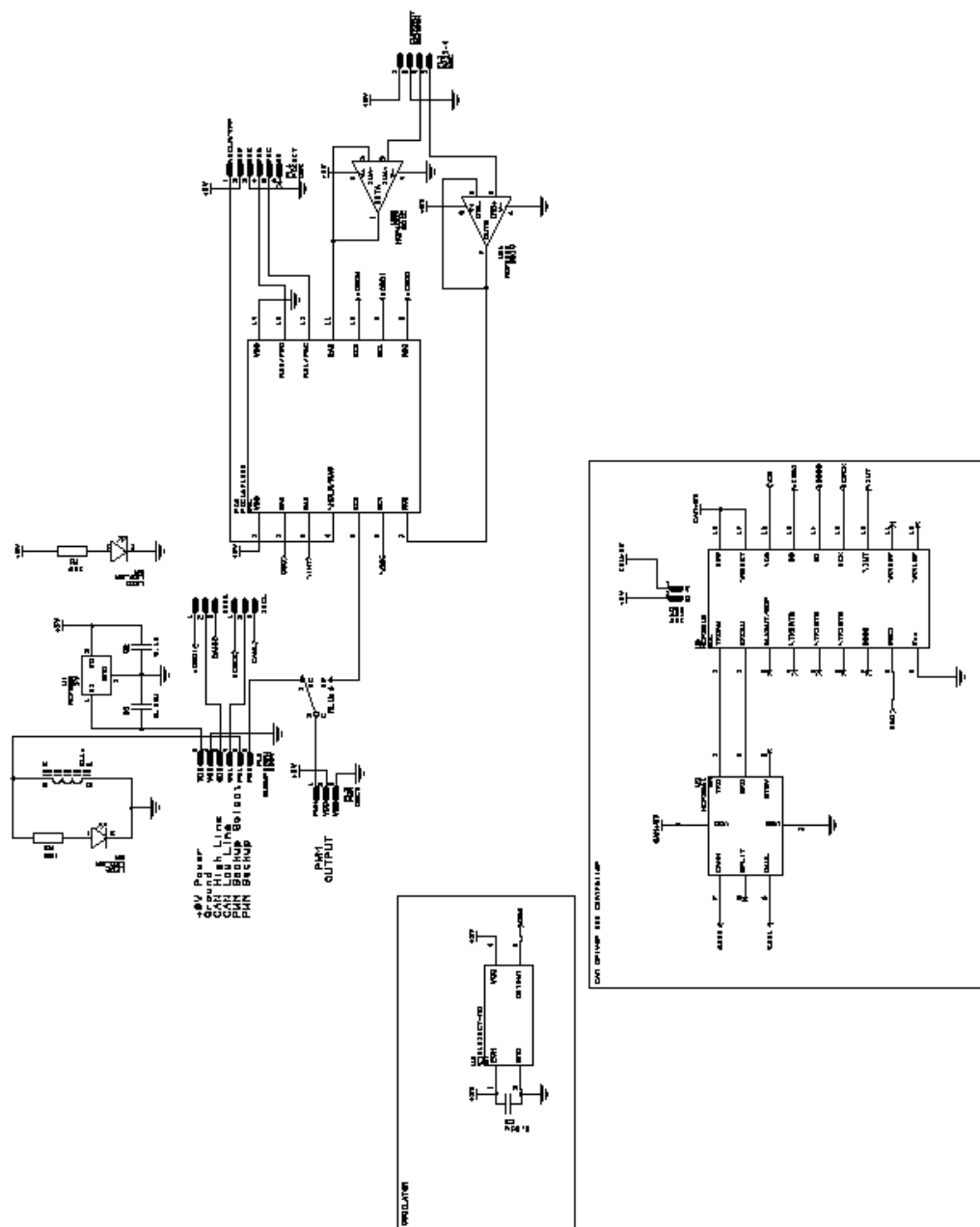


**Figure F.5.** Schematic of the Motor Control Card; starting clockwise on the top: PIC16F1825, CAN controller and transceiver, and PWM select relay and voltage regulator



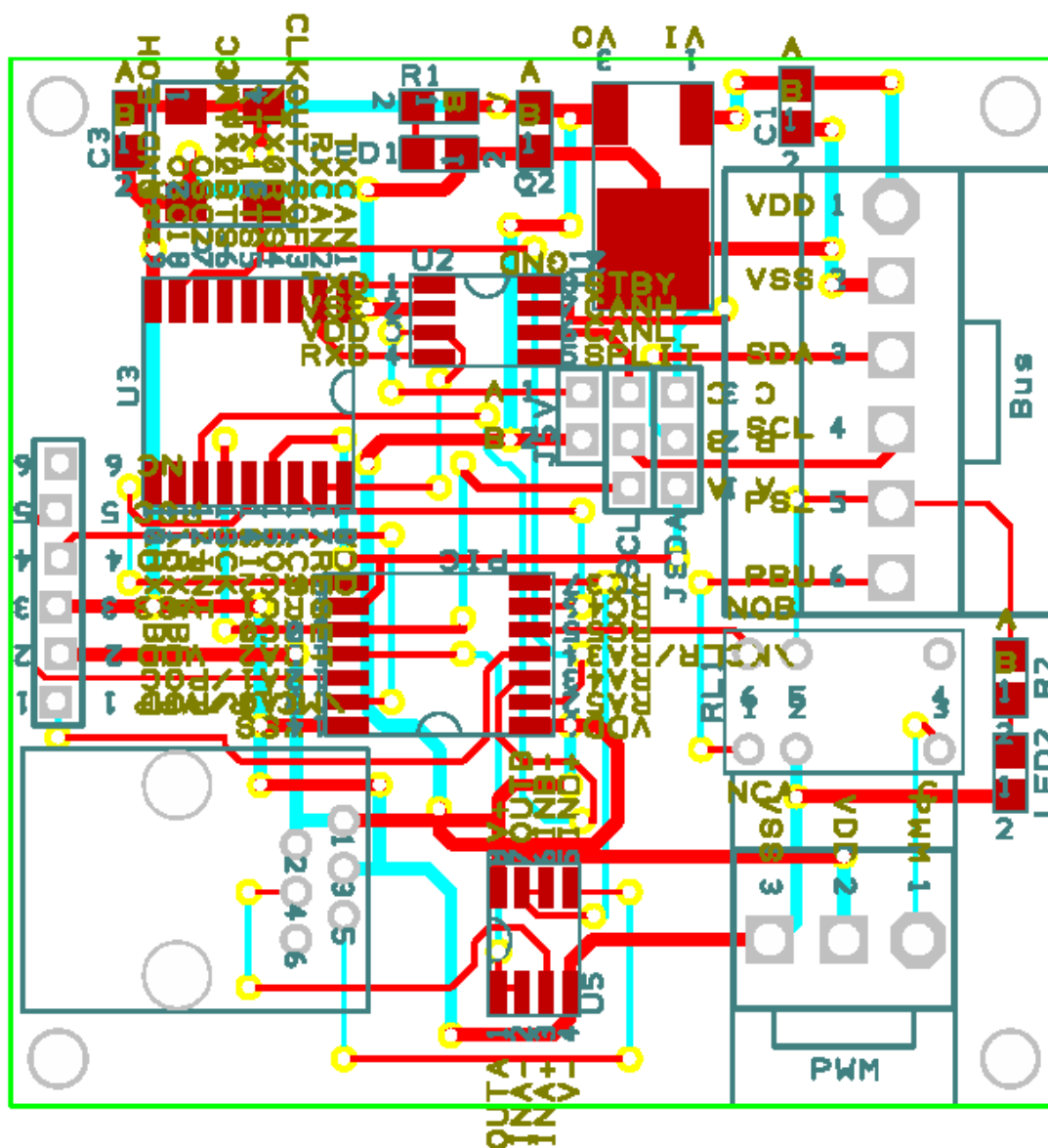


**Figure F.6.** Printed circuit board schematic for the Motor Control Card; refer to Figure T.5 for design details

The circuit's functionality is described below:

- Assume that the batteries are in 12V mode. If the 24V push-button is held closed for at least 100 ms, switches 1 and 2 open instantly.
- After approximately 40 ms the signal relay drive reaches its threshold and closes switch 3: the system is now in 24V mode.
- In between 12V and 24V modes the system enters a “switching mode” where all relays are open and the diodes are conducting. This mode, along with the 300-500 Amps fuse in series with switch 3, allows us to drive the boat in any configuration. This mode is inefficient but allows the battery box to be operated continuously.
- If the 24V mode push-button is pressed again a pulse will be sent to open switches 1 and 2. Later, another will be sent to close switch 3. However, since all of the relays are already in those states, no relays are physically actuated. Operation is therefore not interrupted.
- Pressing the 12V mode push-button from this state opens switch 3 and enters the switching mode again. After another 40ms the signal relays drive the closing coils for switches 1 and 2; the system is once again in 12V mode.

If the 12V button is pressed again the same result occurs as in 24V mode and operation is not interrupted

**Appendix G - Description of AVL**

Athena Vortex Lattice (AVL) is a program that models the induced lift and drag on objects in fluid flow. The program uses lifting line theory to calculate the coefficient of lift on the object modeled. It is only useful for non-symmetrical bodies, as a symmetrical body is treated as a flat plate parallel to flow and there is no resulting lift due to the zero camber. However foil profile shapes can be modeled in AVL and the induced drag and lift components can be obtained for a specific geometry. Using AVL requires external calculations to find the total drag on the system. This was implemented by using a Mat Lab program shown in Appendix H –Additional Hydrofoil Analysis Program. The main file we developed to run AVL for this project is the “.avl” file which contains the system geometry. Figure G.1 outlines the general format for creating a model in AVL.

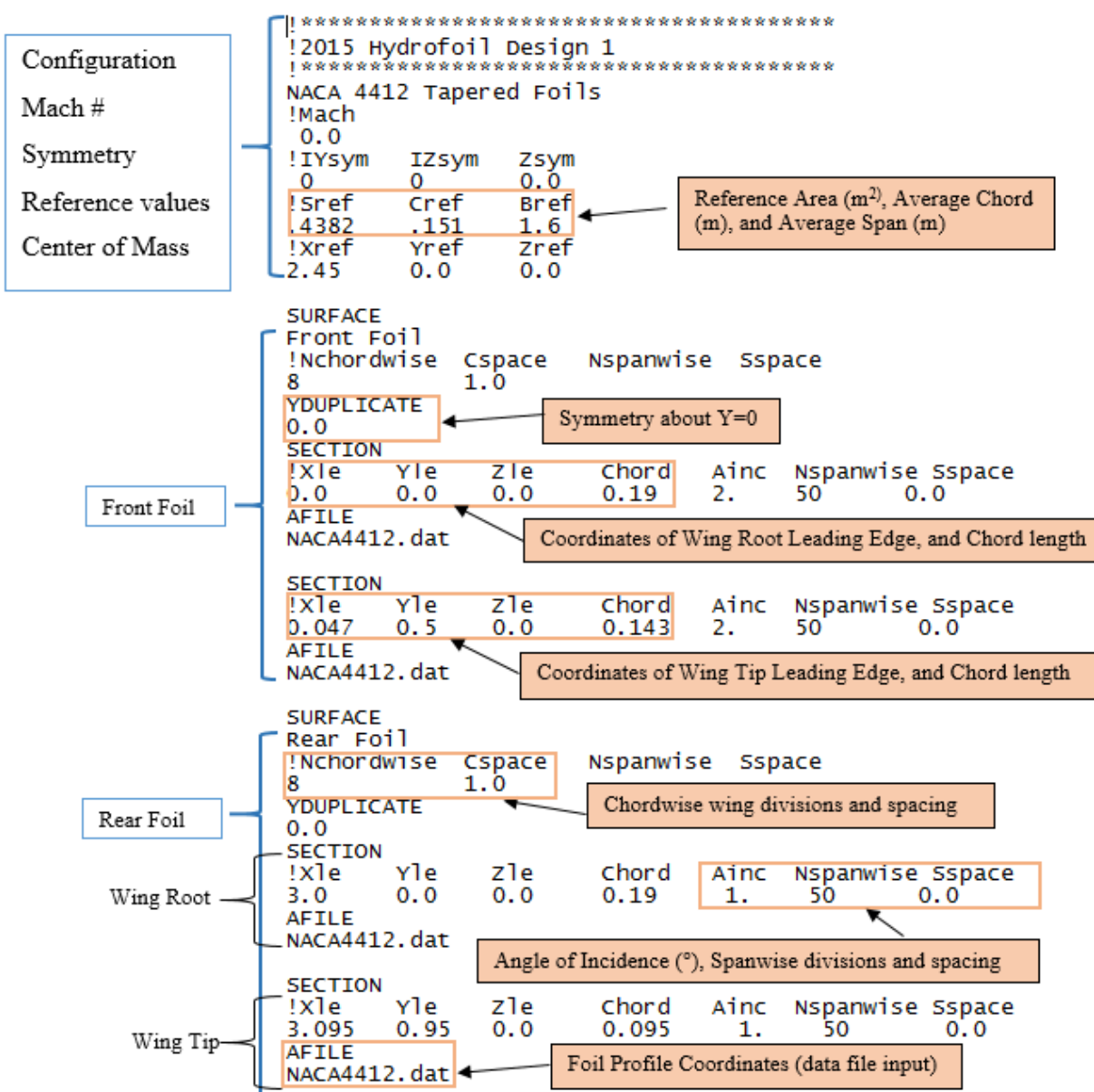


**Figure G.1** AVL input geometry file with callouts annotating the various input parameters

The components of this diagram which are not self-explanatory are the Cspace and Sspace numbers. These are based off of insight given in the AVL Primer 3.0 shown in Figure G.2 (Drela).

### Vortex Lattice Spacing Distributions

Discretization of the geometry into vortex lattice panels is controlled by the spacing parameters described earlier: Sspace, Cspace, Bspace

These must fall in the range -3.0 ... +3.0 , and they determine the spanwise and lengthwise horseshoe vortex or body line node distributions as follows:

parameter		spacing									
-----		-----									
3.0	equal										
2.0	sine										
1.0	cosine										
0.0	equal										
-1.0	cosine										
-2.0	-sine										
-3.0	equal										
Sspace (spanwise) :		first section				==>		last section			
Cspace (chordwise) :		leading edge				==>		trailing edge			
Bspace (lengthwise):		frontmost point				==>		rearmost point			

An intermediate parameter value will result in a blended distribution.

The most efficient distribution (best accuracy for a given number of vortices) is usually the cosine (1.0) chordwise and spanwise. If the wing does not have a significant chord slope discontinuity at the centerline, such as a straight, elliptical, or slightly tapered wing, then the -sine (-2.0) distribution from root to tip will be more efficient. This is equivalent to a cosine distribution across the whole span. The basic rule is that a tight chordwise distribution is needed at the leading and trailing edges, and a tight spanwise distribution is needed wherever the circulation is changing rapidly, such as taper breaks, and especially at flap breaks and wingtips.

**Figure G.2** Chord and span vortex spacing instructions for AVL

In order to obtain the lift and drag coefficients after creating the initial geometry file, the “.avl” program must be executed through AVL.exe. This is a free download from the internet, and AVL.exe operates in the command window. The commands necessary to determine the lift and drag coefficients are “oper” and then “x”. This executes the geometry file and will result in a coefficient of lift and drag. By then pressing “g” a plot of the geometry will appear. To



change the angle of attack of the entire system, in “oper” type “a a 1” to obtain an angle of attack of 1 degree. The program must be executed again, “x” should be pressed to get the new coefficients of lift and drag at an angle of attack of 1 degree.

The coefficients from AVL should be used in the general drag equation (Equation G.1):

$$d = \frac{c_D \rho U^2 A}{2} \quad (G.1)$$

Where  $\rho$  is the density of water,  $U$  is the velocity, and  $A$  is the planform area which is entered into the AVL geometry file under Sref. This area must be used with the coefficients to obtain an accurate drag value, as AVL uses Sref to compute the coefficients. The reference span (Bref) and the reference chord length (Cref) are also important to enter into the AVL file along with the center of gravity which is best found using a SolidWorks model and evaluating the mass properties of the system.

AVL is a useful tool in so far as it provides coefficients for induced drag and lift in an inviscid laminar model. This is a significant limitation, but using AVL for the induced components and equations for the remaining drag produces accurate results as compared with Fluent and experimental data.

## **Appendix H –Additional Hydrofoil Analysis Program**

Because AVL only calculates the induced drag component, formulas are needed to obtain the remaining drag forces, including the skin-friction, form, and interference drag on the wings and struts. The struts and pod which hold the endurance motor must also be accounted for. The AHA program was written in MATLAB to overcome the burden of calculating the total drag by hand each time there was a design change. The program is as shown, with variables clearly labeled and appropriate comments to help the user understand what needs to be entered manually and what each of the equations are used for. The equations are all drawn from Hoerner's *Fluid-Dynamic Drag*.

First, the Reynolds Number must be calculated to determine the coefficient of drag due to skin friction (Equation H.1).

$$Re_{front} = \frac{\rho UL}{\mu} \quad \text{Equation H.1}$$

Where  $\rho$  is the density of the water at 20° Celsius,  $U$  is the fluid velocity relative to the foil,  $L$  is the characteristic length parallel to the fluid flow, and  $\mu$  is the dynamic viscosity. The skin friction coefficient is calculated using a turbulent model because the Reynold's number is on the higher end of the laminar-turbulent transition region. Equation H.2 was used in determining this coefficient.

$$C_f = \frac{0.455}{(\log(Re_l))^{2.58}} \quad \text{Equation H.2}$$

The next step was to calculate the total drag due to skin friction on this front foil using the surface area (Equation H.3). The total surface area for the front foil was obtained by creating the foil in SolidWorks and using the Evaluate tab to calculate the surface area.

$$D_f = \frac{C_f \rho U^2 A_{surface}}{2} \quad \text{Equation H.3}$$

Where  $A_{surface}$  is the surface area of the front foil, see Equation H.1 for an explanation of the remaining variables. The total skin friction drag for the rear foil as well as the struts and the downleg were calculated in the same manner.

Form drag was calculated using experimental data for slender streamlined airfoils and can range from 0.01 to 0.04, where 0.04 is used for thicker streamlined bodies. This value is determined from Figure using a Reynold's number appropriate to the foil or strut. Figure H.1's airfoil data is for a foil of 18% thickness while the foils we are using have a 12% thickness. This chart however, can give a reference point for estimating a form

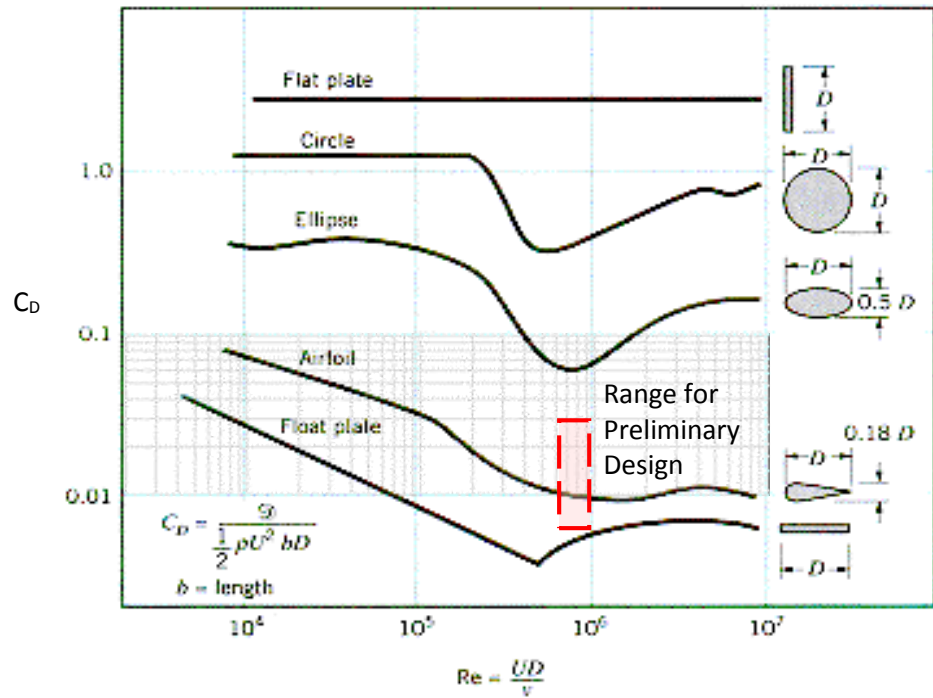


**Figure H.1** Form Drag as a function of Reynold's Number for various body shapes (Munson)

drag coefficient for our hydrofoils. Based on the above figure, we chose  $C_{form} = 0.01$ .

The frontal area must first be calculated (Equation H.4):

$$A_f = c_{average}ts \quad \text{Equation H.4}$$

Where  $c_{average}$  is the average chord length of the foil,  $t$  is the thickness of the foil, and  $s$  is the span of the foil. To then calculate the form drag for the front foil Equation H.5 is used.

$$D_{form} = \frac{C_{form}\rho U^2 A_f}{2} \quad \text{Equation H.5}$$

Where density and velocity are as defined in Equation J.1 and  $A_{frontal}$  is defined in Equation J.4. Then next form of drag which needs to be calculated is the interference drag. The coefficient for this is modeled from *Fluid- Dynamic Drag* by Hoerner in Equation H.6.

$$C_{int} = 17(t)^2 - 0.05 \quad \text{Equation H.6}$$

Where  $t$  is the average thickness ratio of the foil and strut. For this system, the thickness ratio of both the foils and the struts is 12%. The interference drag was then calculated using Equation H.7.

$$D_{int} = \frac{C_{int}\rho U^2 (t_{average})^2}{2} \quad \text{Equation H.7}$$

Where  $t_{average}$  is the average thickness of the foil and the strut. This is calculated by taking the average chord length of each and multiplying by the thickness ratio which is 12% for both foil and strut in this case. All of the previously mentioned equations are summed up in the MATLAB program which follows (Figure H.3), to incorporate the results from AVL as well as the remaining forms of drag to be included such as skin friction, form and interference.

The drag due to the pod is also included as form drag using the frontal area. The coefficients for this are based on Hoerner's work for bodies of revolution in fluid flow (pg 3-12).

```
% Hydrofoil Drag and Lift calculations.
% This program requires several input values which must be calculated by
% the user. Input the necessary information. Use
% SI units. To convert change constant values.

format long

% Input Data enter manually
rho= 998.2; % Density of Water (kg/m^3)
velocity= 5.36; % Velocity of Boat (m/s)
mu= 1.002E-3; % Dynamic Viscosity for calculation of Reynolds number (Ns/m^2)

%Front Foil Geometry
chordf1=0.1665; % Front Foil Chord length (m)
tr1=0.12; % thickness ratio of foil profile (12 percent)
Spanf1=1; % Span of Front foil (m)
SAf1=0.34; % Surface Area of front foil (m^2)

%Rear Foil Geometry
chordf2=0.1425; %m, Rear Foil Chord length
tr2=0.12; % thickness ratio of foil profile (12 percent)
Spanf2=1.9; % Span of Rear foil (m)
SAf2=0.55; % Surface Area of rear foil (m^2)

%Strut Geometry
chordstrut= 0.14; %m, Strut Chord length
trstrut=0.12; % thickness ratio of strut profile (12 percent)
SAstrut=0.064; %Surface Area of 2 struts (m^2)

%Downleg Geometry
chorddown= 0.0689; % downleg Chord length (m)
depth=.2286; % Submerged depth (m)
SAdown=0.164*(depth+.1524); % Surface Area of downleg (m^2)
FAdown=.02921*(depth+.1524); % Frontal Area of downleg (m^2)

%Pod
FApod=.006207; % Frontal Area of the Pod (m^2)

%Preliminary Calculations
Thickf1=chordf1*tr1; % Thickness = chord length*thickness ratio
Thickf2=chordf2*tr2; % Thickness = chord length*thickness ratio
Thickstrut=chordstrut*trstrut; % Thickness = chord length*thickness ratio

FrontalArea= (Thickf1)*(Spanf1)+(Thickf2)*(Spanf2)+(Thickstrut)*2*(depth);
```

% Total Frontal Area for foils and struts (m^2)

Ref1=(rho)\*(velocity)\*(chordf1)/(mu); %Reynold's Number for front foil  
 Ref2=(rho)\*(velocity)\*(chordf2)/(mu); %Reynold's Number for rear foil  
 Restrut=(rho)\*(velocity)\*(chordstrut)/(mu); %Reynold's Number for struts  
 Redown=(rho)\*(velocity)\*(chorddown)/(mu); %Reynold's Number for downleg

%Lift (AVL)

C\_L=.44391; % Coefficient of Lift found from AVL  
 L=1/2\*(C\_L)\*(rho)\*(velocity)^2\*(chordf1\*Spanf1+chordf2\*Spanf2);  
 % Lift force (N) using planform area  
 Lift=L/4.45; % Lift force (lb)

%Induced Drag (AVL)

C\_Dind=.00914; % Coefficient of Induced drag from AVL  
 D\_ind=1/2\*(C\_Dind)\*(rho)\*(velocity)^2\*(chordf1\*Spanf1+chordf2\*Spanf2);  
 % Induced Drag force (N) using planform area  
 D\_induced=D\_ind/4.45; % Drag force (lb)

% Skin Friction Drag

% Foils

C\_f1friction=0.455/(log10(Ref1)^2.58);  
 %Coefficient of skin friction using a turbulent model from Hoerner's Fluid-Dynamic Drag (pg 2-5)  
 D\_f1friction=1/2\*(C\_f1friction)\*(rho)\*(velocity)^2\*(SAf1);  
 % Skin Friction Drag force (N) on front foil using surface area

C\_f2friction=0.455/(log10(Ref2)^2.58);  
 %Coefficient of skin friction using a turbulent model from Hoerner's Fluid-Dynamic Drag (pg 2-5)  
 D\_f2friction=1/2\*(C\_f2friction)\*(rho)\*(velocity)^2\*(SAf2);  
 % Skin Friction Drag force (N) on rear foil using surface area

D\_ffriction=D\_f1friction+D\_f2friction; % Total Foil Skin Friction Drag force (N)  
 D\_foilfric=D\_ffriction/4.45; %Total Foil Skin Friction Drag force (lb)

% Strut

C\_strutfriction=0.455/(log10(Restrut)^2.58);  
 %Coefficient of skin friction using a turbulent model from Hoerner's Fluid-Dynamic Drag (pg 2-5)  
 D\_strutfriction=1/2\*(C\_strutfriction)\*(rho)\*(velocity)^2\*(SAstrut);  
 % Skin Friction Drag force (N) on struts using surface area of both struts

D\_strutfric=D\_strutfriction/4.45; %Total Strut Skin Friction Drag force (lb)

%Form Drag

C\_form=0.01; %Averaged Pressure Drag Coefficient from Figure I.1  
 D\_formn=1/2\*(C\_form)\*(rho)\*(velocity)^2\*(FrontalArea+FAdown);  
 % Pressure/Form drag force (N) using frontal area of foils, struts, downleg  
 D\_form=D\_formn/4.45;



```

%Interference Drag, Drag due to the junction of struts and foils
C_Dinterference=17*(tr1)^2-.05;
%Coefficient of interference drag from Hoerner's Fluid Dynamic Drag (pg 8-1)
D_interference=2*1/2*(C_Dinterference)*(rho)*(velocity)^2*((Thickf1+Thickstrut)/2)^2;
% Interference Drag force (N) due to the junction of foils and struts
D_interfer=D_interference/4.45; % Interference Drag Force (lb)

%Downleg
C_fricdown=0.455/(log10(Redown)^2.58);
%Skin Friction coefficient of drag on downleg using turbulent model from Hoerner's Fluid-
Dynamic Drag (pg 2-5)
D_downfriction=1/2*(C_fricdown)*(rho)*(velocity)^2*(SAdown);
%Skin Friction Drag force (N) on Downleg
D_fricdown=D_downfriction/4.45; %Skin Friction Drag Force on Downleg (lb)

%Pod
C_pod=0.17422;
% Coefficient of drag on an elliptical body from Hoerner's Fluid-Dynamic Drag (pg.3-12)
D_podn=1/2*(C_pod)*(rho)*(velocity)^2*(FApod); %Pressure drag on Pod (N)
D_pod=D_podn/4.45; %Pressure drag on Pod (lb)

%Total Drag
D_Total=D_induced+D_foilfric+D_strutfric+D_form+D_interfer+D_fricdown+D_pod;

format short
D_Total %Display Total Drag
Lift %Display Lift

```

D\_Total =

34.4996 lb

Lift =

625.4346 lb

[Published with MATLAB® R2014b](#)

**Figure H.3** AHA program showing the violation of the drag constraint specified previously and the simplicity of calculating drag force

The data for the geometry of the hydrofoil system must be taken from the AVL file, and the surface area can be easily calculated using a SolidWorks model, or estimating that it is a little more than twice the planform area. This program can also be modified to model struts, foils or the pod alone. In several instances such adjustments have been made to eliminate the need to calculate forces by hand. By selecting only portions of this program to run, each component can

be run alone. This was done to model the 2013 system as well as the NACA 66014 strut to make analysis easier.

The program is most effective for design changes such as speed and angle of attack. It allows the user to have the ability to calculate the total drag and determine at what angle of attack and speed the boat will begin to fly. This is valuable in estimating the speed and angle of attack at which the boat will begin to rise out of the water. Using this program we were able to determine the speed at which the Solar Splash boat would begin to lift out of the water, as well as the speed at which the boat would normally fly on the designed foils. This is a unique function of AVL and AHA programs to analyze such a system. Achieving the same result in Fluent would require intensive work to run many cases at different angles and different flow rates. This would take significantly more time than completing similar tasks in AVL with the addition of the remaining drag calculations.

## Appendix I - Hydrofoil Design Analysis

Data for Lift to Drag ratio of varying foil profiles at 1 degree angle of attack. The geometry is 1.9 m wing span with a chord length of 0.19 m and appears as in Figure I.1 with .74 taper ratio.

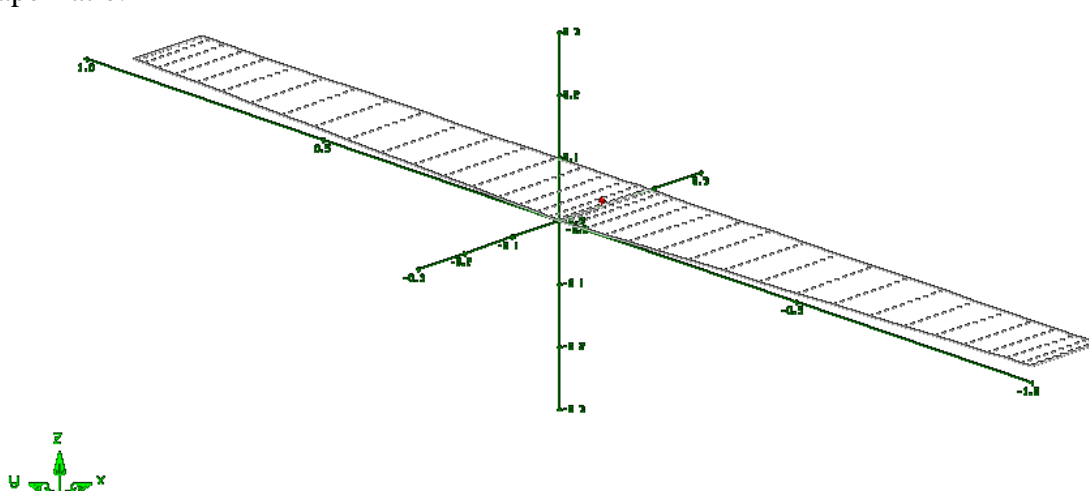


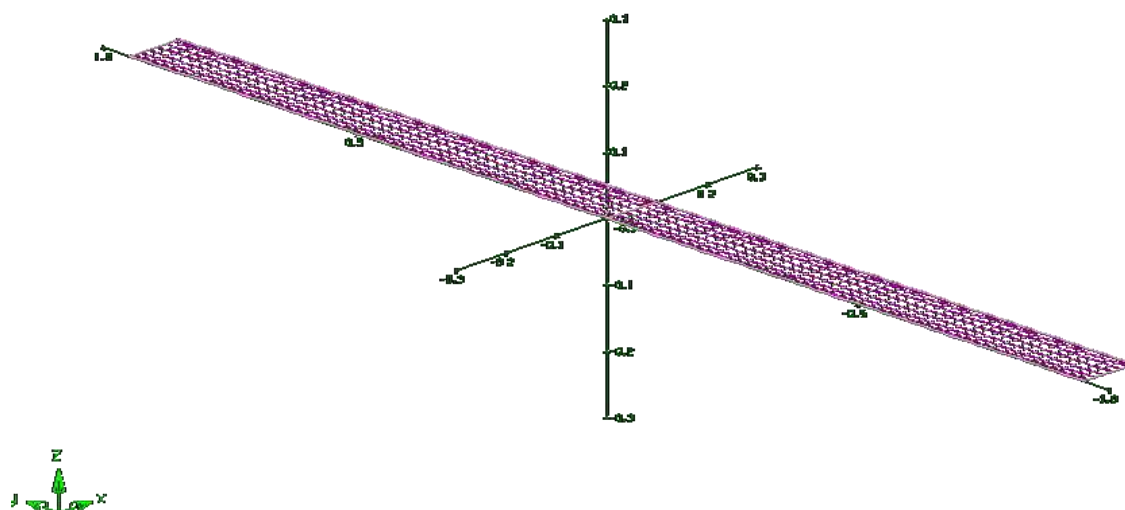
Figure I.1 General geometry tested

The raw resultant data can be found in Table I.1. The coefficients of lift and induced drag were found using AVL. This analysis was completed before the development of the MATLAB program in Appendix H and thus, the drag due to viscous effects is not included. The viscous drag for each foil would be approximately the same, as the geometry is the same for each. Comparatively speaking, this does not change the results in terms of which foil profile produces the highest lift to drag ratio. While the Eppler 420 profile has the highest coefficient of lift in Table I.1, the NACA 4412 has the highest lift to drag ratio and was selected for further analysis of a hydrofoil system.

The next parameter study consisted of determining the optimal aspect ratio. To complete this test a foil was generated with a NACA 4412 profile with a constant span of 1.9 m. The chord was then varied to determine the effect of aspect ratio on the lift to drag ratio for the foil. Figure I.2 shows the set up for the aspect ratio test in AVL. Additional formulas found in the MATLAB program in Appendix H –Additional Hydrofoil Analysis Program, were used as it pertains to the design for this test.

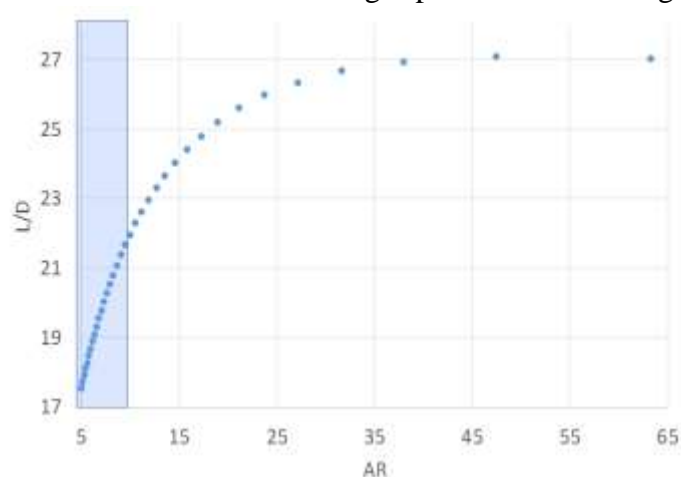
Table I.1 Lift to Drag Ratios for high camber foil profiles

Foil Profile	Coefficient of Lift	Coefficient of Drag	L/D ratio
Eppler 393	0.52653	0.00811	65
Eppler 395	0.68113	0.01358	50
Eppler 396	0.69969	0.01578	44
Eppler 420	1.09814	0.03479	32
Eppler 421	0.85523	0.021	41
Eppler 422	0.63077	0.01131	56
Eppler 434	0.49279	0.00702	70
Eppler 554	0.47828	0.00684	70
Eppler 561	0.69429	0.01415	49
Eppler 748	0.69112	0.01417	49
Eppler 1211	0.50246	0.00732	69
NACA 4412	0.47263	0.00629	81
NACA 6409	0.63786	0.01174	54
NACA 6412	0.63319	0.01155	55
NREL'S S826	0.66934	0.01339	50



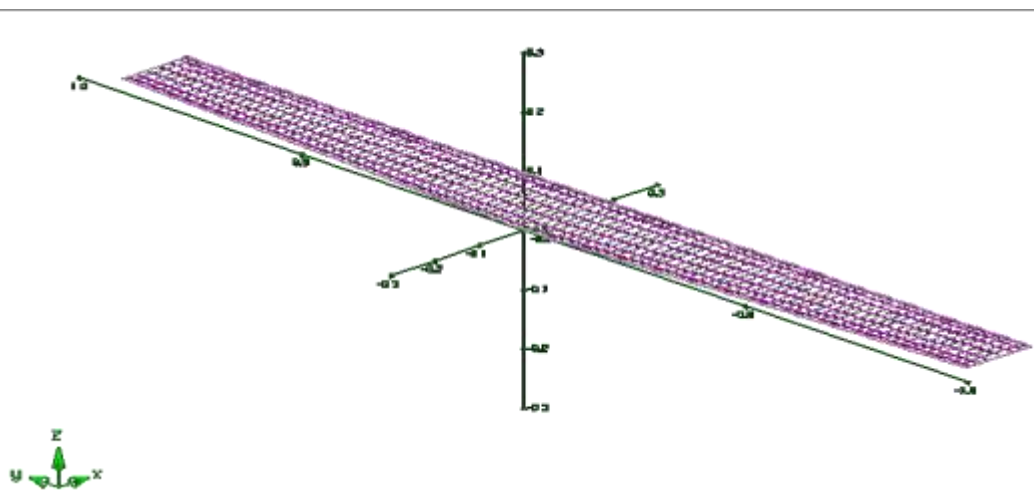
**Figure I.2** Foil at 0.19 m chord; chord length was varied to test aspect ratio

Figure I.3 displays the lift to drag ratio as a function of increasing aspect ratio. The drag includes the additional drag due to skin friction, form and wing tip drag. Figure I.3 shows that there is a maximum aspect ratio which is optimal for obtaining the best lift to drag ratio ( $AR \approx 47$ ). However, this foil is not easily made, and is too thin for structural purposes. The shaded region in Figure I.3 shows the acceptable range from which the optimal aspect ratio was determined. This range includes foils that have a chord length which will withstand bending moments produced by the 1.9 m span and the required lift on this foil. We chose a chord length of 0.19 m which is the minimum chord length within our design constraints. Having a lower aspect ratio reduces the chance of flutter and torsion in the wing.



**Figure I.3** Lift-to-drag ratio as a function of aspect ratio for a NACA 4412 foil profile and a 1.9 m span

The next test performed in AVL was to determine the effect of taper on the foils. This was done by taking the 0.19 m chord, 1.9 m span NACA 4412 foil and decreasing the tip chord by small increments. This was measured as taper ratio which is the ratio of tip chord to root chord. A print out of an AVL tapered wing design is found in Figure I.4.



**Figure I.4** NACA 4412, 0.19 m chord, 1.9 m span tapered foil

The conclusion of this test indicates that the lift to drag ratio increases for decreasing taper ratio. This is because there is less tip loss with a smaller tip chord length. Figure I.5 shows that for decreasing taper ratio the lift to drag ratio increases while the lift force decreases. There must be a balance found in designing a wing with taper so that the lift requirement is maintained while the wing is also made as efficient as possible by decreasing tip chord length. At a 50% taper ratio the minimum lift requirement was reached for the rear foil, thus 50% taper was chosen for the rear. These tests were valuable in showing the effects of individual parameters on foil lift and drag and are essential for an excellent hydrofoil design.

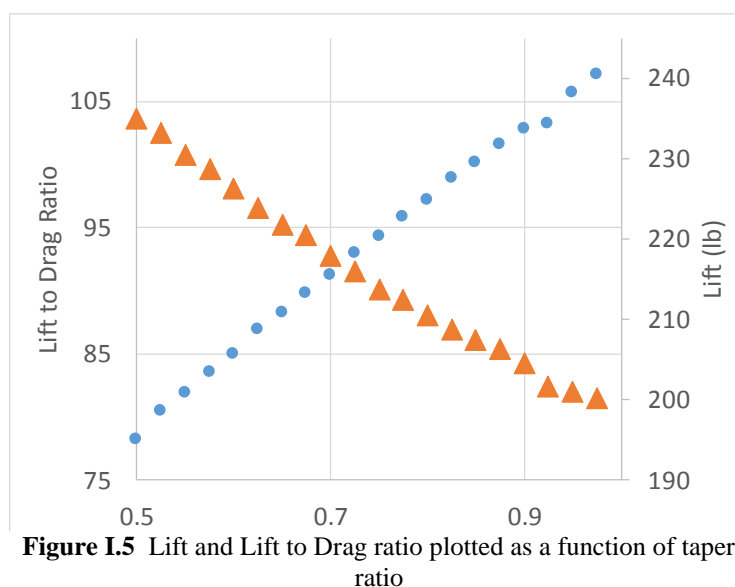


**Figure I.5** Lift and Lift to Drag ratio plotted as a function of taper ratio

By testing one parameter at a time, we were able to understand the effect that that parameter alone had on the overall system. With this as a method of designing an experiment we were able to determine critical information in the design of a hydrofoil system. In conclusion these parameter studies can be completed with varying two variables, however this is much more complicated than the simple single variable tests completed in this report.



## **Appendix J - Ohio Supercomputer Input Files**

Running a Fluent calculation on the Ohio Supercomputer requires interaction with both the Supercomputer's "job submission" system and Fluent's command line. There are therefore two files necessary: a ".job" file to submit the calculation to the Supercomputer and a ".jou" Fluent journal file to define the parameters of the calculation. Each of these documents simply contains text; create the documents as ".txt" and rename them to the appropriate file extension.

It should be noted that before any such documents may be created, however, that the Fluent-readable ".cas" case and ".dat" data files must be created and placed in on the Supercomputer file system in an easily accessible location. The "crimson\_files" folder automatically generated on the user root directory is a generally a good default choice. The data file should have the solution initialized and the desired set-up for writing out data files during the solution (every five time steps, for example). If these data files are not set up to write (or write infrequently) it will be impossible to post-process results for visualization. It should also be noted that all files and folders within this "tree" must not have spaces or else the Bash language will interpret them incorrectly.

The ".job" file (seen in Figure J.1) uses the Bash scripting language to communicate with the Supercomputer. Its purpose is to create an environment where the Supercomputer may execute the desired Fluent calculations and report them to the user. A sample code is given below. The "-N" tag sets the name of the job, the "walltime" sets the time that the Supercomputer will designate to the job before forcibly interrupting it, and the "nodes" tag sets whether serial or parallel processing will be used (parallel processing uses more than 1 node). The solution given is serial. The next commands open Fluent on the designated Supercomputer nodes. The next batch of lines copy the requisite Fluent files to a the nodes to create a temporary workspace for computation; these files must exist in the given location in order to be copied without error. Finally, the ".job" code invokes the ".jou" file to run the desired Fluent calculations. When the calculation has completed (and the "date" has been printed again on the Supercomputer ".o" log file) all of the created files are copied back to the original directory. Further information on programming in this format may be found in Linux Bash tutorials.

```
#PBS -N Single_GOE776_Downleg_Reference_7
#PBS -l walltime=160:00:00
#PBS -l nodes=1:ppn=8
#PBS -l software=fluent+1
#PBS -j oe
#
# The following lines set up the FLUENT environment
#
module load fluent/15.0.7
#
# Move to the directory where the job was submitted from
# You could also 'cd' directly to your working directory
#
# Copy files to $TMPDIR and move there to execute the program
#
cd crimson_files
cd Ansys
```

```

cd Single_GOE776_Downleg_Reference_7
cp Single_GOE776_Downleg_Initialized.cas Single_GOE776_Downleg_Initialized.dat
Single_GOE776_Downleg.jou $TMPDIR
cd $TMPDIR
#
date
#
# Run fluent
fluent 3d -g < Single_GOE776_Downleg.jou
#
date
#
# Finally, copy files back to your home directory
cp * $PBS_O_WORKDIR

```

**Figure J.1.** Job (“job”) file used to submit a Fluent job through the Linux mainframe of the Ohio State Supercomputer

The “.jou” file (seen in Figure J.2) contains commands to Fluent that tell it to execute the desired solution. This file is much shorter and must only designate the iteration limits of the solution. The code below first has Fluent read the case and data files in the workplace (thus setting up the solution) and thereafter commands it to run the solution for 10,000 time steps at 20 iterations per time step. After this calculation is completed the file commands Fluent to write a new, final, data file describing the final fluid configuration of the job. This file, along with the “.job” file described previously, may be named arbitrarily so long as Bash special characters are not used. However, the more descriptive a name is, the easier it is to interpret the purpose and outcome of a job retroactively. Since a first-time job submission will likely involve multiple attempts, use descriptive naming and heavy commenting to track changes and identify which corrections result in a successful submission.

```

/file/read-case-data Single_GOE776_Downleg_Initialized.cas
/solve/dual-time-iterate 10000 20
/file/write-case-data Single_GOE776_Downleg_on_OSC.dat
/file/confirm-overwrite yes

```

**Figure J.2.** Journal (“jou”) file used to give commands to Fluent through the Ansys Workbench

## Appendix K – Boundary Layer Mesh Procedure

All bodies within fluid flow will develop a “boundary layer.” This is a thin film of fluid around the body in which the velocity profile transitions from stationary (relative to the body) to the free-stream velocity. This behavior is due to the no-slip condition at the body’s wall (imposed by fluid theory). Since this transition to the free-stream velocity takes place over a short distance, there is a large velocity gradient within this region. This general situation is depicted in Figure K.1.

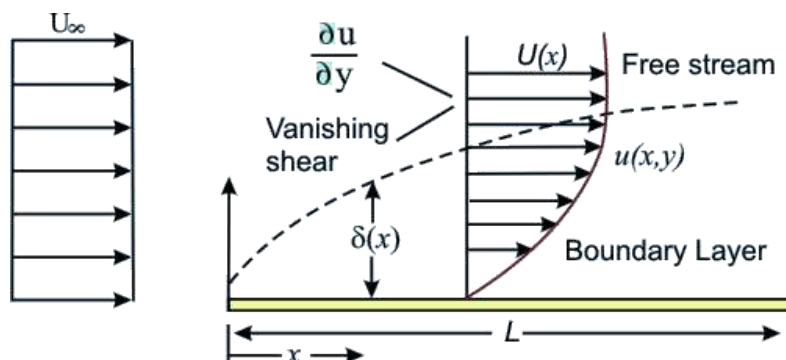


**Figure K.1.** Illustration of boundary layer theory describing the change in x-velocity

over the direction transverse to the flow; this creates shear and thus viscous drag<sup>1</sup>

This, in turn, causes a large amount of shear stress  $\tau_{yx}$ . This relationship is given by Equation K.1 where  $\mu$  is the fluid viscosity. Therefore drag is distributed over the area of the submerged body. This line of reasoning leads to the “viscous boundary layer theory,” which posits that fluid viscosity is only relevant to behavior within the boundary layer and that all other behavior can be described by inviscid models. These inviscid models may also be described as “potential flows,” or an “ideal fluid model” based on the preference of the source.

$$\tau_{yx} = \mu \frac{\partial u}{\partial y} \quad (\text{K.1})$$

To apply this theory to computational fluid dynamics we may first note that the presence and treatment of viscosity is dependent upon the solver used. Such treatment is necessary since viscosity is not strictly isotropic or endemic to a fluid—presence of turbulence and temperature fluctuations can change a fluid viscosity throughout a flow. It is not possible to have a solution with both a viscous and an inviscid domain; a viscous solver must be used for the whole domain to capture the viscous boundary layer behavior.

Viscous solvers are differentiated in that they may or may not model this turbulent fluid behavior. Laminar models use one equation to model viscosity and cannot capture turbulent behavior. Turbulent models range from the one-equation Spallart-Allmaras model to the seven-equation Reynolds Stress model. Selection between these turbulent models is dependent upon the quality of the mesh used; the more complex models are less likely to diverge but also take longer to compute on any given computer. It is thus possible to think of the choice between solvers as a balancing act between solver stability and the potential speed of the solution. Turbulent models are also known to over-predict drag compared to experiments in three-dimensional meshes. The general process for selecting a solver therefore involves asking and answering three questions: Is boundary layer (viscous) behavior needed? Is the flow of interest laminar or turbulent (based on Reynolds number)? Finally, in what proportion are speed and stability of solution desired?

<sup>1</sup> <http://www.efm.leeds.ac.uk/CIVE/CIVE1400/PDF/Notes/section1.pdf>

Consider now the meshing strategy required to capture the boundary layer behavior. Accurate drag modeling requires the shear stress and thus the velocity profile close to the airfoil to be accurate. It is therefore necessary to create a fine mesh of points around the body of interest so that the grid points of the mesh could accurately contain the tightly-curved boundary layer velocity profile. One of the best means of accomplishing this is to extrude a “prism” mesh from the body of interest such that there are a large number of cells concentrated around it. Completing this step in ICEM allows the user to control the thickness of each prism so that the boundary layer is defined only with the requisite thickness. This allows the viscous behavior to be captured without an unnecessary number of cells and a longer convergence time.

We will now consider the procedure for creating a prism mesh. In ICEM prism extrusion requires the original mesh to exist before starting. To create the original mesh follow the two-phase tutorial written by John Howland for the Solar Boat team’s 2013-2014 Final Report. Following this tutorial will allow the user to specify the maximum size of the cells adjacent to any part in the model; ensure that these values create a preliminary mesh that is still fine enough to capture the desired geometry. An example of one such mesh (of a NACA0012 airfoil) is given in Figure K.2 below. This example mesh has three parts: HYDROFOIL\_DOWNLEG, HYDROFOIL\_DOWNLEG\_LEADING\_EDGE, and HYDROFOIL\_DOWNLEG\_TRAILING\_EDGE. These latter two parts use a finer mesh size to capture the more drastic curvature of their geometry and accordingly can be seen to have a higher surrounding cell density.

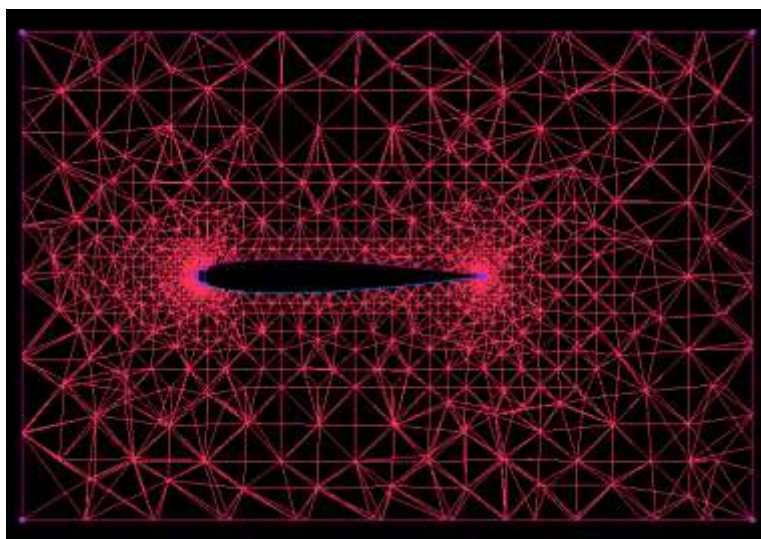


**Figure K.2.** Tetrahedral mesh surrounding a NACA0012 foil profile in ICEM

Now, calculate the boundary layer thickness for the problem of interest. Since turbulent boundary layers are thicker than laminar ones, it is best to calculate the boundary layer thickness for the turbulent boundary layer—even if the flow is laminar—to fully capture the viscous shearing effects on the body. No analytical formulation for boundary layers on bodies other than flat plates exist. It is therefore necessary to estimate the boundary layer thickness for the problem at hand using the formulation for a flat plate of the same Reynolds number. This maximal boundary layer thickness  $\delta_{max}$  is estimated by the formula below (Equation K.2). Here  $Re_L$  is the Reynolds number based on the characteristic length  $L$ .

$$\delta_{max} \approx \frac{0.382L}{Re_L^{1/5}} \quad (K.2)$$

It is now possible to set up the prism meshing parameters. To begin this process enter the “Mesh” tab in the ICEM taskbar and click the rightmost icon to open the “Compute Mesh” dialog box in the lower-left hand corner of the document. Within this dialog box click the rightmost icon (with the arrow) to launch the “Prism Mesh” sub-dialog box. The ICEM layout should now resemble the one shown in Figure K.3.

The “Select Mesh” drop-down menu should have “Existing Mesh” selected; for this reason it was necessary to complete the previous meshing steps. Click on the “Select parts for Prism Layer” button. This will launch the “Part Mesh Setup” menu shown in Figure K.4. Check the “Prism” radio button next to the parts where a boundary layer is required.

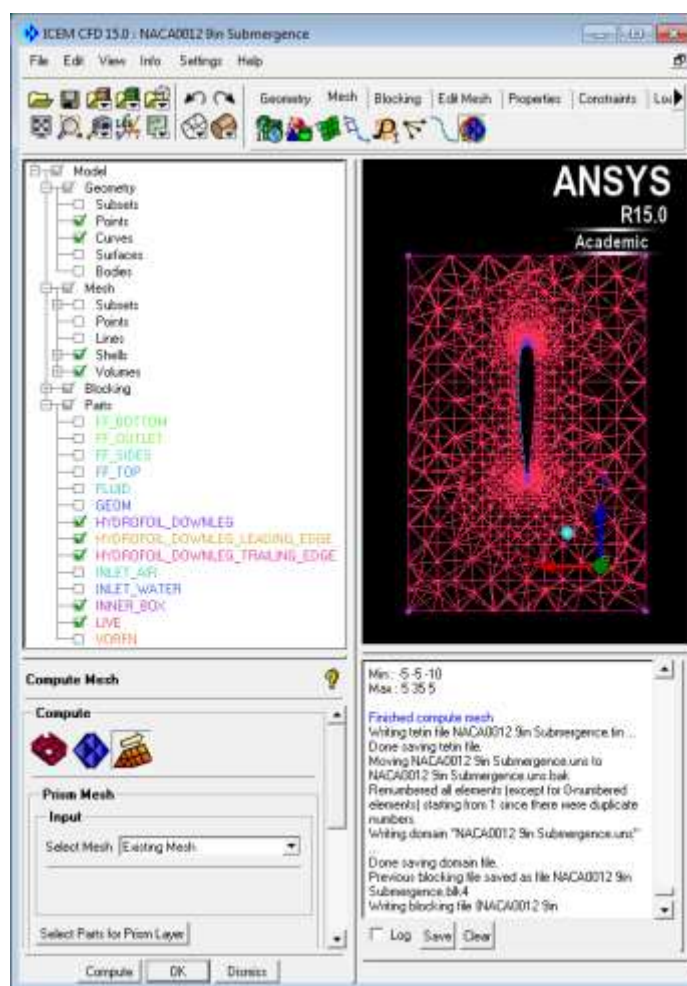


**Figure K.3.** Prism mesh creation menu in ICEM



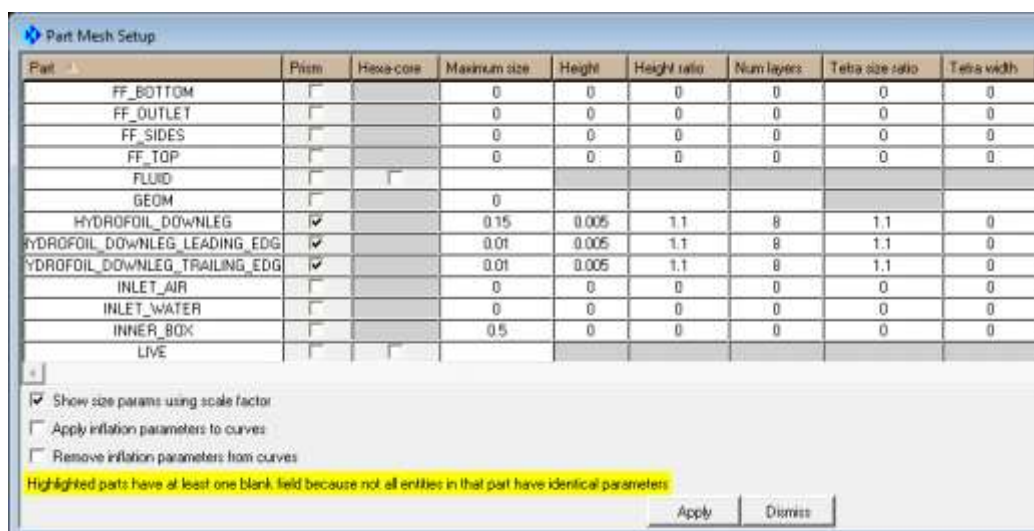


**Figure K.4.** “Part Mesh Setup” Menu in ICEM which allows the user to designate prism parameters

Then, set the “Height,” “Height Ratio,” and “Num Layers” options to numbers that comport with the computed boundary layer thickness. “Num Layers” is the number of layers of prisms that will be extruded from the selected parts. “Height” is the thickness of the first prism layer’s extrusion from the associated part. “Height Ratio” is the ratio of the second prism layer’s thickness to the first layer’s thickness and so on. A Height Ratio value of 1 would result in uniformly thick prism layers and any value greater than 1 will result in a geometrically-growing series of prism thicknesses. From these numbers it is possible to compute the total thickness of all of the prism layers taken together; be careful that the units used here are the same as was used in the original SolidWorks geometry model. Also be careful that the “scale factor” is taken into account: only if the “Show size params using scale factor” is unchecked will the “Height” displayed be in the original units.

With all of these parameters set, click the “Apply” button on the “Part Mesh Setup” menu to close it. Back in the “Compute Mesh” dialog box, click “Compute” at the bottom of the window. The mesh will compute (likely taking several minutes) and display. If this mesh is unsatisfactory for some reason (or the prism mesh causes ICEM errors), re-compute the original tetrahedral mesh with smaller size parameters and attempt the prism creation again. An example of a successfully-created mesh is shown for a symmetrical airfoil in Figure K.5.

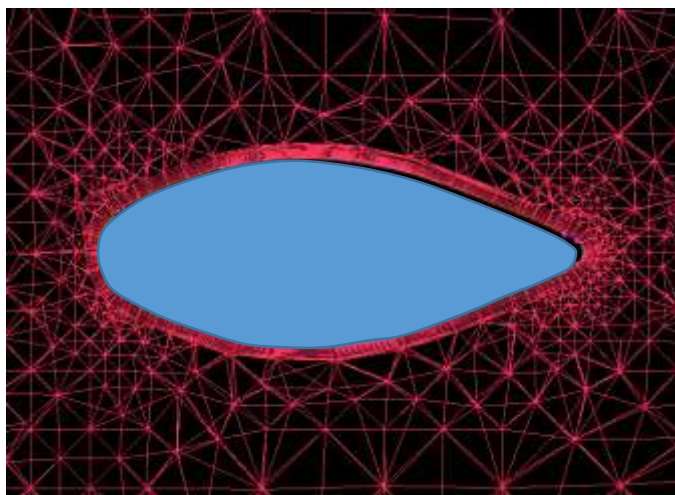


**Figure K.5.** Symmetrical airfoil with tetrahedral mesh and successfully extruded prisms; the prism mesh can be seen to surround the blue airfoil body

## Appendix L – SolidWorks Model of Foil and Mold

The following tutorial describes the foil modeling process, and included many details. It is assumed that the user only has a very basic understanding of Solidworks. Therefore “simple” details have been included to make the process more explicit.

To make a foil in SolidWorks (SW), you will first need to create a text file with the coordinates of the foil profile. There are several online databases ([http://www.ae.illinois.edu/m-selig/ads/coord\\_database.html](http://www.ae.illinois.edu/m-selig/ads/coord_database.html) or <http://www.airfoiltools.com/>) which provide 2D coordinates of most standard foil shapes (NACA, Eppler, etc.). These data points can be copied into an Excel spreadsheet. Creating separate columns for X, Y, and Z coordinates is useful. The Z column should simply be populated by zeros. Since the coordinates are given with a chord length of 1, simply multiply each column by the new desired chord length. In some cases it is necessary to shift the curve in the X or Y direction, and this must be done here by adding the constant distance to each cell. Z-offsets will be done in SW at a later step. Copy the resulting three columns into Notepad to convert the 3D coordinates to a **.txt** file. Do this for both the root and the tip profiles.

At this point, open a new file in SW and check your units. Make sure they match the units in your Excel file. Select, “Curve through XYZ points” in the drop down menu of the “Curves” button under the “Features” tab. (see Figure L.1)

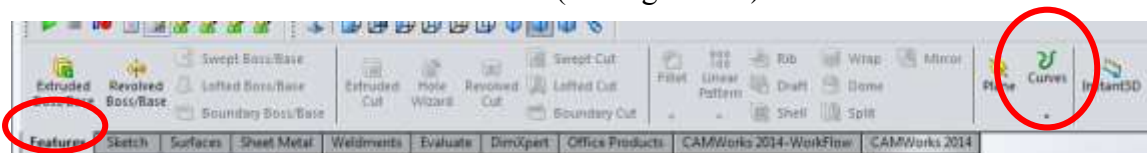


Figure L.1 Inserting a curve using a .txt file.

A dialogue box will appear (Figure L.2) and you will be able to browse for the file you created earlier. Initially SW will only show **.sldcrv** files, simply change file type to **.txt** and your file will show up. If this is successful a blue outline of the foil will appear.

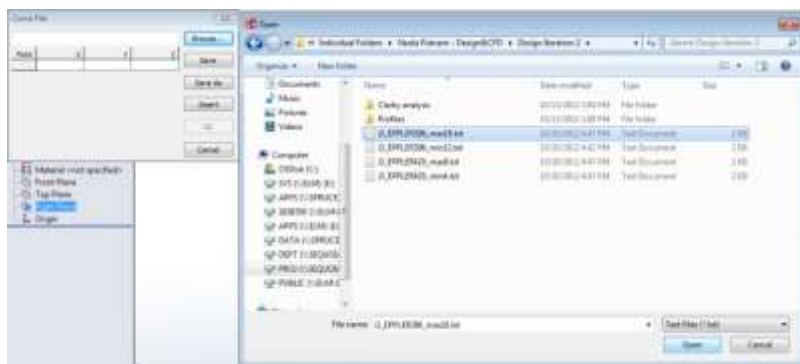


Figure L.2 Finding the .txt file

Once both the root and the tip profiles have been imported, they must be converted to a sketch and lofted together. Open a new sketch by clicking the **Sketch** button under the **Sketch** tab. For the root, create this sketch on the front plane, and for the tip create this sketch in another plane parallel to the front plane. By creating another plane parallel to the front plane and placing the tip profile sketch in this plane, you will be able to adjust the span by simply changing this distance (Figure L.3).

To add a parallel plane, return to the features tab and select **Plane** from the dropdown menu off the **Reference Geometry** button under the features tab. Select the front plane as your first reference and enter the desired distance. This will fully define the plane and allow you to easily adjust the span of the foil.

It is possible to use the “Convert Entities” tool in the **Sketch** tab to convert the curve into a sketch, but this causes problems later in the process. To avoid this, trace the curve with a spline (an option under the **Sketch** tab). By tracing the top of the foil and the bottom of the foil as separate splines, the sharp trailing edge will be maintained. Figure L.4 shows a spline tracing the top half of the foil. Notice that more points are required at the leading edge, and less towards the trailing edge.

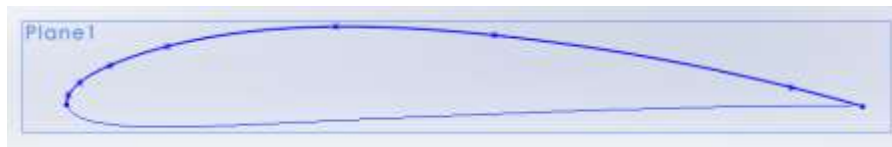


Figure L.4 Foil profile sketch using a spline.

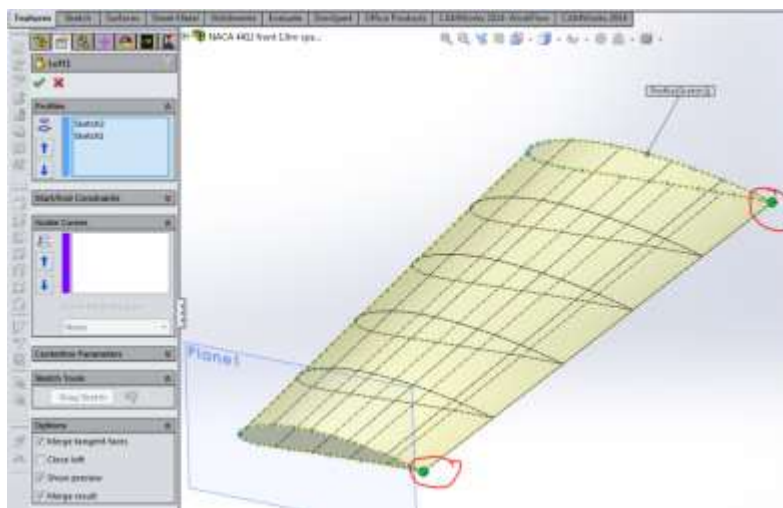


Figure L.5 Lofting the sketches together.

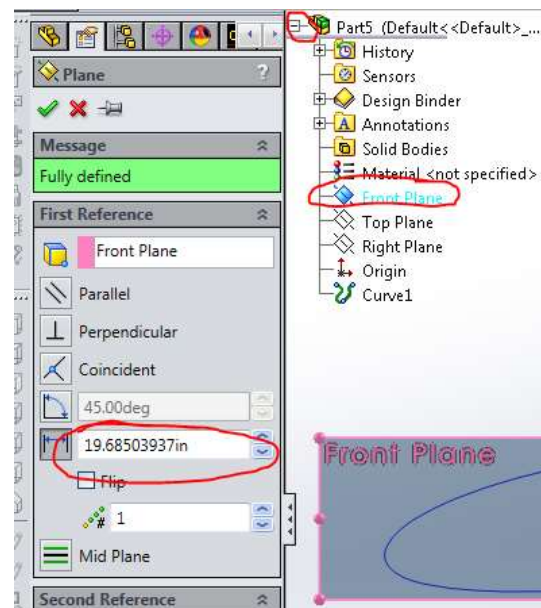


Figure L.3 Addition of a plane parallel to the Front Plane

Once the root curve has been traced with a spline on the front plane, and the tip curve has been traced with a spline on the offset plane, you will loft the two curves together. The loft feature (found under the **Features** tab) requires you to select at least two curves to loft between. The green dots should be moved to comparable points on the two curves, in this case the trailing edge is convenient (Figure L.5).

Once this part of the foil has been modeled, use the **Mirror** feature (found under the **Features** tab) to mirror the foil. The face of the root will be convenient to use as the “Mirror Face/Plane” and if the loft feature is not automatically selected as the body to be mirrored, click any part of the foil to select it.

The final step is to use the **Shell** feature (found under the **Features** tab). Enter the desired thickness of the foil (a function of how many layers of carbon you plan to use) and select the two faces at the tips. This will remove all the inner material and allow for accurate weight calculations. This feature can be found under the **Evaluate** tab, and is called **Mass Properties**.

## Appendix M - Moth Foil Results

The paper titled *Full Scale Measurements on a Hydrofoil International Moth* outlines several strut and foil types tested for drag measurements. Figure M.1 shows the types of strut profiles which were used. We used the Vendor 2 NACA 66014 strut profile to run cases in both Fluent and the MATLAB program found in Figure M.3. The results from the paper (Figure M.2) as well as results from Fluent and the MATLAB program were then compared.

The results found in the paper *Full Scale Measurements on a Hydrofoil International Moth* are shown in Figure M.2. This figure outlines the different forms of drag on the foil and strut tested. However, we are only looking at the strut data for the purpose of this comparison. As noted for the NACA 66014 strut, the drag comes out to 2.72 lb (12 N) which is a summation of the “Strut Section” drag as well as “Strut Wave and Spray” drag.

The equations used in the analysis of the NACA 66014 strut profile at the same speed and submerged depth as in the paper are found using the following MATLAB program (Figure M.3):

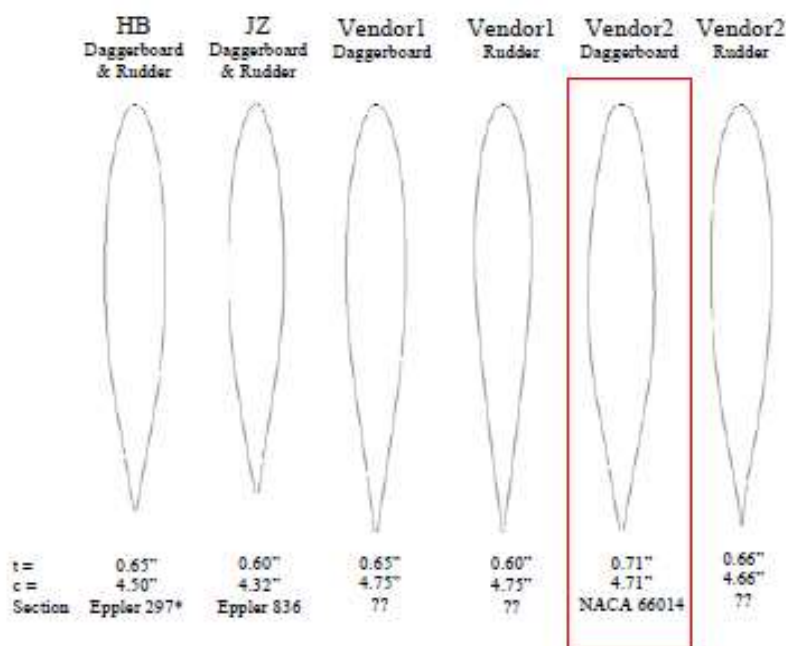


Figure M.1 Geometry of Tested Struts

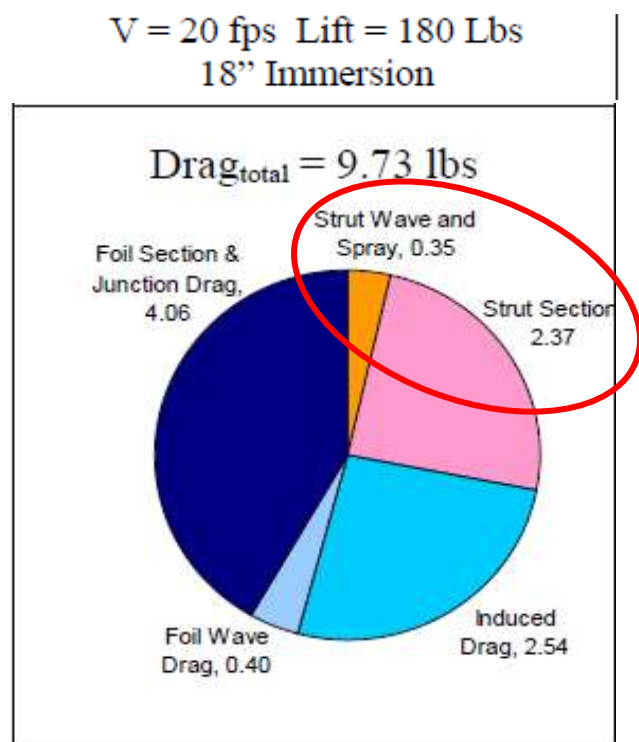


Figure M.2 Drag results for moth foils from *Full Scale Measurements on a Hydrofoil International Moth*



```

% Hydrofoil Drag and Lift calculations.
% This program requires several input values which must be calculated by
% the user. Input the necessary information. Use
% SI units. To convert change constant values.

format long

% constants, enter manually
rho= 998.2; % Density of water kg/m^3
velocity= 5.36; % Velocity of fluid with respect to strut (m/s)
mu= 1.002E-3; % Dynamic Viscosity (Ns/m^2)

%Strut
chordstrut= 0.1196; % Strut Chord length (m)
trstrut=0.14; % 12 percent thickness ratio
SAstrut=0.1116; % Surface Area of struts (m^2)
depth=.4572; % 18" submerged (m)

%Preliminary Calculations
Thickstrut=chordstrut*trstrut; % Thickness = chord length*thickness ratio
FrontalArea= (Thickstrut)*(depth); % Frontal Area of strut (m^2)
Restrut=(rho)*(velocity)*(chordstrut)/(mu); %Reynold's Number for strut

%Skin Friction on Strut
C_strutfriction=0.455/(log10(Restrut)^2.58);
D_strutfriction=1/2*(C_strutfriction)*(rho)*(velocity)^2*(SAstrut); %Newtons
D_strutfric=D_strutfriction/4.45; %Pounds

%Form Drag
C_form=0.035; %General Value
D_formn=1/2*(C_form)*(rho)*(velocity)^2*(FrontalArea); %Newtons
D_form=D_formn/4.45;

%Tip Drag
C_tip=0.15*(Thickstrut/chordstrut)^2;
D_tipn=1/2*(C_tip)*(rho)*(velocity)^2*(chordstrut)^2;
D_tip=D_tipn/4.45;

%Total Drag
D_Total=D_strutfric+D_form+D_tip;

format short
D_Total

```

D\_Total =

2.75 lb

[Published with MATLAB® R2014b](#)

**Figure M.3.** MATLAB program for NACA 66014 strut drag

The result from the MATLAB program in Figure M.3 show that the total drag on the strut using a turbulent skin friction model comes to 2.75 lb (12.0 N). The results from the same analysis in Fluent are 2.7 lb (12.0 N). Fluent results are for a laminar model, and are sufficient as Fluent tends to over predict drag based on the fineness of the mesh. The result of this comparison aided in the decision to further use the MATLAB program in calculating the skin friction, form, and spray drag on struts. This confirmation of the program also allowed for the further use of the same formulas in the hydrofoil system as a whole.

## Appendix N – Raw Free-Surface Study Data

Vellinga reports that Beason and Buckle found the following relationship between hydrofoil lift and surface proximity, where  $F_S$  is the “surface factor” based on chord length  $C$  and foil submergence distance  $S$  (Equation (N.1)) (Vellinga).

$$F_S = 1 - 0.222 \left( \frac{1.5C-S}{C} \right)^2 \quad (\text{N.1})$$

This surface factor can be used to calculate the foil lift coefficient as a fraction of the “fully submerged” lift coefficient. It may be noted from the above formula that it is only sensible to calculate the surface factor if the foil is submerged more than 1.5 chord lengths (Equation (N.2)).

$$C_{L, \text{surface proximity}} = F_S * C_{L, \text{fully submerged}} \quad (\text{N.2})$$

Lift may then be calculated by the general formula (Equation N.3).

$$L = \frac{C_L \rho A v^2}{2} \quad (\text{N.3})$$

To test whether the 2-phase VOF would replicate these results we used an existing tapered hydrofoil geometry with an Eppler 420 cross-section. By running the Fluent solution at various submergence depths we obtained several lift results. The foil submerged beneath 1.5 chord lengths was taken as having the “fully submerged” lift coefficient for calculation purposes. We could then calculate the surface factor and multiply by the “fully submerged” lift coefficient to find the coefficient of lift predicted by the experimental model for the same geometry as the Fluent test. Sample results of such calculations are shown in Table N.1.

**Table N.1.** Sample of free-surface lift and drag results

Chord Length (in)	Depth (in)	D/C	Lift (lb)	Drag (lb)	C_L	C_D		F_S	C_L (Vellinga)
5.25	3	0.571	57.6	13.1	0.412	0.094		0.809	0.491
	6	1.143	76.8	15.8	0.550	0.113		0.972	0.590
	9	1.714	82.25	16.125	0.589	0.115		1.000	0.608
	12	2.286	84.9	15.28124	0.608	0.109		1.000	0.608

Fluent’s coefficient-of-lift results can be seen to drop off sooner and more steeply than the experimentally-determined formula. The discrepancy between these two, however, is not drastic. Furthermore, Fluent’s under-prediction of lift (compared to the Vellinga formula) is preferable to over-prediction since it would result in a more robust design if the Fluent results were taken at face value. Fluent may therefore be said to satisfactorily model the free-surface lift-loss seen experimentally.

Fluent’s VOF formulation also indirectly captures the position of the free-surface of the water-air interface. This behavior is captured “indirectly” since in this mode Fluent does not calculate a mathematical plane describing the interface. Rather, Fluent calculates the fraction (by volume) of each material present in each cell of the model. A cell with a volume fraction of water of 1 (and thus a volume fraction of air of 0) is fully submerged, then, and a cell with a volume fraction of water of 0.5 (and thus a volume fraction of air of 0.5) contains half water and half air.

Figure N.1 and Figure N.2 display the Fluent phase results for two of the E420 hydrofoils flying at 3” and 12” submergence, respectively. As predicted by the experimental results, the 3” submergence results display substantial wave behavior, thus contributing to wave drag. It should be noted, however, that this is offset by an decrease in standard form drag due to lower pressure values near the water surface. By contrast, the 12” submergence results in display virtually no

wave formation as a result of the hydrofoil (a very slight “bump” may be observed directly above the hydrofoil).

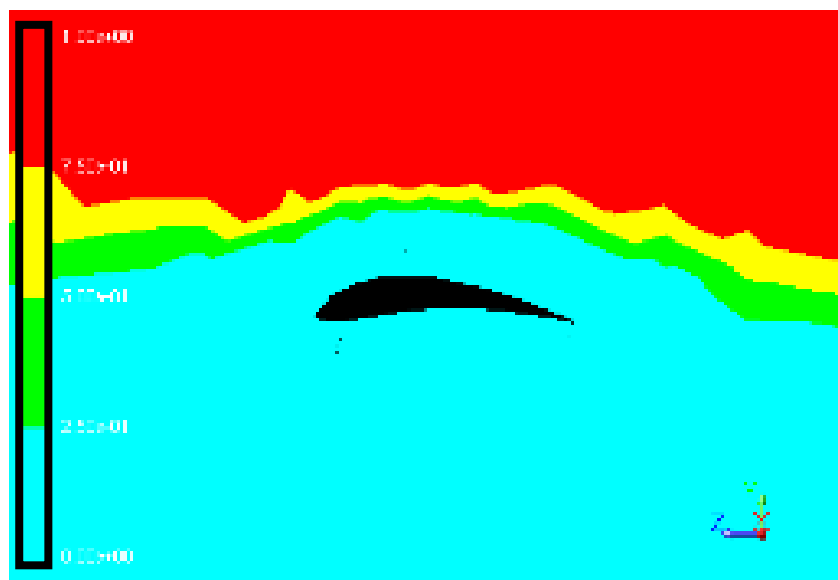


**Figure N.1.** Fluent phase results for an Eppler 420 airfoil with a submergence surface factor of 0.808; blue represents a cell full of water and red represents a cell full of air; wave formation is clearly visible



**Figure N.2.** Fluent phase results for an Eppler 420 airfoil with a submergence surface factor of 1; blue represents a cell full of water and red represents a cell full of air; wave formation is minimal

## **Appendix O - 2015 Endurance Motor Design**

First semester the team's goal was to gather good test data on the 12 V Endurance motor, and then to begin research on a new motor for the 2016 Netherlands competition. The design specifications for the 12 V Endurance motor are 2.8 Nm of torque at 3000 rpm at 93% efficiency. Soon after beginning preliminary Endurance tests with the 12 V motor, a low efficiency of about 70% was discovered. After determining the low efficiency in the 12 V motor a series of tests were conducted in order to determine if the efficiency problem lay with the test setup, motor controller, or the motor.

The 12 V motor was connected to the dynamometer in the EPL to test its efficiency. The power into the motor was calculated by multiplying the current and voltage together going into the motor controller and the power out of the motor was measured by the dynamometer. Motor efficiency was determined by dividing the output power by the input power. Types of efficiency tests conducted with the 12 V Endurance motor include partial throttle tests, wide open throttle (WOT) tests, and tests with three different motor controllers. The primary motor controller used for these tests was the Mamba XL2. Identical tests were also conducted with the Phoenix ICE 300 and the Jeti SpinPro 300 to see if the different motor controllers had an effect on motor efficiency.

Partial throttle tests were conducted with the 12 V motor at torques between 2-4 N-m at speeds between 2000 and 4000 rpm to determine how efficient the motor was at different operating points. The majority of our dynamometer tests were performed at partial throttle because that is how the motor is run at competition. The partial throttle tests we performed showed the motor efficiency to be between 65-75% efficient depending upon the torque and speed the motor was run at. To verify that our test set up was not causing any inefficiencies we performed additional partial throttle tests at the same torques and speeds with the 2010 team's 24 V Endurance motor. These tests allowed us to compare our efficiency data with the 2010 team's efficiency data. While our test data did not align exactly with the 2010 team's data, we decided it was close enough, within 4%, considering we used a lovejoy coupler instead of a rigid coupler. Additionally, we swapped the rotors and stators between the 12 V and 24 V motors to see if switching them had any effect on efficiency due to possible demagnetization.

We performed WOT tests with the 12 V motor to test the hypothesis that the motor controller is more efficient when it is run wide open and we wanted to see how much it affected the motor's efficiency. The downside of the WOT tests are that they do not accurately reflect how we would run our motor during competition because on race day we may have to run the motor faster or slower at different points during the event. Our WOT tests with the 12 V motor consisted of performing a torque sweep between 0-2.75 N-m of torque to find the motor's most efficient operating point. Unfortunately, the motor ran most efficiently at 1.75 N-m instead of at the values described in our power budget.

A series of voltage and current tests were performed to try and narrow down the reason for the 12 V motor's inefficiency. We used an oscilloscope during several of the dynamometer tests to view the current and voltage waveforms going into each of the motor's three wires. The waveform tests with the oscilloscope allowed us to see if there were any inconsistencies in current or voltage between each of the motor's three phases. The motor was also spun as a generator by spinning its shaft in a lathe. While the motor was spinning, the back EMF voltage was measured between each of the motor's wires. We spun the motor as a generator to see if the voltage waveforms differed compared to when it was operating as a motor. From the voltage and current tests we learned that the current going through each of the phases was identical but the

voltage was not. The voltage passing through the third wire was significantly lower than the voltage passing through the first and second wires. The lower voltage signified that there was probably a short somewhere within the stator.

The last series of tests performed to determine the motor's efficiency problem were measuring its resistances to try and determine any short circuits. A large transistor bank was set up in series with the motor's wires and current was measured across two of the phases. With the known voltage and measured current the resistance between each of the three windings was determined. The resistance was also measured between each of the motor's three phases and the stator's outer aluminum casing to determine if any of the motor's internal wires were shorted to the housing. During our resistance tests we discovered a short between the aluminum housing and the same winding that had the lower voltage.

Even though we could not guarantee with one hundred percent certainty that the short was causing the 12 V motor inefficiency we knew we needed to take action to get a more efficient motor. We began by calling Jeff Keesaman, an engineer at Neu Motors, who designed and built most of the motor. He agreed that the inefficiency was most likely being caused by the short. However, he told us that it would be easier to build an entirely new motor than it would be to rewind the current motor. Keesaman also told us that he would help with the design and manufacturing of the new motor.

We planned for the new motor to run at the same efficiency and speed as described in our power budget, and it needed to be constrained to the same outer diameter and approximate length as the current motor so that it could fit into the motor pod. These constraints limited the number of modifications we could make on the motor. To meet our design specifications Keesaman made several changes to the laminations. For the laminations, the number of poles was increased from 9 to 36 and the inner diameter was increased from 42.3 mm to 56.4 mm. A positive side effect of the new lamination design is that it requires a shorter stack than the 2014 motor. The shorter stack will take up less space and allow more room for Keesaman to make the windings within the housing. He also said he would design and build the magnet sleeve that would go around the rotor. This left us to design and build the housing, rotor shaft, rotor slugs and end bells.

Since the stack was shorter, we needed to redesign the inside of the motor's aluminum housing. With the extra 1.44 inches we gave Keesaman one extra inch of space on the non-drive and the last 0.44 inches on the drive end. This would give him plenty of space to make nice turns for the motor. Additionally, we needed to increase the inner diameter of the drive ends openings to make room for the new rotor's larger outer diameter.

For this year's rotor we decided to utilize a new design to attach the magnets to the shaft. The new design will use two rotor slugs that will slide onto the shaft to hold a sleeve of magnets. The advantage of this design is that it is easy to achieve a large rotor outer diameter which is needed for the larger inner diameter of the laminations. Additionally, the new rotor shaft and slugs needed line up with the laminations. Also, the outer diameter of the slugs needed to be precise so that we would have the right air gap. To hold the slugs onto the rotor shaft we added a keyway for each slug and to lock them down with Loctite 38. In addition, to help hold the magnetic sleeve on the slugs we added a 1 x 1 mm shoulder on each end.

The end bells are largely unchanged from the 2014 design except for where the concentricity shoulder is located. The 2014 design has the concentricity shoulder sliding around the outside of the motor housing. The issue with the 2014 design is that the shoulder is in the way of the screws that hold the end bell to the housing. As a result, the screws had fewer threads



into the housing. For the 2015 design we have the concentricity shoulder sliding within the motor's housing. The advantage of the new design is that the shoulder will no longer interfere with the screw threading.

The new design is shown in Figure O.1 and an exploded view is shown in Figure O.2.



**Figure O.1** External drawing of the 2015 Endurance motor

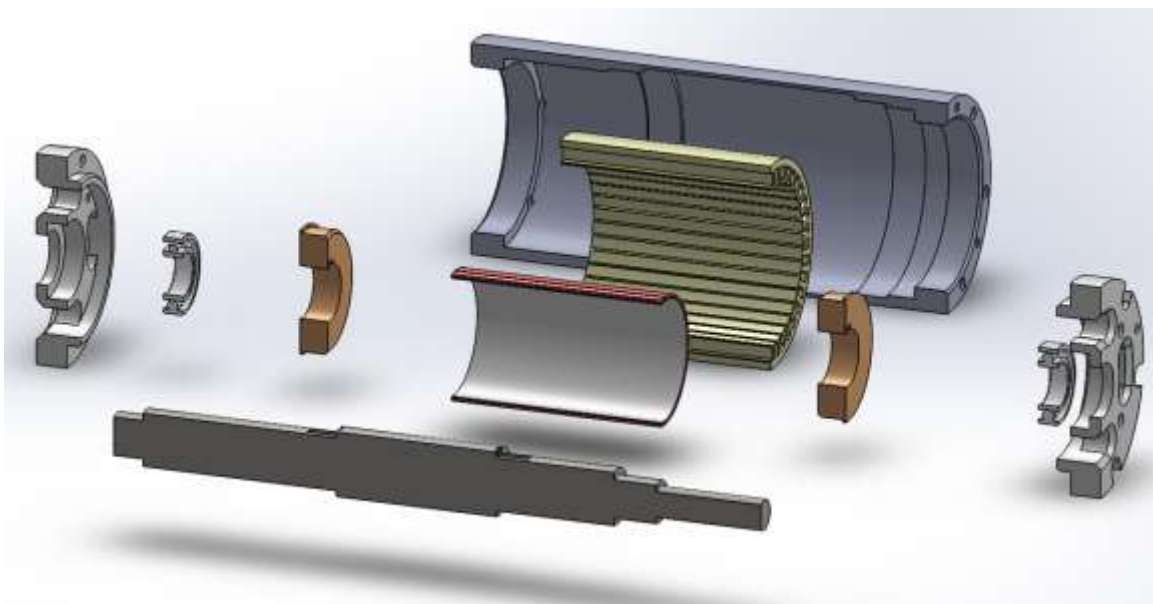


**Figure O.2** Exploded section view of 2015 Endurance motor

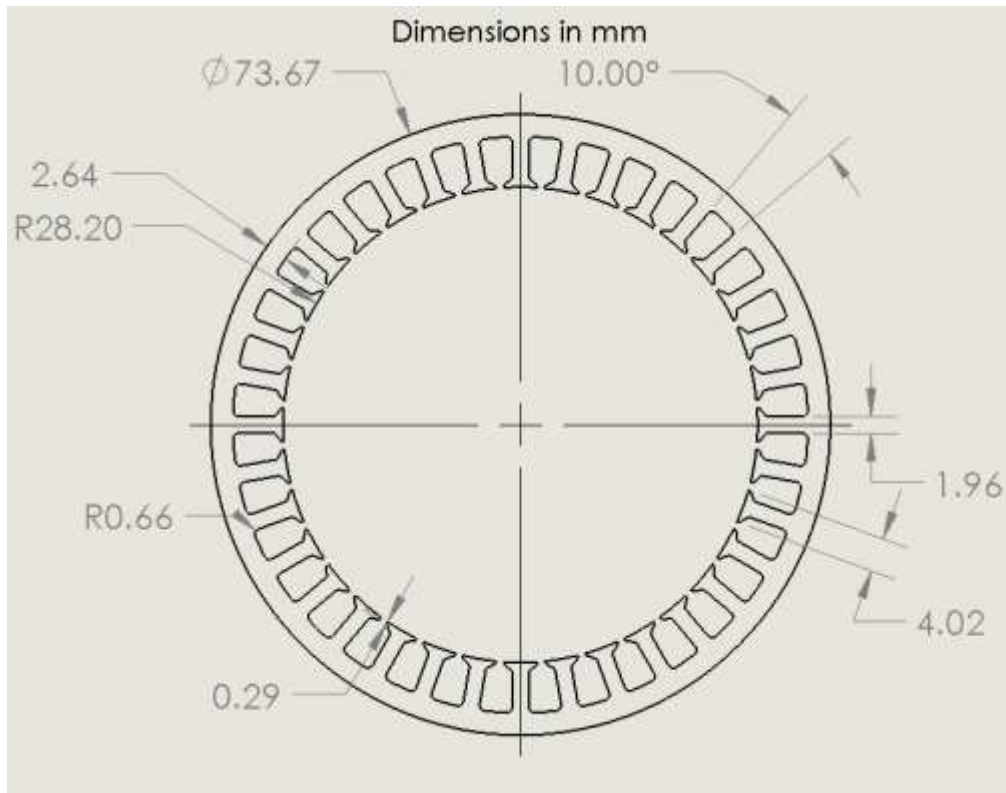


**Figure O.3** 2015 endurance motor lamination drawing

Figure O.3 is new lamination pattern for the 2015 endurance motor. The new lamination pattern and pole number is the main feature the new motor is designed around. The space limitation of the motor pod constricted the new motor design to have the same outer diameter with only the potential for small adjustments in length. Since the major design flaw of the 2014 12 V motor was in the windings, to keep the same targeted power output and efficiency many adjustments needed to be made to the lamination pattern. We increased the number of poles from 9 to 39 and we increased the inner diameter from 42.9 to 56.4 mm.

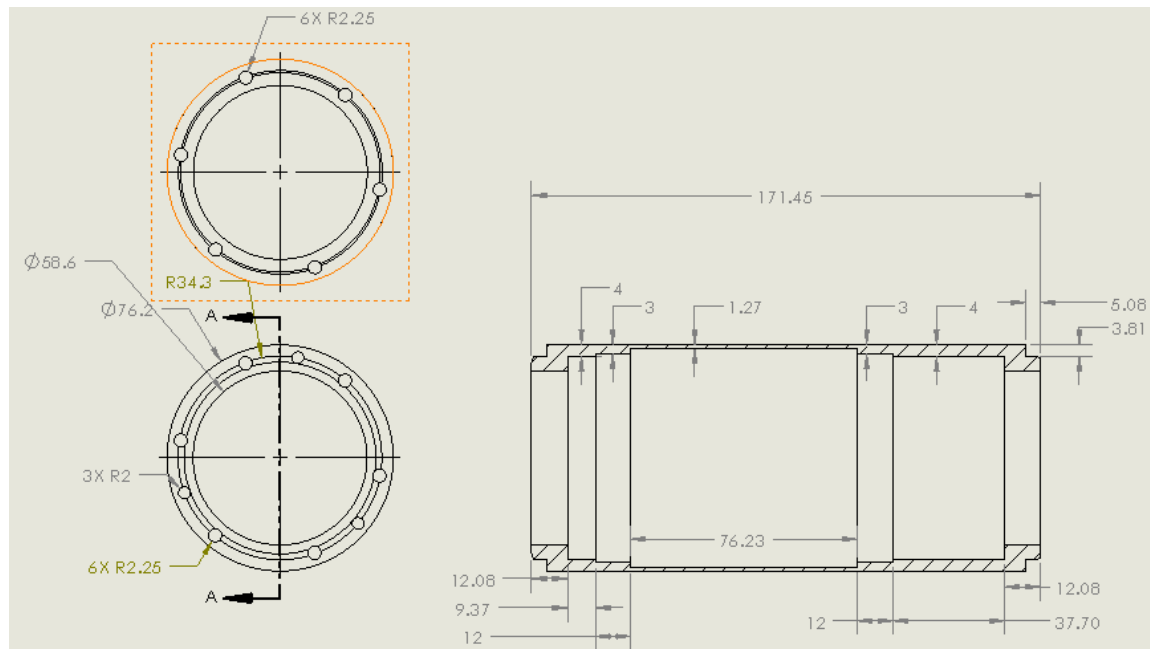


**Figure O.4** 2015 endurance motor aluminum sleeve drawing



**Figure O.5** 2015 endurance motor sleeve

Figure O.4 and Figure O.5 are of the 2015 motor's new sleeve design. The length and outer diameter of the sleeve are the same as the 2014 motors. The inside of the motor was modified to fit the new laminations. With the extra 36 mm of space due to the shorter lamination stack we gave 25.4 mm of extra space to the non-drive and the rest to the drive end. Extra space on each end will make it much easier for our manufacturer to make perfect windings.

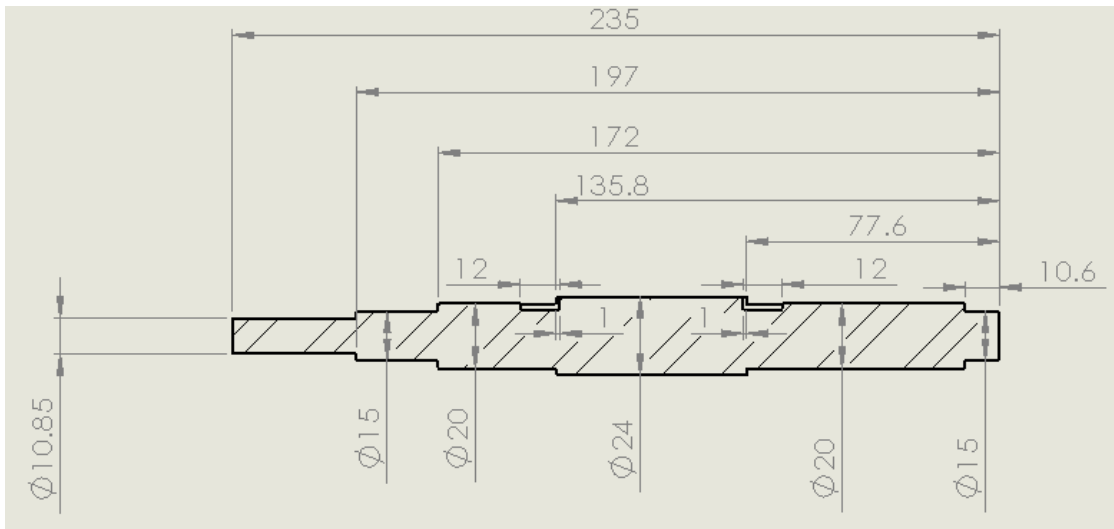


**Figure O.6** 2015 endurance motor shaft drawing

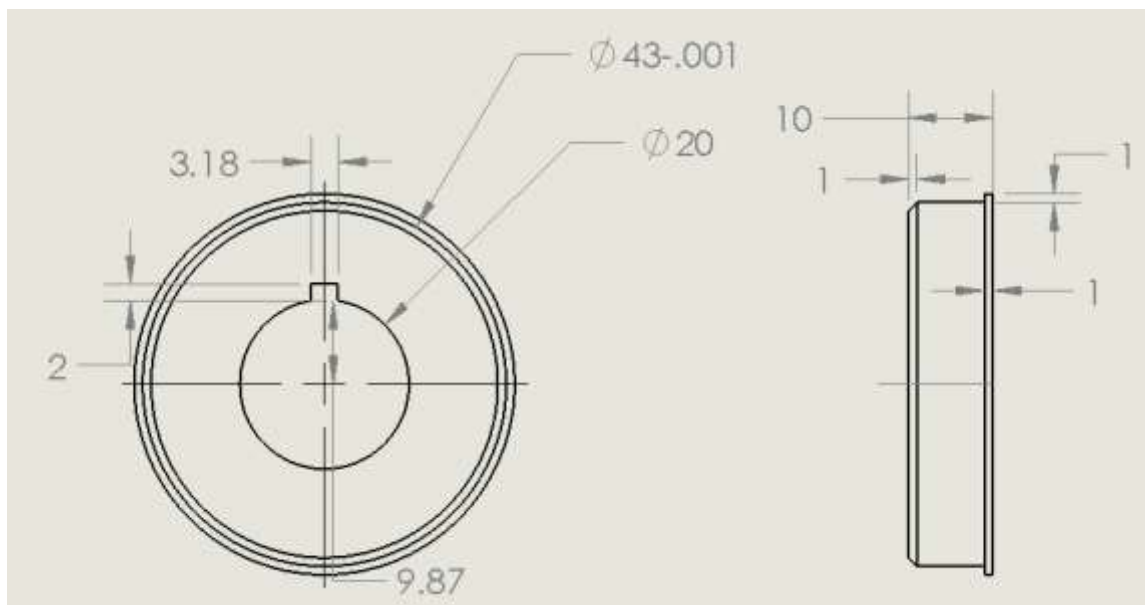


**Figure O.7** 2015 endurance motor rotor slug drawing

Figure O.6 is the new rotor shaft design and Figure O.7 is of the rotor slugs. The rotor needed to be redesigned because we decided to alter the way we would attach the magnets to our shaft. The magnets are on a thin aluminum sleeve that will slide on top of the slugs. We chose to use the magnetic sleeve design because it can better support more poles which is needed to work with our new lamination design.

Figure O.8 is a section view of the four motor parts we are building assembled together.

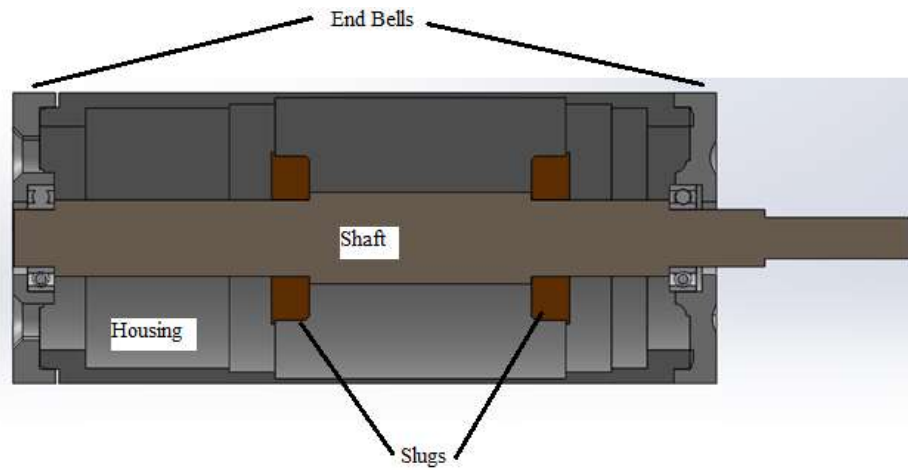


**Figure O.8** 2015 Motor Sleeve, slugs, shaft, and end bell assembly

## **Appendix P – Contra-Rotating Gear Box Design**

The first step in the design of the gear assembly was to choose between a bevel gear system and a planetary gear system. In the past the solar boat team has used a bevel gear CRP system with some success. The previous bevel gear system used bevel gears sourced from the sprint drivetrain that were not the ideal match for an endurance drivetrain. We decided to use a planetary gear system because we already had two planetary gearboxes that were advertised as 94% efficient. The goal was to design a CRP system that could utilize one of the current planetary gearboxes.

The decision was made to use parts of an existing planetary gearbox with some modifications to transform a single power input into concentric contra-rotating power outputs. The first design challenge was to determine how the existing gears could be used to generate contra-rotating motion. We observed that in a simple system of planetary gears, the rotation of the sun gear (power input) causes the planet ring (power output) to rotate by pushing against the ring gear (stationary and attached to the body of the gearbox). This concept is shown in Figure P.1 using a picture of the gearbox. We determined that the force applied to the pod by the ring gear could be applied to another propeller instead, producing contra-rotating motion.

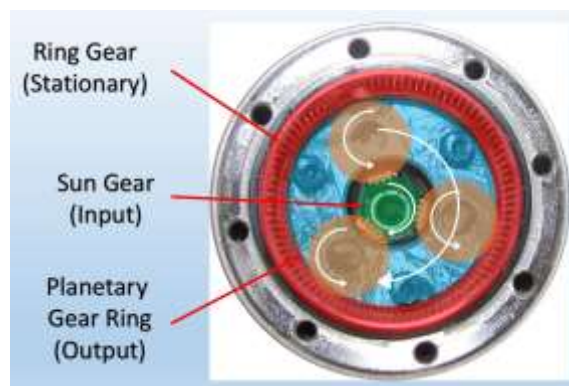


**Figure P.1.** Planetary gearbox primary components

The first design was a sectional hand sketch to sort out the shape and assembly of the parts. We then generated a rough CAD assembly of the design as a dimensioned proof of concept. The hand sketch and CAD model are shown in Figure P.2. This design was discarded immediately for many reasons, including the fact that the gearbox is completely exposed to water. The concept, however, was maintained throughout all additional design iterations.

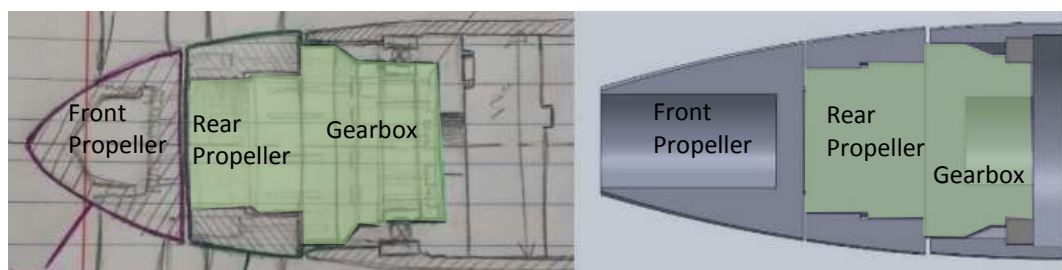


**Figure P.2.** Initial design sketch and subsequent CAD model

We redesigned the whole assembly to include a pair of nested shafts. This design was also originally drafted by hand which allowed us to work out some design issues before devoting time to the creation of CAD models. The addition of shafts afforded the use of smaller seals to keep the water out and also moved the gearbox back into the pod. We were also able to spread out the pairs of bearings that supported each prop for improved alignment. We determined that each piece of the assembly should fit into the back of the next larger piece so that thrust was transmitted through bearings from the inner shaft to the outer and finally to the pod. This also



allows the system to be easily assembled. Finally, we generated CAD drawings from the revised sketches. The revised hand sketch and preliminary CAD model are shown below in Figure Q.3.

We decided to pursue this design and spent the majority of the remaining time revising this design to fit available parts and decrease manufacturing difficulty. The final design is shown in Figure P.4.

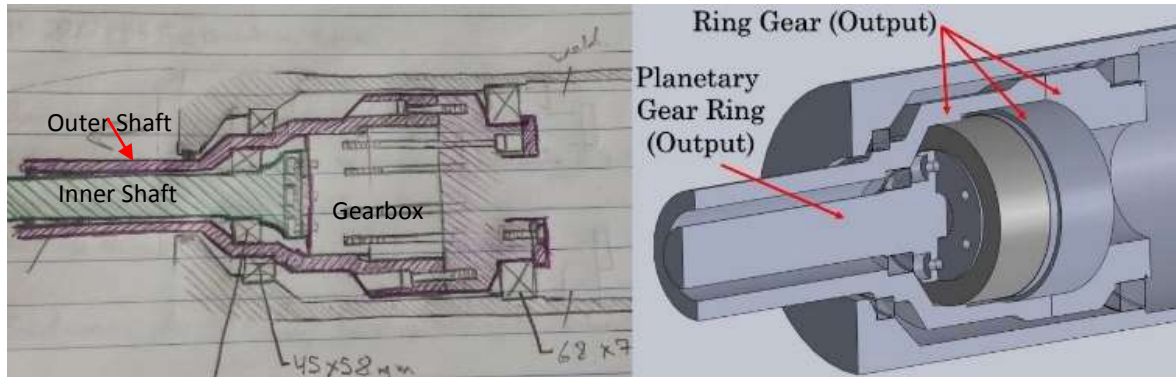


**Figure P.3.** Early Sketch and subsequent CAD model of revised design including shafts

Finally, we decided to use snap rings to secure the aft propeller for ease of removal since a threaded nut that large (~1.6" diameter) would be difficult to remove with limited tools. There is also an internal snap ring in the end of the outer shaft that retains the inner seal and shaft alignment bearing. The outer seal is set into the face of the pod and seats around the outer shaft. The fore propeller is secured with a nut that is screwed onto the threaded end of the inner shaft.

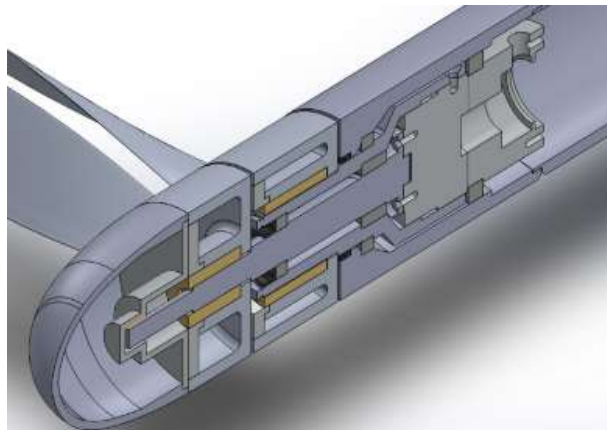


**Figure P.4.** Section view of CRP Assembly.

## **Appendix Q - Instructions, Sample Inputs, and Outputs from Iterative CRP Version of OpenProp**

This year a significant part of our propeller work was to edit OpenPropSingle.m to create OpenPropCRP.m. This appendix describes the use and structure of this program.

### *How to use OpenPropCRP.m*

To use OpenPropCRP.m, first download the program's files and have MATLAB software downloaded to the computer. Then within the highest-level folder navigate to the SourceCode folder and open the file OpenPropCRP.m. Click "Run" and the image shown in Figure Q.1 will be displayed. At the left-hand side input the specifications. The image below shows the Solar Splash 2015 Endurance specifications. Each propeller can have different specifications except for the grayed-out "aft" fields. The default direction of rotation is a right-handed front prop and left-handed rear prop. Click the checkbox at the top to switch those. The default number of panels, 20 in each direction, has been shown to be sufficient for most purposes by the creators of OpenProp. We calculated 998 kg/m as the fresh water density in Ohio in June. The hub diameter is 0.0888 m for a 3.5" hub. This number should be slightly less than the actual hub diameter so that the two bodies meet in SolidWorks. If the hub diameter is tapered, one may run into issues with mating the two bodies. We are not sure how to solve that problem, but it seems to have been done in previous years.

For cavitation analysis, the shaft centerline depth for the Solar Splash forward-facing drivetrain is currently 0.57 m. We assumed no inflow variation. We did not edit anything in Blade Design Values except thickness ( $t_0/D$ ). The chord length column ( $c/D$  or  $XCL_{max}$  depending on if Chord optimization is checked) sometimes has issues but right now seems OK. We have not looked into the reasons for the default  $XCL_{max}$  (max lift coefficient) and  $C_d$  (drag coefficient) values. That is something that should probably be done.  $X_s/D$  is rake. Inflow profile values we always left blank. Those are only needed if the incoming flow is anything other than the boat speed. In reality it is a little slower than the boat speed since the friction of the hull causes the water to speed up, but we assumed it was not significantly slower.

On Options, one will generally want to create a propeller, with hub effects, chord optimization, and viscous forces. The optimization plots are not very helpful. OpenPropCRP.m can perform three primary functions: on-design analysis, geometry generation, and off-design analysis. The first of these is always performed and forms the first step of predicting performance at the specified boat and shaft speeds. Check geometry plots perform the geometry generation as well, which displays propeller geometry and enables exporting to SolidWorks as well. Check performance curve to run an off-design analysis. This should only be done if an on-design analysis has already been performed and the program is being run on a fast computer, as the CRP performance curve creation takes a long time—about ten minutes on one of the senior design computers.

Due to the original code's operation cavitation analysis cannot be run unless off-design analysis is also run. This may be possible to fix since we think the cavitation analysis is only for the on-design case. For Airfoil type, literature suggests that the NACA a=0.8 (modified) meanline and the NACA 65A010 (modified) thickness offer good performance for marine propeller applications, including low risk of cavitation. Once inputs have been completed, enter a filename prefix, save the inputs, and select the run button. At later sessions, simply load the \_GUIsd file to avoid having to re-enter all the inputs.

## OpenProp v3.3.4 CRP

☐ LH front prop

Number of blades:  
 Rotation speed (RPM):  
 Rotor diameter (m):  
 Torque per prop (Nm):  
 Ship speed (m/s):  
 Hub diameter (m):  
 Fluid density (kg/m<sup>3</sup>):  
 # radial panels:  
 # chordwise panels:  
 CRP separation (m):

Fore  
 2  
 333  
 .5  
 11.6  
 4  
 .0888  
 998  
 20  
 20  
 .05

Aft  
 2  
 333  
 .5  
 11.6  
 4  
 .0888  
 998  
 20  
 20  
 -0.05

Blade Design Values

r/R	XCLmax	Cd	t0/D	Skew	Xs/D
0.2	0.5	0.008	0.021933	0	0
0.3	0.4625	0.008	0.018733	0	0
0.4	0.425	0.008	0.015933	0	0
0.5	0.3875	0.008	0.0132	0	0
0.6	0.35	0.008	0.010667	0	0
0.7	0.3125	0.008	0.0083333	0	0
0.8	0.275	0.008	0.0060667	0	0
0.9	0.2375	0.008	0.004	0	0
0.95	0.21875	0.008	0.003	0	0
1	0.2	0.008	0	0	0

Inflow Profile Values

r	Va/Vs	Vt/Vs

Options

☒ Propeller  
☐ Turbine  
☒ Hub  
☒ Chord optimization  
☒ Viscous forces  
☐ Optimization plots  
☒ Geometry plots  
☒ Performance curve

**Airfoil type**  
 Meanline type:  
 NACA a=0.8 (modif...  
 Thickness type:  
 NACA 65A010 (mo...

**Cavitation Analysis**  
 Shaft centerline depth (m):  
 Inflow variation (m/s):  
☒ Perform cavitation analysis

Fore  
 .57  
 0

**Non-dimensional Parameters**

Fore  
 $J = V/nD =$   
 $L = \omega \cdot R/V =$   
 $KQ = Q/(\rho \cdot n^3 \cdot D^5) =$   
 $CQ = Q/(1/2 \cdot \rho \cdot V^2 \cdot \pi R^3) =$

Aft  
 $J = V/nD =$   
 $L = \omega \cdot R/V =$   
 $KQ = Q/(\rho \cdot n^3 \cdot D^5) =$   
 $CQ = Q/(1/2 \cdot \rho \cdot V^2 \cdot \pi R^3) =$

1.4414  
 2.1795  
 0.012075  
 0.029598

1.4414  
 2.1795  
 0.012075  
 0.029598

**Tools**  
 Filename prefix:  
 Laskowski\_SS\_CRP\_0\_0\_1  
 Load  
 Save  
 Run OpenProp

Figure Q.1. Input screen to OpenPropCRP.m

## OpenProp v3.3.4

### On-design Performance - Front

**Figures**

From Inputs:

Expanded Blade

Blade Thickness

Inflow Profile

Parametric:

Effy vs D

Effy vs N

Design results:

Design Performance

Circulation Distribu...

Induced Velocity

Inflow Angle

Expanded Blade

Blade Thickness

Lift Coefficient

2D Geometry

3D Geometry

Performance Curv...

☒ SI    ☐ Engli...

J =	1.4414	Ship speed (Vs) =	4	m/s
KT =	0.049209	Rotation speed (N)	333	RPM
KQ =	0.012075	Diameter (D) =	0.5	m
EFFY =	0.94694	Thrust (T) =	94.5452	N
EFFYo =	0.93491	Torque (Q) =	11.6	Nm
CT =	0.06031	Power (P) =	404.5114	W
CQ =	0.029598			
CP =	0.064509			
P/D =	1.4736			
Slip =	0.021811			

**Figure Q.2.** On-design Performance Output Screen

The first page that will be displayed is the on-design performance output screen (Figure Q.2). EFFYo is the open water efficiency and is the value that we really care about generally. The other efficiency is proportional to the incoming flow rather than the boat speed. I also added the pitch to diameter ratio P/D and Slip to this page.

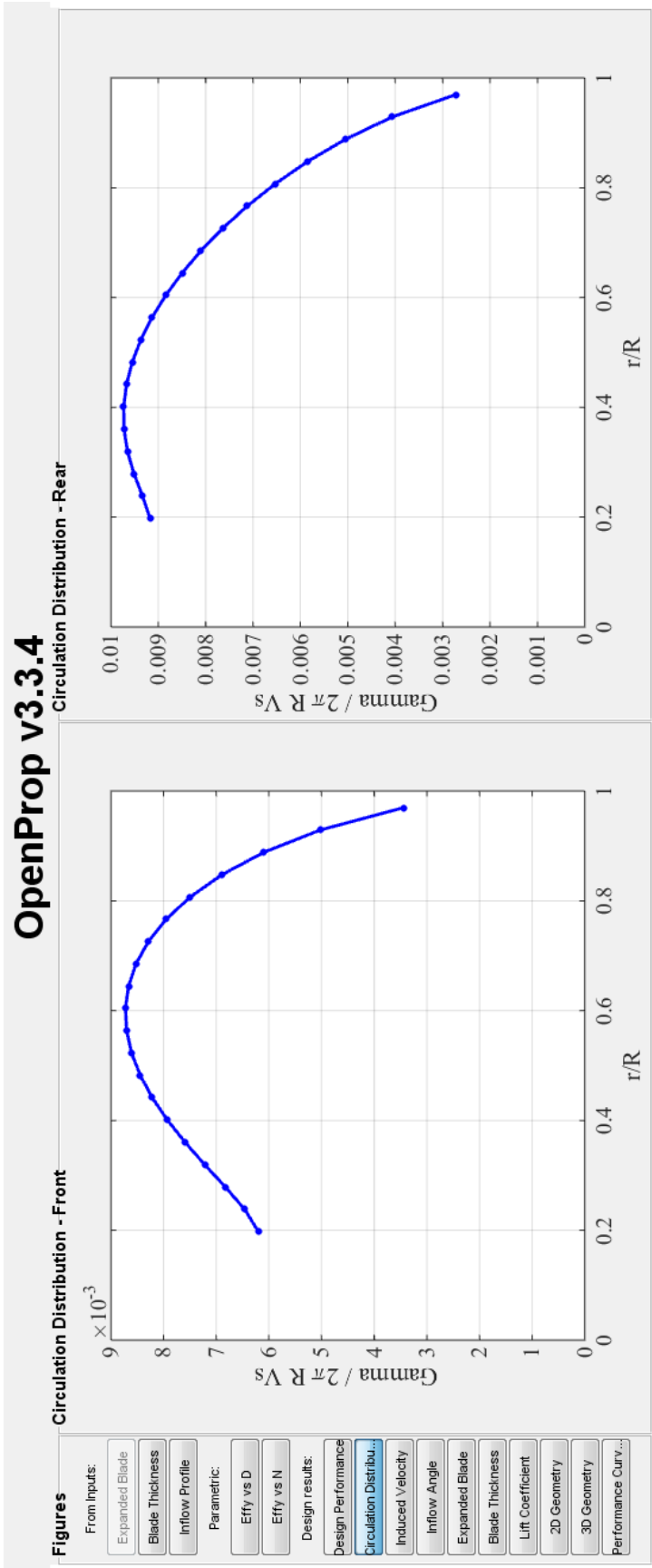
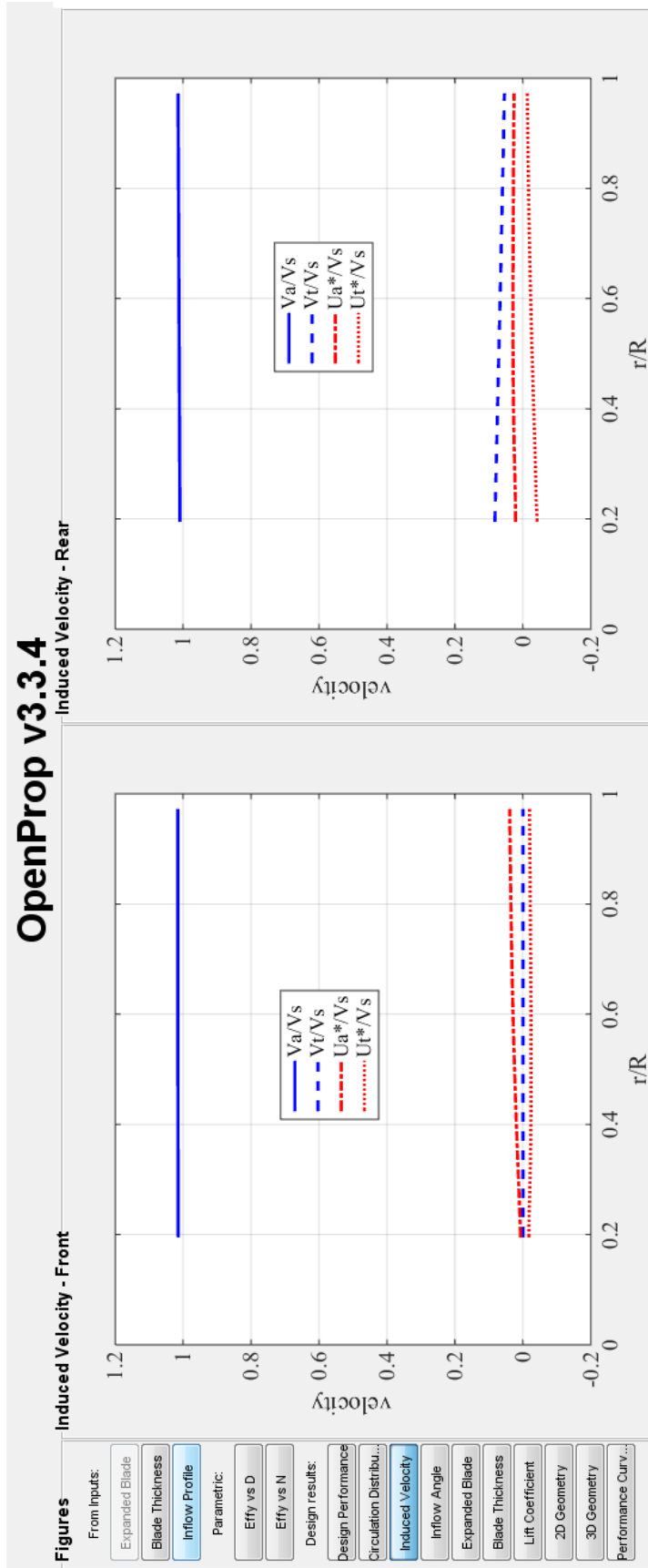


Figure Q.3. Circulation distribution plots

The next tab down is the circulation distribution plots (Figure Q.3). The textbook *Marine Propellers and Propulsion* available at the Cedarville University library has a good explanation of what circulation is. It is basically equivalent to the force that the propeller exerts on the water.



**Figure Q.4.** Incoming and induced velocity plots

The next tab is the incoming and induced velocity plots (Figure Q.4). Notice how the incoming tangential velocity of the rear propeller is non-zero. On this graph, the tangential velocities are positive in the direction of apparent incoming flow. Thus the induced tangential velocity for the front propeller in this case is negative, while the incoming flow to the rear propeller is positive.



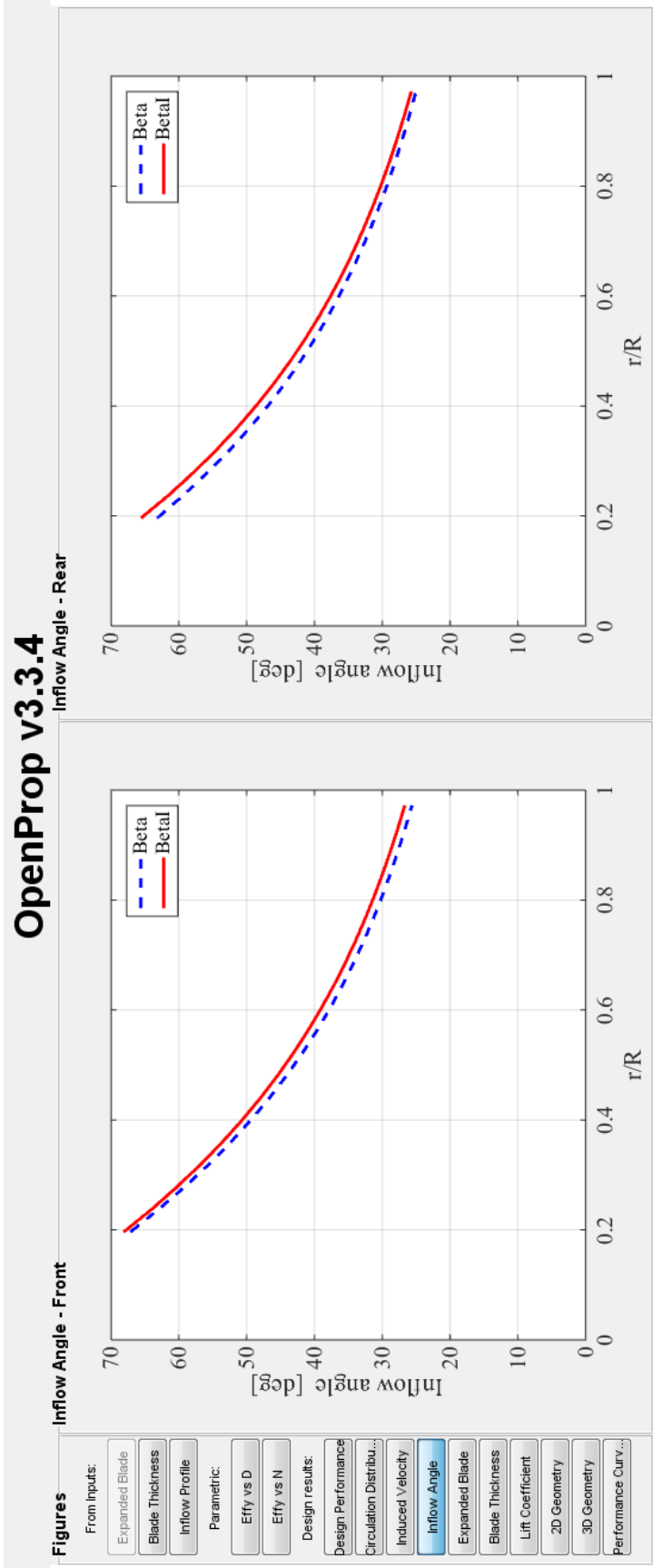


Figure Q.5. Flow angle plots

The next tab is the flow angle plots (Figure Q.5). Beta is the undisturbed inflow angle and Betal is the hydrodynamic pitch angle.

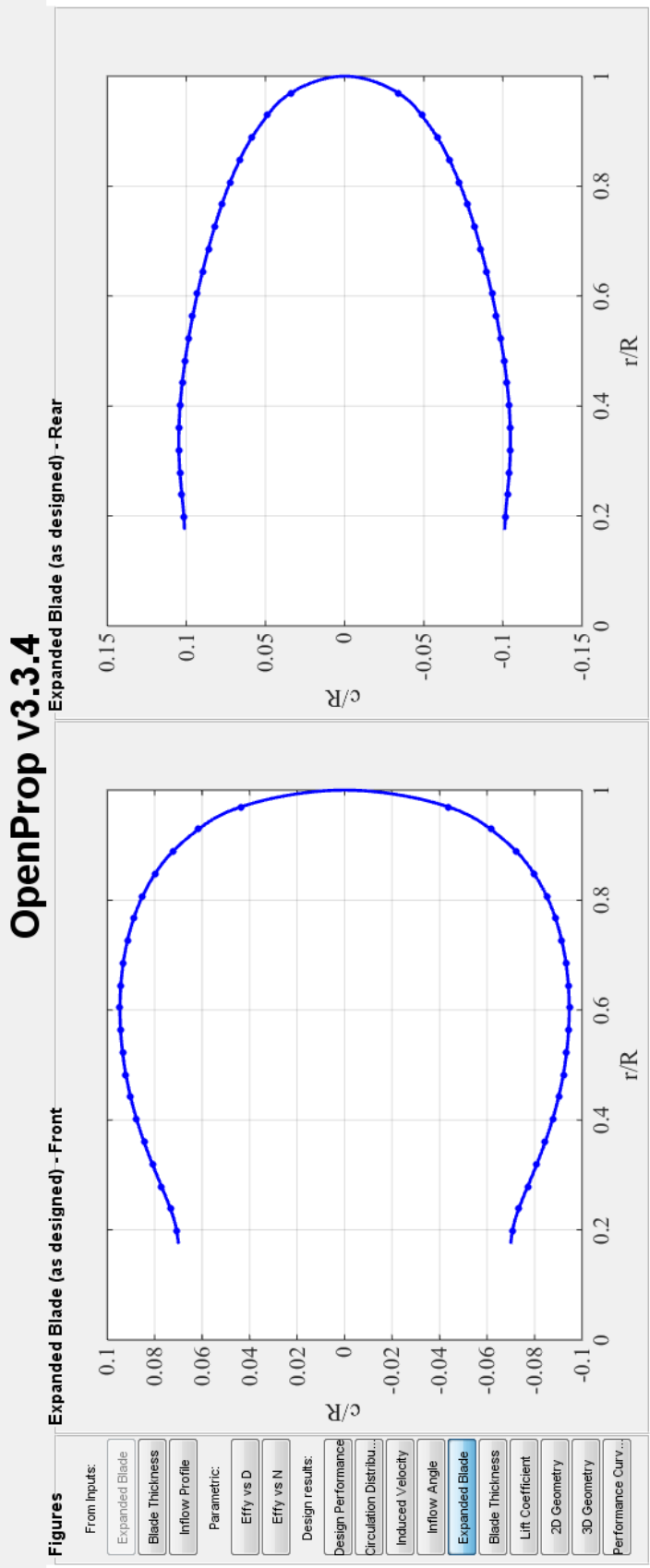


Figure Q.6. Expanded Blade Plots

The next tab is the expanded blade plots (Figure Q.6).

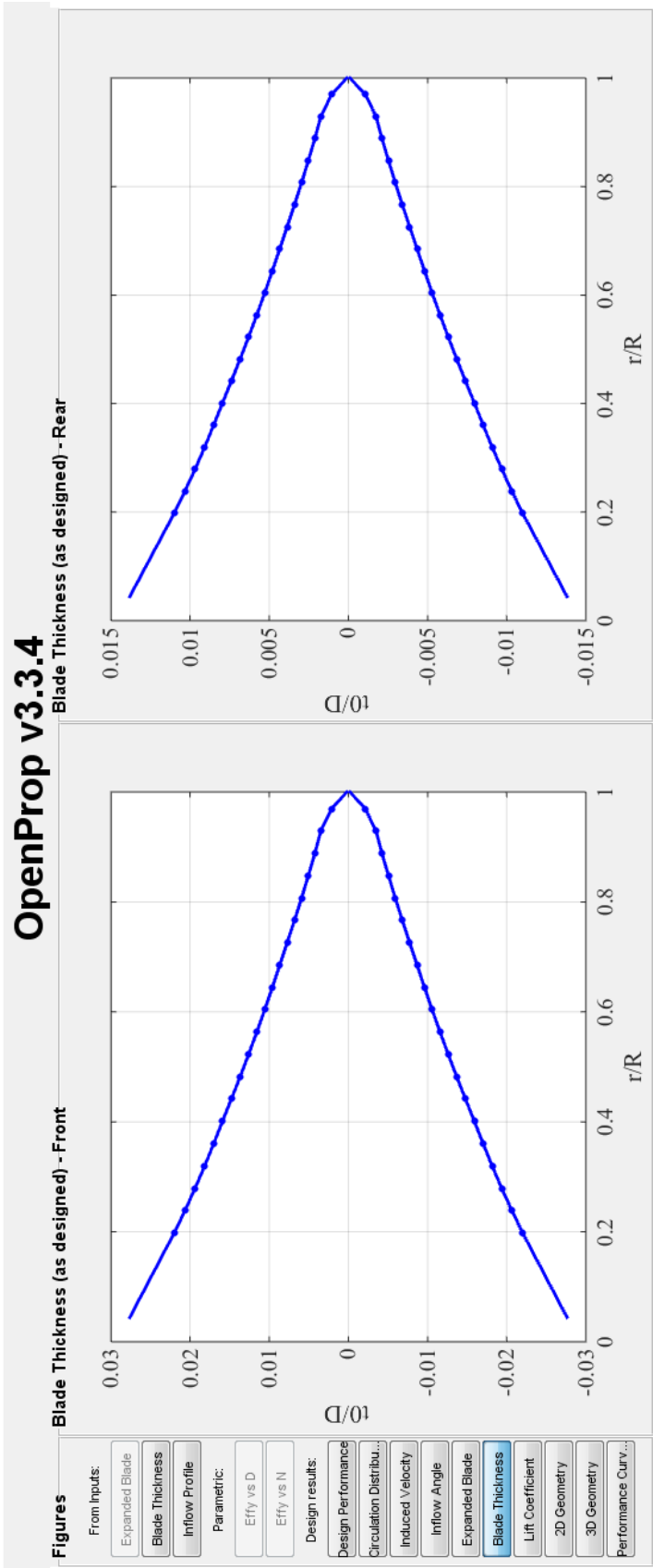


Figure Q.7. Blade Thickness Plots

The next tab is the blade thickness plots (Figure Q.7).

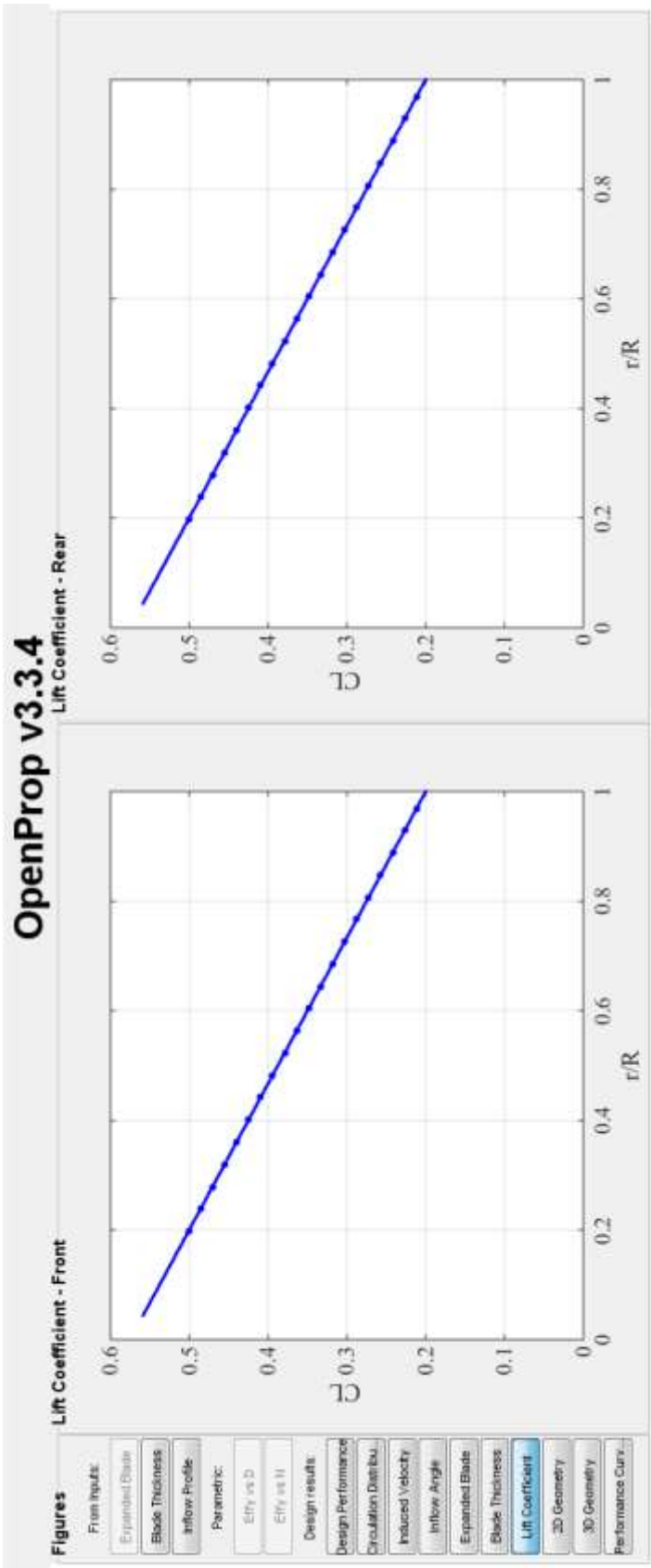


Figure Q.8. Lift Coefficient Plots

The next tab is the lift coefficient plots (Figure Q.8).

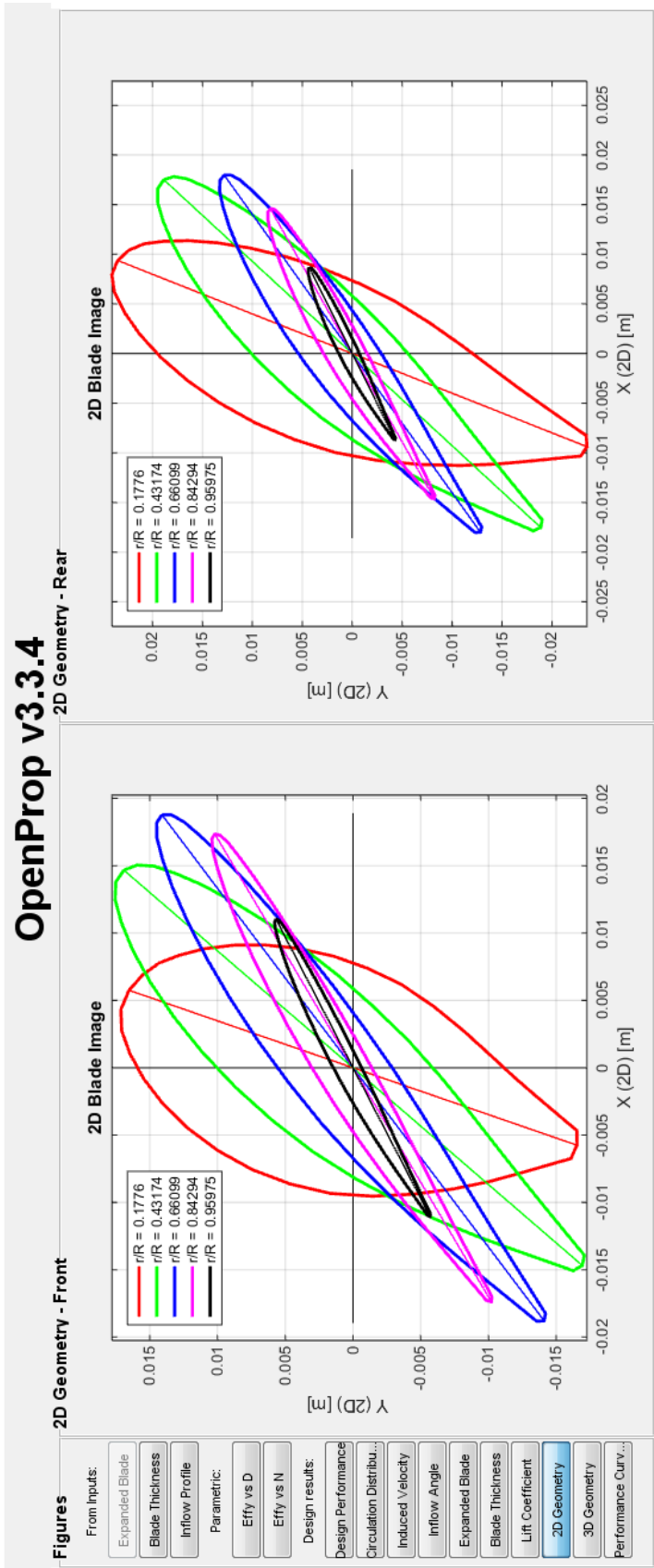


Figure Q.9. 2D Geometry Plots

The next tab is the 2D geometry plots (Figure Q.9).

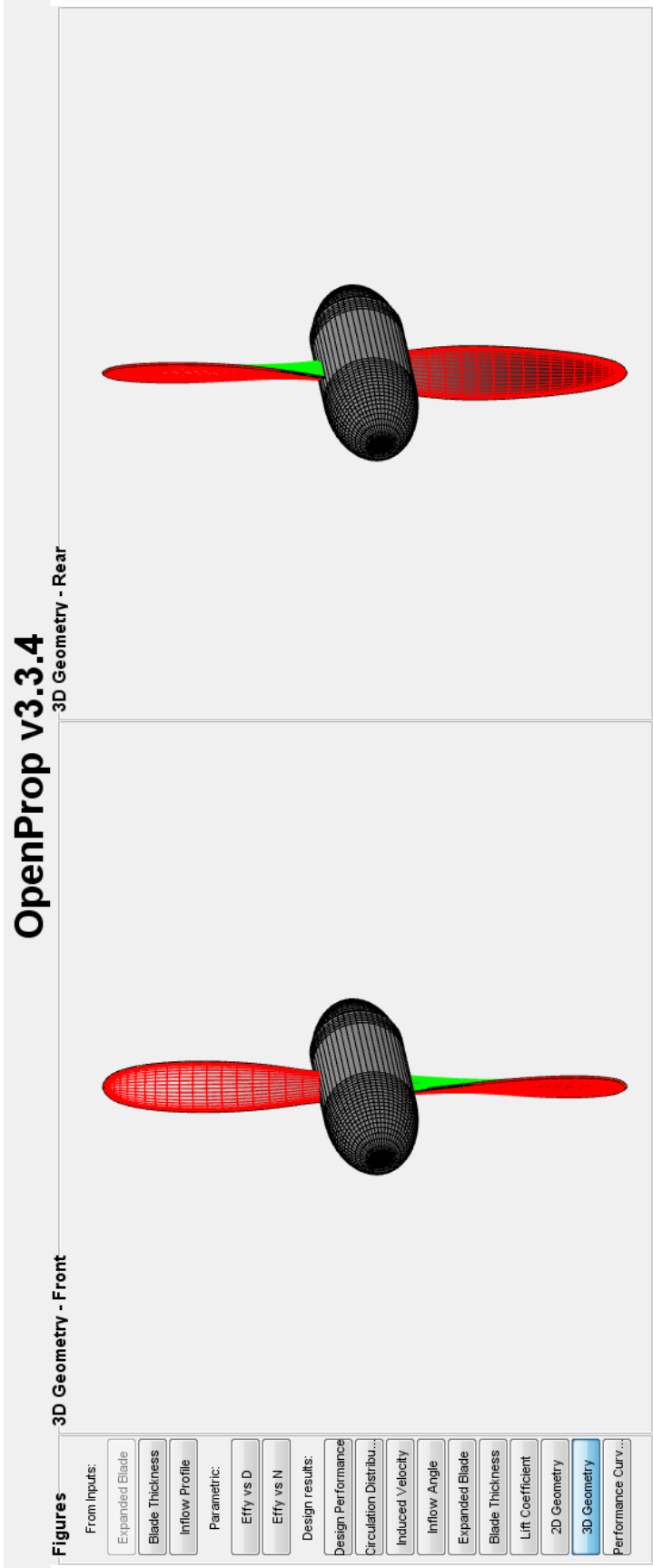


Figure Q.10. 3D Geometry plots

The 3D geometry plots found on the next tab (Figure Q.10) can be rotated in all three axes for visualization purposes.



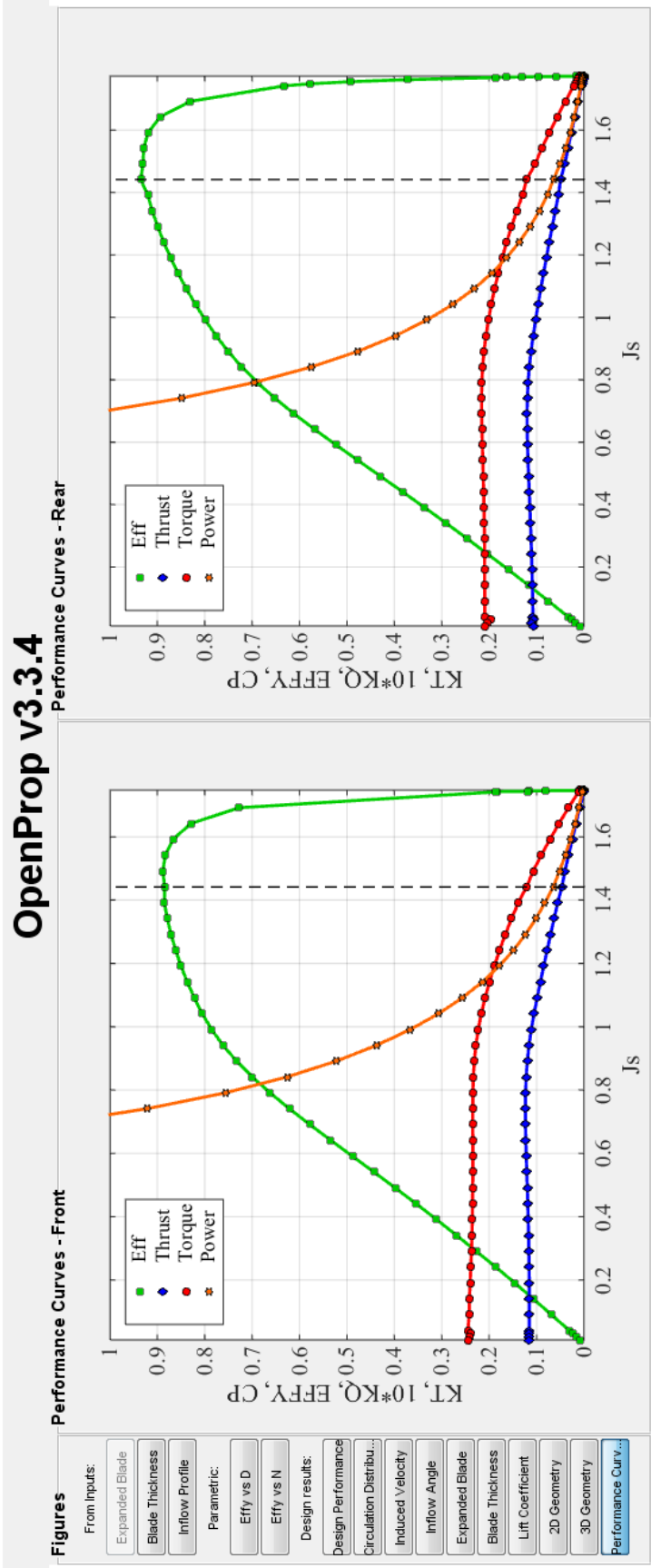


Figure Q.11. Off-design performance curves

The last tab, shown in Figure Q.11, shows the predicted off-design performance of the design.  $KT$  and  $KQ$  are non-dimensional thrust and torque based on blade tip speed.  $CP$ , which we added to this graph, is non-dimensional power based on boat speed. We had a hard time understanding how to interpret this graph since it is non-dimensional and hard to dimensionalize since when the boat speed changes, so does the tip speed. One way we tried to dimensionalize it was by assuming that thrust, which should be the same as drag, was proportional to boat velocity squared. However, that did not seem to help anything. The most basic understanding we have grasped about this graph is that power is low at the right-hand side. At a certain point, increasing power has diminishing returns in terms of thrust. What we tried to make sure of on this graph was that the operating point (the dotted line) was somewhat centered on the efficiency curve and on the sloped regions of the thrust and torque curves. It is possible to use an off-design point as the inputs to `OpenPropCRP.m` in order to try to improve the off-design performance.

The next pages show cavitation analysis figures. The first figure is a simplistic plot with either green (no cavitation predicted), yellow (risk of cavitation), and red (cavitation predicted). The second and third sets of figures shows more detail.

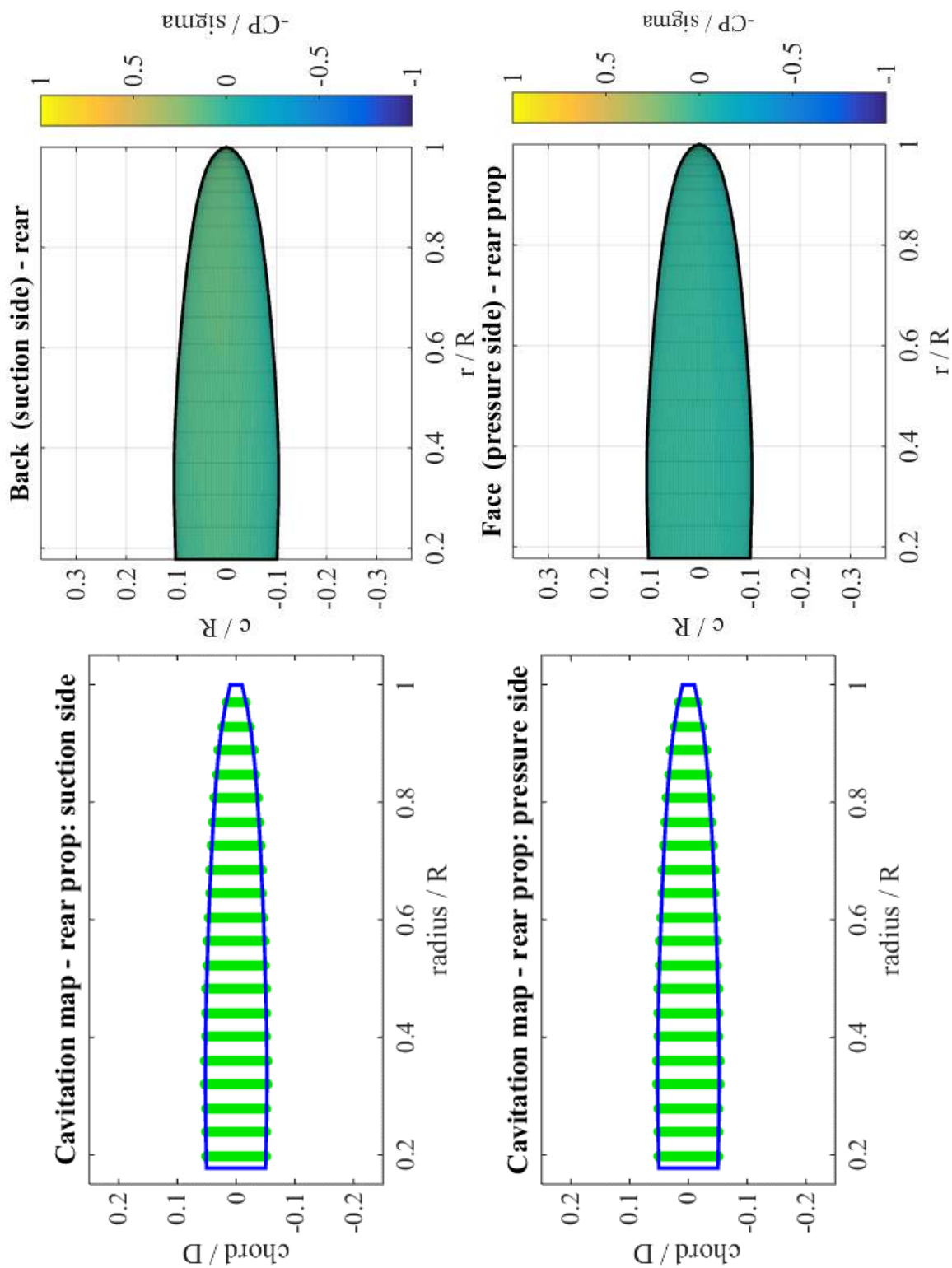
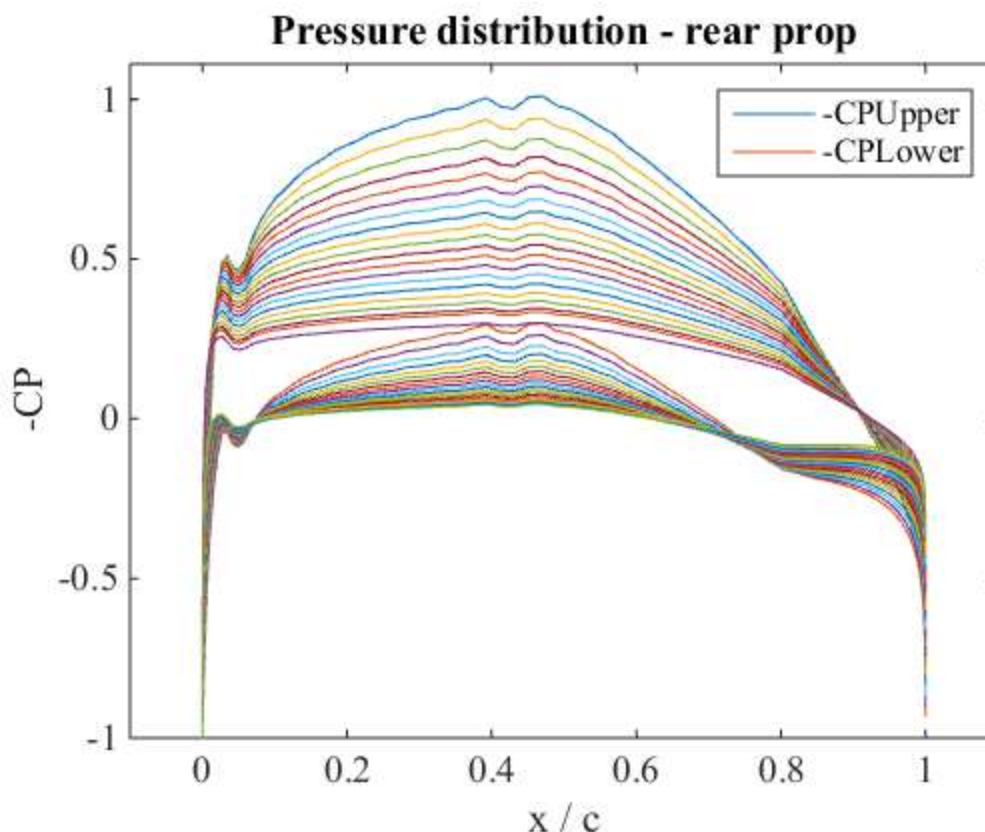


Figure Q.12. Cavitation plots of the rear propeller



**Figure Q.13.** Pressure distribution plot for the rear propeller

In separate windows, the cavitation plots (see for example Figure Q.12) and pressure distribution plots (see for example Figure Q.13) are produced for each propeller. Each line on the pressure distribution plots represents a different radius (20 total). The plot shown here has smooth curves without spikes on the upper surface, which indicates that the chosen foil shape avoids low pressure regions that can lead to cavitation.

Using the Edit > Copy Figure functionality of MATLAB works well for copying a lot of these results to Word for documentation.

After finishing with OpenPropCRP.m, another helpful tool to use is stress analysis. To perform a stress analysis, open MATLAB and open the primary .mat file that was created by OpenPropCRP.m (for example MyCRPs.mat). The pt1 and pt2 variables should appear in the Variables window. Set the working folder to SourceCode, then type 'Stress\_Analysis(pt1);' into the command window. The command window will display the maximum root stress at design conditions and the maximum rate of change of shaft speed (in rev/s) to keep that value under half the yield stress of aluminum 6061. Make sure this is a reasonable proportion of the design shaft speed. It will also produce a 3D plot of the stress. Confirm on this plot that the maximum stress (indicated by the red square) occurs at the root, since the analysis makes this assumption. Then do the same for pt2 (the aft propeller). Following is a sample, including the output figure shown in Figure Q.14.

```
>> load('Laskowske_SS_CRP_0_0_3.mat')
>> Stress_Analysis(pt1);
```

```
MAX_STRESS =
```

```
6.7040e+07
```

```
MAX_n_dot =
```

```
219.1221
```

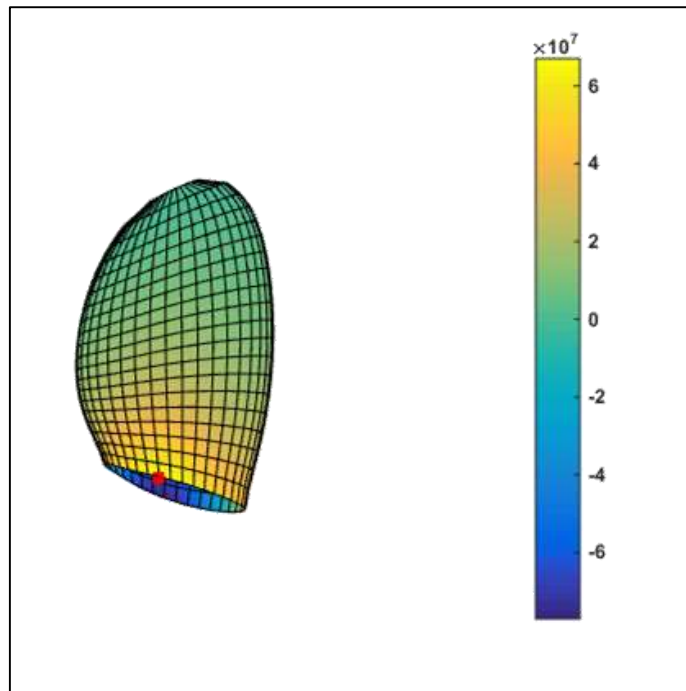


**Figure Q.14.** Stress analysis plot on a plot

### *OpenPropCRP.m Program Structure*

OpenPropCRP.m is a modification of OpenPropSingle.m. Both of these programs are tied together with many of the other .m files in the SourceCode folder. We have made modifications to a variety of these files. If the changes were only applicable to the CRP case, we renamed them with a CRP suffix.

The vast majority of the actual file OpenPropCRP.m is taking care of logistics such as GUI creation. It is also the “hub” of activity, taking inputs and sending them to various functions to produce results. However, very little actual activity takes place in OpenPropCRP.m. What follows is a general description of the “skeleton” of the program. Besides reading this, we also encourage going through the program reading comments and seeing where the different functions are called. Also very helpful is the file OpenProp\_v2\_4\_theory.pdf found in the Reference folder.

First, OpenProp closes all current figures and variables. It then initiates several global variables. It defines the default input values and creates the input GUI. After that it waits for the user to interact with the GUI. Upon entering values, clicking on checkboxes, etc., the GUI updates the input variables as well. That is all that lines 60-950 do.

The primary function within OpenPropCRP.m is “execute,” which is initiated by clicking the Run OpenProp button. At this point the Plots figure is initiated, and two very important global variables are created that will hold all the information about the propellers, pt1 (fore) and pt2 (aft). These two variables are structure variables and have values stored inside them in different fields. We think of them like apartment complexes. In the pt1 “apartment complex” there is the “input” building, the “design” building, the “geometry” building, and the “states” building. The first is for the inputs, the second for the design results, the third for the geometry results, and the fourth for the off-design results. Within each building there are rooms holding different variables. After running OpenPropCRP.m, one can find the primary .mat file it created and open it up in MATLAB to examine it to understand these structure variables better.

After creating pt1 and pt2, the execute function populates their input structures with the input variables from the GUI (lines 1015-1300). Next, the design optimization is run in a while loop (1305-1355). First, the fore propeller is optimized ignoring the aft propeller using the function EppsOptimizer, which uses linear optimization following the Lagrange Multiplier method to optimize the circulation. It also performs the chord optimization. We modified EppsOptimizer to also calculate the induced velocities at the plane of the other propeller by calling Horseshoe\_intr\_110830. The next step in the while loop is therefore to update the inflow inputs of the rear propeller based on the front propeller design, and optimize the rear propeller. This in turn modifies the inflow to the front propeller, and the procedure is repeated until the circulation results do not change between two consecutive iterations. Convergence typically occurs after about 3-5 iterations if it occurs at all.

Lines 1355-1580 populate the “From inputs” and “Design Performance” panels of the Plots figure. At lines 1587 and 1588, the Make\_Reports function is run to populate the Circulation Distribution, Induced Velocity, Inflow Angle, and Expanded Blade panels. Next, lines 1590-1640 plot the thickness profile and lift coefficient. 1640-1900 calculate and plot the geometry via the Geometry function, as well as plot the parametric study results if they exist. We have commented out the portion that plots the parametric study results because it was preventing the input structures from updating. We think it may have something to do with the way it temporarily switches out the pt variables for temp variables. Lines 1900-2085 run the off-design analysis. This was a very difficult portion to update for the CRP case. The OpenPropSingle off-



design analysis assumes a constant inflow velocity profile. We went to a lot of trouble to make sure that the inflow velocity profile for each off-design state was updated to include the influence from the other propeller. The document *Iterative CRP documentation.docx* documents the results of these modifications.

Lines 2085 to 2100 call `Cav_CavitationMap` to produce the cavitation figures. The rest of the `execute` function saves the GUI inputs and the structure variables to `.mat` files. There is much more to this file and to all the files it calls. Examine the file further as the need and desire arises. We have tried to leave good comments on our modifications to assist with understanding.

## Appendix R – CRP Design Process

First we compared tools available to perform the design task. OpenProp is an open source MATLAB-based program that the team has used in the past. OpenProp is primarily used for conventional geometry propeller design and a description of how to use it for CRP design is available. We also considered three unconventional propeller geometries (square tip, Contracted & Loaded Tip, and Kappel). However, the design methods for these geometries are complex and proprietary. Additionally, the tools that the University currently has available are insufficient (SolidWorks) or too complex (Fluent) for analyzing these geometries. Therefore, we chose to carry out the design using OpenProp. OpenProp has two basic features: Parametric Study and Single Design. Parametric Study is used to choose propeller angular velocity, number of blades, and diameter. Single Design is used to predict more detailed on-design performance, predict off-design performance, and generate blade geometry. In order to gain a working knowledge of OpenProp as well as to help make some design decisions, we first performed three Parametric Studies using last year's modified version of OpenProp. First, we ran a study that showed that propellers designed for the 2015 Endurance specifications could achieve near maximal efficiency at 333 RPM, which was the angular velocity that the proposed new contra-rotating gearbox would produce for the motor design speed of 3,000 RPM. Second, we ran a study for a single propeller for predicted Frisian Solar Challenge 2016 specifications in order to help choose the best propeller angular velocity, an input to the motor design. This study showed that the propeller should operate in the range of approximately 1,000-2,000 RPM. Finally, we also ran a study that indicated that increasing the hub diameter to the diameter of the pod did not reduce propeller efficiency, which helped to decide to use a dome-shaped hub.

Next, we moved on to learning the Single Design feature. In this process, we noticed several differences between the old and new versions

of OpenProp. First, we discovered that several results from the modified version used by the 2014 team did not make physical sense. Next, we discovered that the old and new versions of OpenProp gave very different results. For example, for the 2014 specifications the old version predicted maximal efficiency would be achieved by a propeller 0.37 m (15 in) in diameter, while the new version pointed to a diameter of 0.60 m (24 in), a difference of 62% (see Figure R.1). Upon investigating the differences between the two versions of OpenProp, we discovered that the new version incorporates significant improvements to the propeller model that seem to be responsible for these large differences.

Next, we learned more about CRP design using OpenProp by first replicating the 2009 method using the new version of OpenProp. In order to go through this design method using the

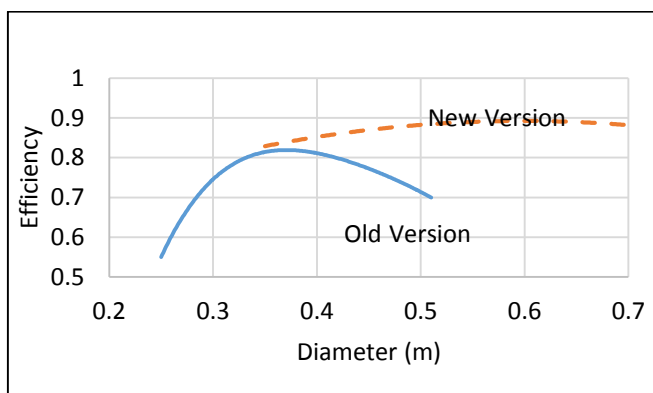


**Figure R.1.** Differences between old and new versions of OpenProp

new version of OpenProp, we modified it to allow the velocity induced by the front propeller at the front propeller plane to be easily transferred to the input of the rear propeller using the GUI. We also modified the code to allow the direction of rotation to be modified using the GUI. In addition, we modified the GUI to enable cavitation analysis. Finally, we learned how to use the stress analysis tool from the command line.

After successfully replicating the 2009 method, we moved on to implement Laskos's 'uncoupled' method. Since the code included in his thesis was incomplete and intended for use with a much older version of OpenProp, we followed his method, but for the most part did not use his code. The basic idea of his 'uncoupled' method is to optimize the front propeller without regard to the rear propeller, then calculate the induced velocities at the plane of the rear propeller, then optimize the rear propeller, calculate the velocities the rear propeller induces at the plane of the front propeller and repeat this procedure until convergence is achieved.

In order to implement Laskos's 'uncoupled' method using the newest version of OpenProp, we first made a plan for how we would go about implementing it. We identified the functions which would be used for the optimization and the induced velocity calculations. We also identified each component that would have to be modified or added to the code. The first modification that we made was to add a second structure variable, for the additional propeller, to the output file. Second, we modified the output figures to show the results of both propellers. Third, we modified the input GUI to allow specification of the direction of rotation, the axial distance between the propeller planes, and a different diameter, number of blades, and torque for each propeller. Fourth, we modified the code to optimize the propellers based on a torque specification rather than a thrust specification. Fifth, we incorporated the while loop from Laskos's code to implement the iterative optimization routine. Finally, we modified the off-design analysis to make it applicable for analysis of CRPs. Instructions to use the modified version of OpenProp, a sample of the primary input and output figures, and a basic description of how the program works can be found in Appendix Q.

In order to validate the modifications we made to OpenProp, we compared the results with published data. First, we found a CRP study that included both theoretical and experimental results. A reproduction of the study in OpenProp predicted a similar geometry and thrust. Next, we compared the 2009-method CRP design with the iterative CRP design for the 2015 Endurance specifications. In most respects, the designs produced by the two CRP methods were fairly similar. The key difference was that the iterative CRP method predicted a significantly higher tangential velocity induced by the front

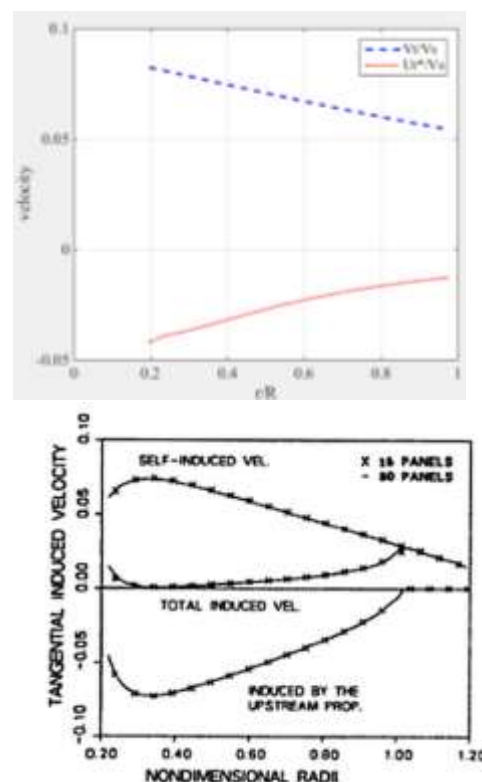


**Figure S.2.** The shape of the induced tangential velocity curve predicted by the iterative CRP method (top) agrees with published scholarly predictions (bottom).

propeller near the root of the aft propeller resulting in a greater chord length and lower pitch in this region. This prediction matches well with the paper presented by Kerwin, Coney and Hsin in 1987, as shown by Figure S.2 (Kerwin, 53-60).

### **Appendix S - 12 V Endurance Motor Testing and Evaluation**

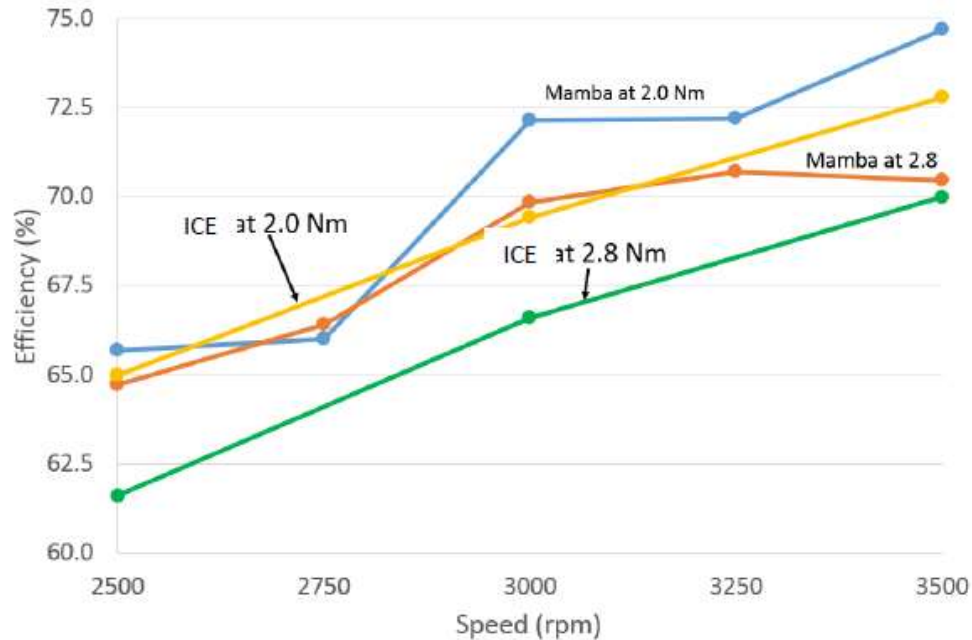
While the new motor is still under construction, lots of testing was conducted to determine the need of a new motor. Table S.1 is a brief summary of the partial throttle efficiency tests conducted with the 12 and 24 V motors. Both motors were tested at the same torques at a speed of 3000 rpm. Then the rotors were swapped between the two stators and the same tests were performed again. The majority of our partial throttle tests were conducted with a Mamba XL2 motor controller.

**Table S.1** 12 and 24 V motor efficiency results with swapped rotors at 3000 rpm

				Rotor	
				12 V (black)	24 V (yellow)
		Voltage (V)	Torque (Nm)	Efficiency (%)	Efficiency (%)
Stator	12 V Al	12 V	2.0	66.4	69.0
			2.5	65.4	65.8
			3.0	63.2	63.8
		24 V	2.0	70.9	63.5
			2.5	63.7	62.3
			3.0	60.1	59.8
	24 V steel	24 V	2.0	80.3	79.8
			2.5	79.1	79.4
			3.0	77.6	78.1

The results from Table S.1 show that the 12 V motor efficiency is significantly lower than it should be and the 24 V motor efficiency is the same. The 24 V motor having the same efficiency as recorded in 2010 let us verify that we had a good test setup. Also, the table shows that swapping the rotors had little effect on the motor's efficiency which let us know that the neither of the rotor's magnets were demagnetized.

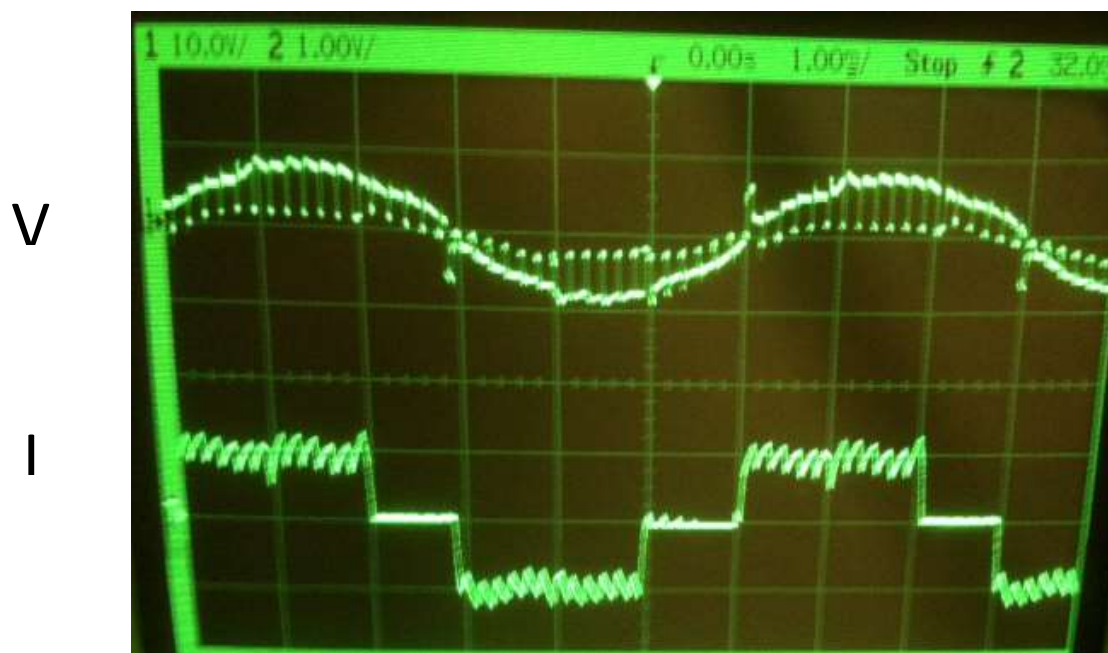
Several of the same partial throttle tests were also conducted with our other motor controllers: the Phoenix ICE 300 and the Jeti SpinPro 300. Figure S.1 is an example of several efficiency tests conducted at different torques and speeds with the Mamba and ICE controllers.



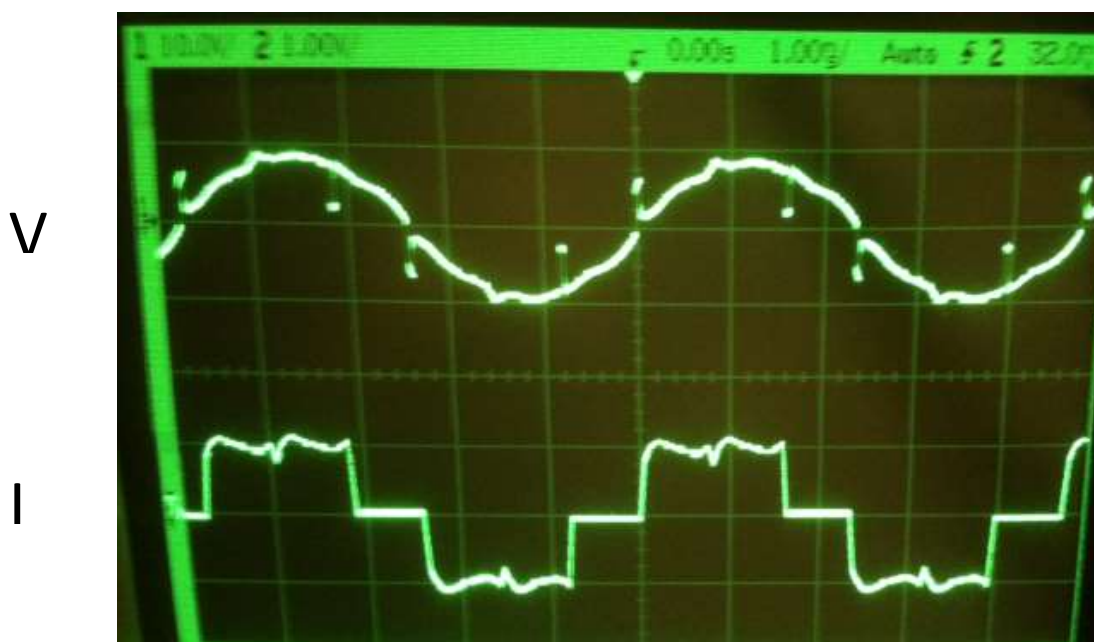
**Figure S.1.** Efficiency test results with Mamba and ICE motor controllers

Figure S.1 shows that the efficiency is affected very little by the different motor controllers. At most the efficiency difference was 3%. The same was true when the Jeti was compared with the Mamba.

We performed tests at WOT (wide open throttle) to see how much more efficient the motor controller would be would become. During these dynamometer test runs an oscilloscope was used to capture the waveform of the current and voltage after the motor controller going into each of the motor's three wires. The voltage was measured using a standard probe and the current was measured using a Rogowski coil. The Rogowski coil was set to X1-10mV/A. Table S.2 shows the data collected during these tests runs. Figures for the 2 Nm test runs have been included for observation. Note: the partial throttles were not all set to exactly the same PWM which is why the data differs for those runs. Also, voltage is the wave form on top and current is the waveform on the bottom.



**Figure S.2** Wire 1 at partial throttle and 2 Nm of torque



**Figure S.3** Wire 1 at WOT and 2 Nm of torque



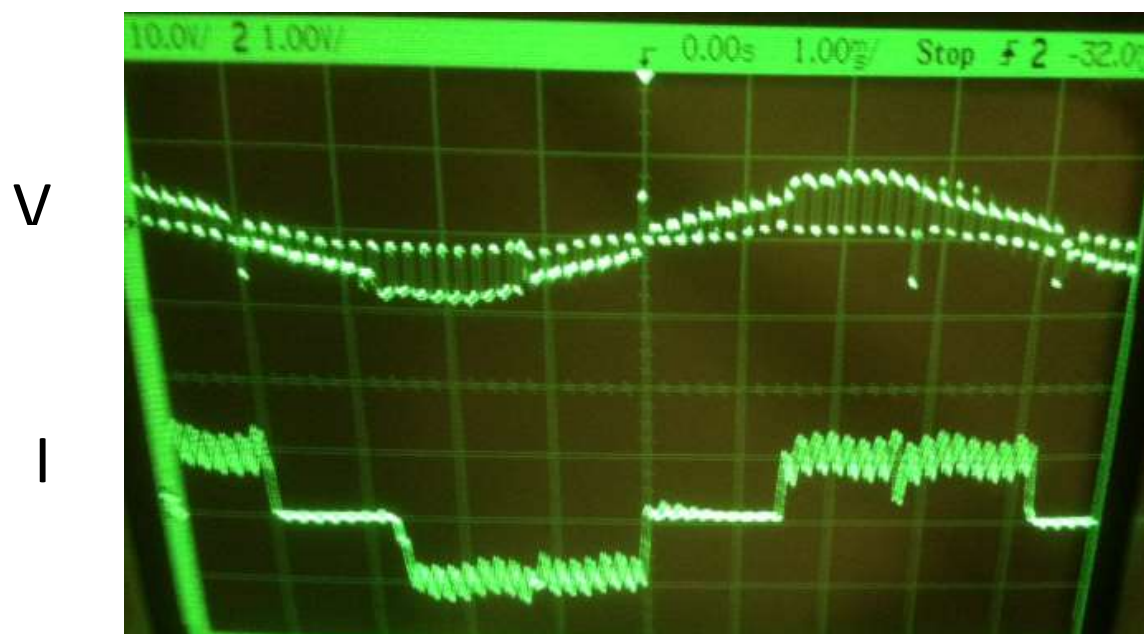


**Figure S.4** Wire 2 at partial throttle and 2 Nm of torque

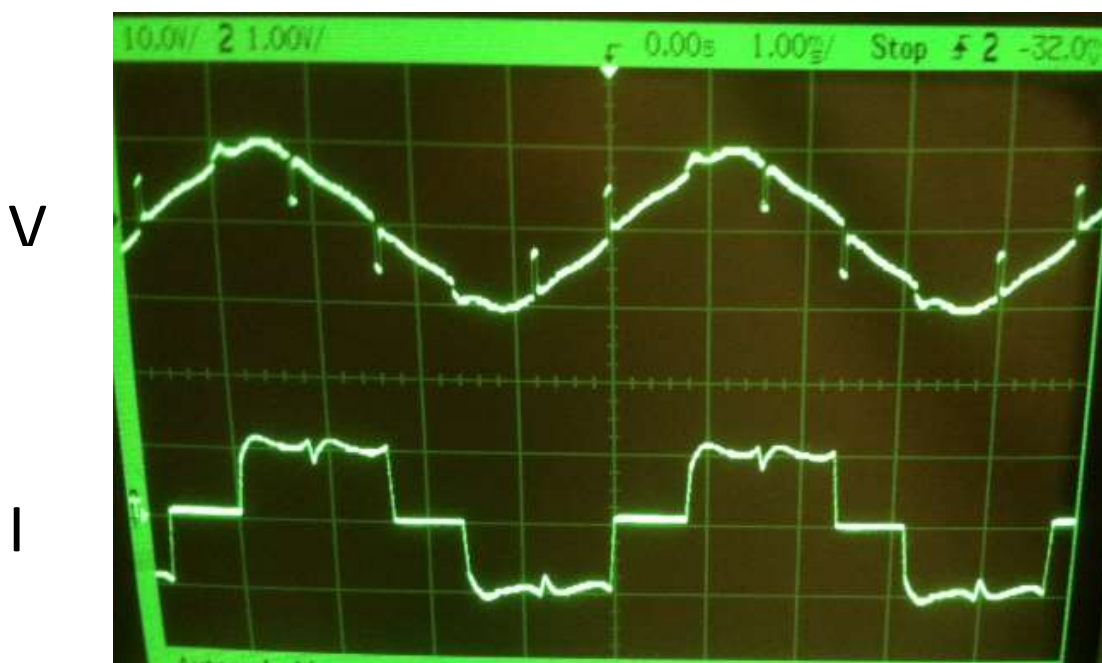


**Figure S.5** Wire 2 at WOT and 2 Nm of torque

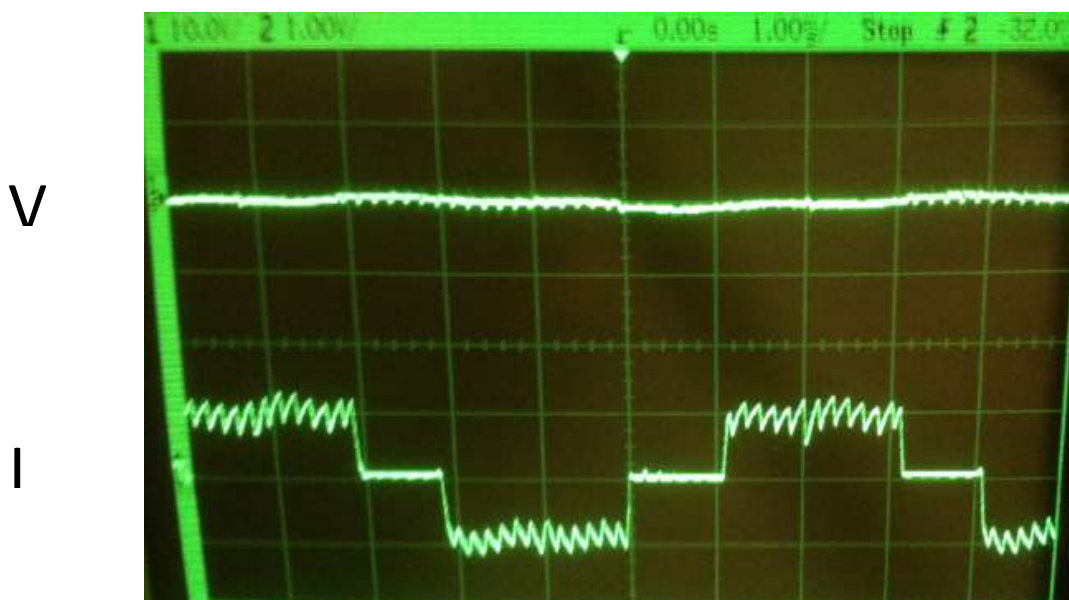


**Figure S.6** Wire 3 at partial throttle and 2 Nm of torque

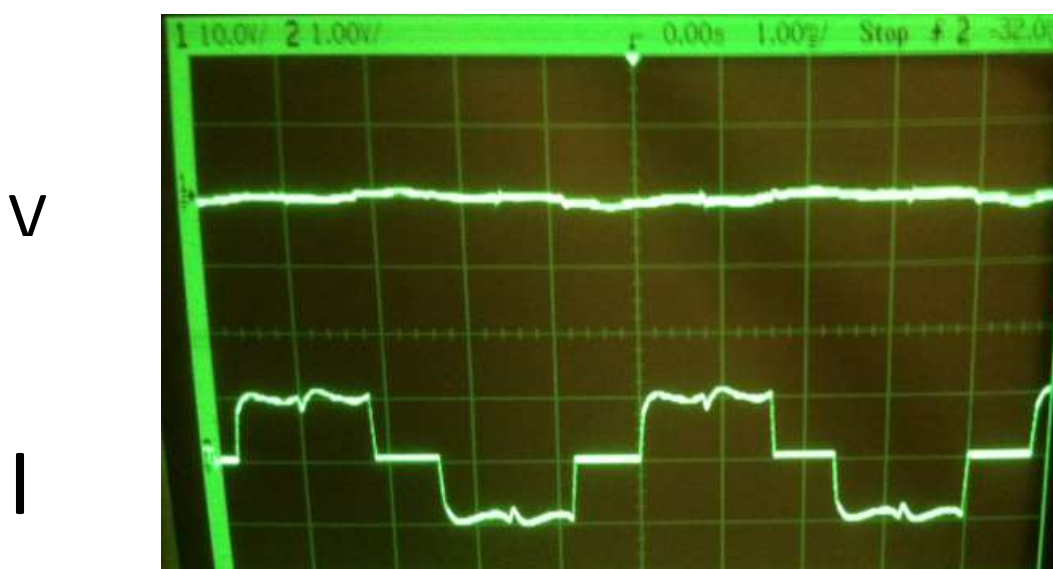


**Figure S.7** Wire 3 at WOT and 2 Nm of torque

As seen in Figure S.2 – Figure S.7, the current waveforms are the same but the voltage waveforms differ. The voltage coming through wire terminals one and two have an amplitude of about 20V/div and the voltage coming through wire terminal three has a voltage amplitude of about 5V/div. The unusually low voltage going through the third terminal wire led us to believe that there might be a short in one of the windings.

Table S.2 includes the speed, current, voltage, power, and efficiency for each of these partial throttle and wide open throttle test runs.

**Table S.2** 12 V motor Efficiency data at partial and wide open throttle

Test	Throttle	Wire	Torque (Nm)	Speed (rpm)	Power into motor controller			Pout (W)	Efficiency (%)
					Current DC (A)	Voltage DC (V)	Pin (W)		
1	partial throttle	1	1	4570	52.6	12.1	635	478	75.3
	WOT	1	1	4830	54.7	12.0	659	505	76.7
2	partial throttle	2	1	4330	47.1	12.2	574	452	78.7
	WOT	2	1	4910	53.0	12.2	645	515	79.8
3	partial throttle	3	1	3880	43.2	12.1	521	406	77.9
	WOT	3	1	4850	53.3	12.0	640	507	79.2
4	partial throttle	1	2	2660	67.5	12.0	808	560	69.3
	WOT	1	2	4230	96.7	11.8	1137	889	78.2
5	partial throttle	2	2	2450	63.4	11.9	753	512	68.0
	WOT	2	2	4210	96.7	11.7	1130	880	77.8
6	partial throttle	3	2	3209	78.7	11.8	925	672	72.7
	WOT	3	2	4180	96.8	11.6	1127	875	77.7

Another voltage test we performed with the motor was measuring the back EMF by spinning it as a generator. Our back EMF testing results are shown in Table T.3.

**Table S.3** 12 V motor back EMF voltages

VMS	900 rpm	1800 rpm
V13	1.27 Vrms	2.65 Vrms
V12	1.27 Vrms	2.65 Vrms
V23	1.27 Vrms	2.65 Vrms

The consistency of the voltages at the different speeds and the near doubling of the voltage by doubling the speed are signs of a good motor. These results perplexed us because the voltages were not consistent when the motor was motoring.

We performed two tests to check for shorts in the motor's windings. The resistance of the motor windings was measured by using a large transistor bank with three 12 V batteries in parallel. Voltage was measured across two wires using a voltmeter and current was measured using a shunt. Resistance was calculated from the voltage and current. Table S.4 shows the resistance between each of the wires.

**Table S.4** 12 V motor winding resistances

Motor Wires	mV	A	mΩ
1→2	20.3	10	2.03
2→3	19.5	10	1.95
3→1	21.3	10	2.13
1→2	41.0	20	2.05

Resistance was also measured between the motor's three phases and the stator's outer aluminum casing. Using an ohmmeter, the resistance between each of the three individual wires and the case was open circuit. When the third wire is shifted from its stationary position a resistance of 30 Ohms results between any of the three wires and the casing. The motion of the third wire, which is the same one that had the poor voltage waveform, is most likely the cause of the motor's low efficiency.

## Appendix T – Team Member Task Gantt Charts

At the beginning of this project each team member created a Gantt chart describing their planned tasks for the remainder of the year. These charts are included in Figure T.1 below.

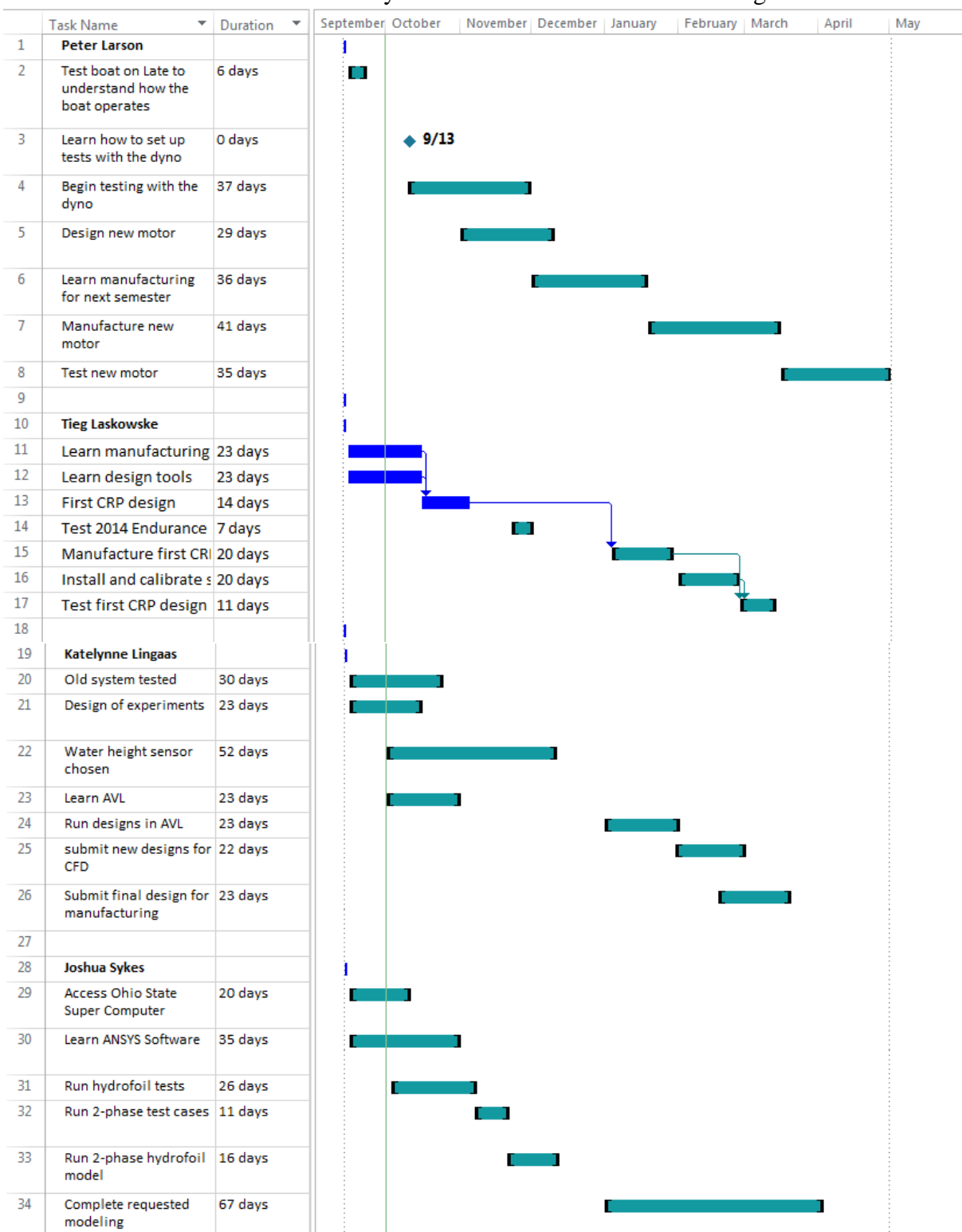


Figure T.1. Team project timeline broken up by team member (1 of 2)

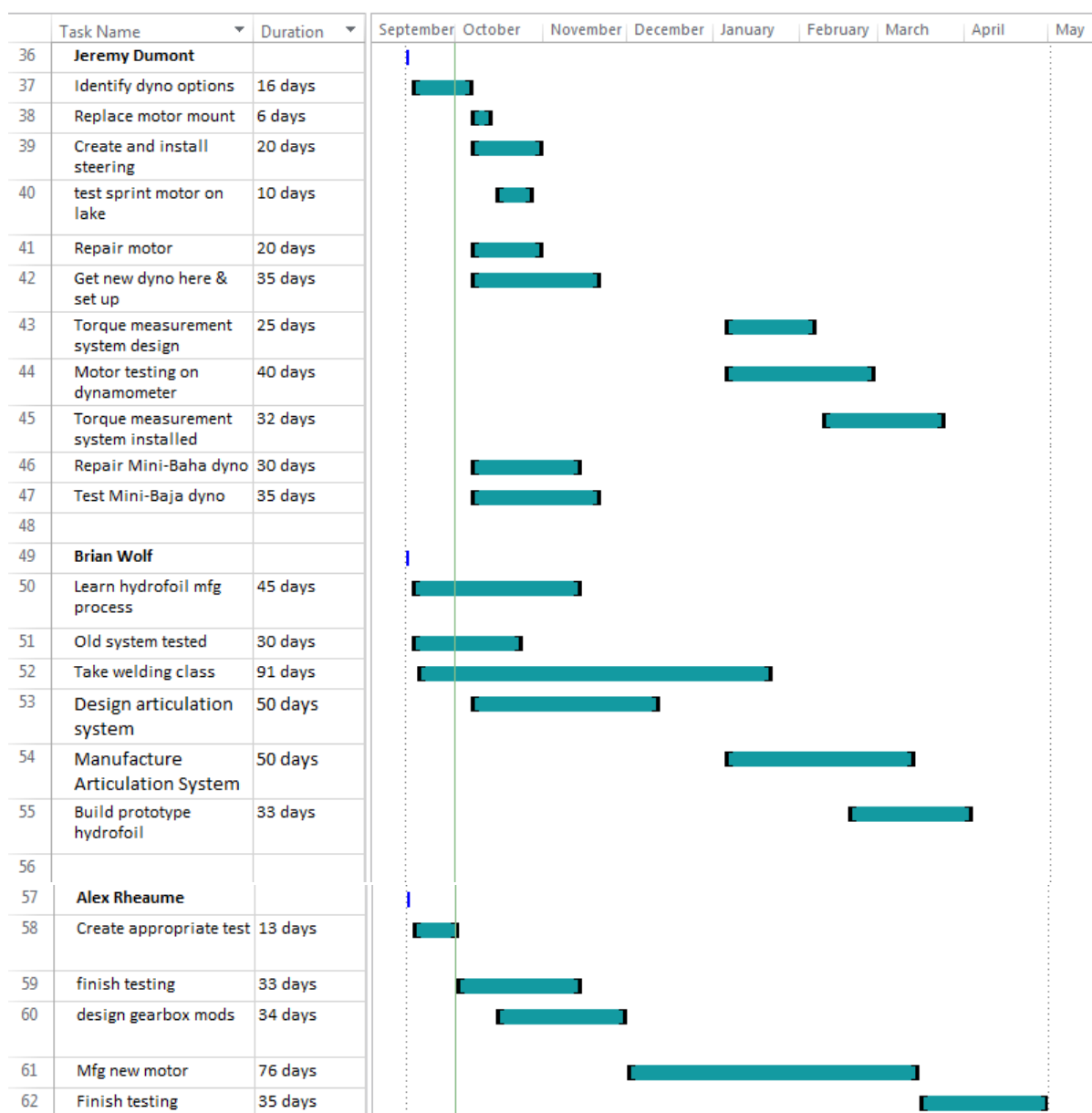


Figure T.1. Team project timeline broken up by team member (2 of 2)

## Appendix U – Monetary Budget Summary

At the beginning of this project each team member created a monetary budget describing their financial outlays for the remainder of the year. This chart is included in Table U.1 below.

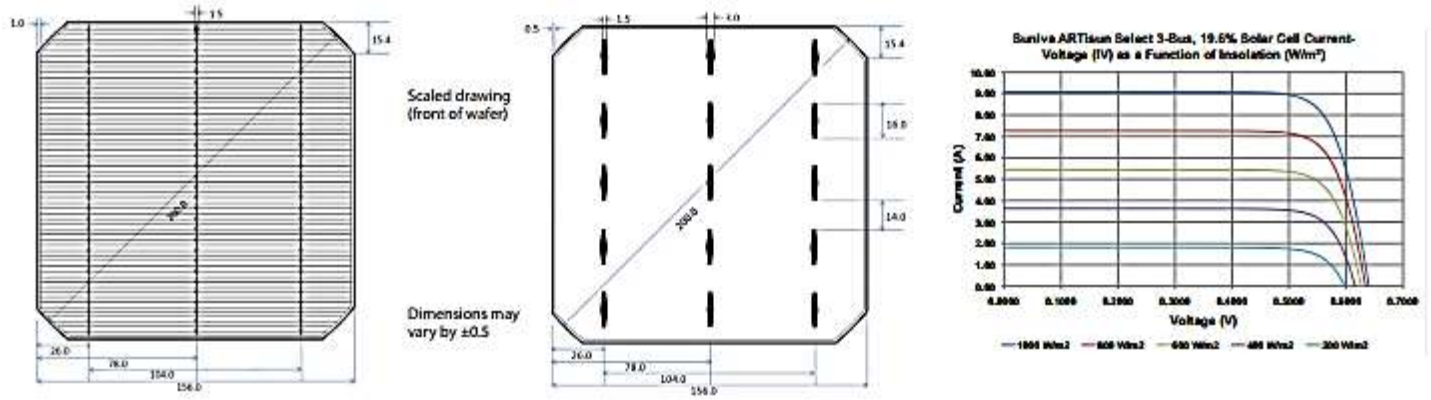
**Table U.1.** Predicted monetary budget for both semesters of the Senior Design experience

Item	Cost			Potential Donor
	Material	Donations/Sponsorship	Total	
Competition Expenses				
Solar Splash 2015	\$400	\$0	\$400	
Sprint Motor and Dynamometer				
Aluminum	\$150	\$0	\$150	
Various hardware	\$100	\$0	\$100	
Motor Controller	\$500	\$250	\$250	Jeti (Esprit) Model
Sub-Total	\$750	\$250	\$500	
Endurance Motor				
Copper Wire	\$200	\$0	\$200	
New Electric Motor	\$650	\$200	\$450	
Laminations	\$1,000	\$1,000	\$0	Laser Laminations
Motor controller	\$250	\$0	\$250	
Steel	\$50	\$0	\$50	
Aluminum	\$50	\$0	\$50	
Sub-Total	\$2,200	\$1,200	\$1,000	
Gear Train				
Bearings	\$80	\$0	\$80	
Aluminum	\$150	\$0	\$150	
Sub-Total	\$230	\$0	\$230	
Propeller Design				
Aluminum	\$500	\$0	\$500	
Testing	\$150	\$0	\$150	
Tooling	\$80	\$0	\$80	
Sub-Total	\$730	\$0	\$730	
Computational Fluid Dynamics				
Software Licenses	\$0	\$0	\$0	
Supercomputer Use	\$0	\$0	\$0	Ohio State University
Computing Cluster	\$2,000	\$0	\$2,000	Cedarville I.T. Department
Sub-Total	\$2,000	\$0	\$2,000	
Hydrofoil Design and Articulation				
Articulation Materials	\$2,000	\$0	\$2,000	
Articulation Design	\$200	\$200	\$0	SeaLandAire
Hydrofoil Design	\$0	\$0	\$0	
Sub-Total	\$2,200	\$200	\$2,000	
Hydrofoil Manufacturing				
Carbon Fiber Sheets	\$200	\$200	\$0	SeaLandAire
Resin	\$50	\$50	\$0	SeaLandAire
MDF	\$85	\$0	\$85	JMS composites
Stock Aluminum	\$200	\$0	\$200	
Foam Core	\$20	\$20	\$0	JMS composites
Aluminum Extrudes	\$50	\$50	\$0	
Sub-Total	\$605	\$320	\$285	
Team Total				
	\$9,115	\$1,970	\$7,145	



## Appendix V- Solar Array Electrical Calculations

Our solar array uses monocrystalline cells from Everbrite Solar. The solar cell specifications provided by Everbright Solar are shown in Figure F.1.



### TYPICAL CELL ELECTRICAL PROPERTIES<sup>1</sup>

ARTisun Select - Bin (Pos.Tol.)	18.6%	18.8%	19.0%	19.2%	19.4%
Efficiency (%)	18.60-18.80	18.80-19.00	19.00-19.20	19.20-19.40	19.40-19.60
Power Pmp (W)	4.44-4.49	4.49-4.54	4.54-4.59	4.59-4.64	4.64-4.68
Max Power Current Imp (A)	8.330	8.390	8.440	8.490	8.540
Short Circuit Current Isc (A)	8.850	8.890	8.930	8.970	9.010
Max. Power Voltage Vmp (V)	0.637	0.638	0.639	0.640	0.641
Open Circuit Voltage Voc (V)	0.536	0.538	0.541	0.543	0.546

<sup>a</sup> All electrical parameters valid under Standard Testing Conditions (STC): Intensity: 1000 W/m<sup>2</sup>; Spectrum: AM1.5 Global; Temperature: 25°

**Figure F.1. Cell Specifications for 19% efficient solar cells from Everbright Solar**

Note that  $V_{mp}$  and  $V_{oc}$  are mislabeled.  $V_{oc}$  should be 0.639 V, and  $V_{mp}$  should be 0.541 V. Using the maximum nominal power (4.59 W) we calculated the nominal power of the solar array.

$$P_{array} = n_{cells} * P_{mp} \quad (F.1)$$

Where  $P_{mp}$  is the nominal peak power of a cell,  $n_{cells}$  is the number of cells in our array, and  $P_{array}$  is the nominal power of the entire array. We created a spreadsheet to calculate the nominal power of the array as well as the open circuit voltage of each series. The series open circuit voltage is calculated by multiplying the individual open circuit voltage by the number of cells in

$$V_{panel_{oc}} = n_{cells} * V_{oc} \quad (F.2)$$

a series. To be conservative we used the high end nominal power of 4.59 W.



These power and voltage values are shown in Table F.1

**Table F.1.** Solar Array  $V_{oc}$  and  $P_{mp}$  calculations

Solar Cells			
Cell Specifications for 1000 W/m <sup>2</sup>			
Type	Everbright Solar Monocrystalline		
% Eff.	19.0		
$I_{mpp}$ [A]	8.45		
$V_{mpp}$ [V]	0.543		
* $P_{mpp}$ [W]	4.59		
$I_{sc}$ [A]	8.89		
$V_{oc}$ [V]	0.639		
	Panel 1	Panel 2	Panel 3
Number of Cells Per Panel	36	36	43
$V_{mpp}$ of Panels [V]	19.5	19.5	23.3
$V_{oc}$ of Panels [V]	23.0	23.0	27.5
Power of Panels [W]	165.2	165.2	197.4
Total Array Power [W]	115	Total # of Cells	
		115	

From the table our solar array's nominal power is 527.9 W, and our maximum source open voltage is 27.5 V both values are under the max allowed, 528 W<sub>mp</sub>, and 52 V<sub>oc</sub> respectively.

